FINAL TECHNICAL REPORT

A Long Record of Earthquakes With Timing and Displacements for the Imperial Fault: A Test of Earthquake Recurrence Models

U.S.G.S GRANT NO. G10AP00003

Thomas Rockwell, P.I.

Aron Meltzner,

Rebecca Tsang

Geological Sciences
San Diego State University
San Diego, CA 92182
Trockwel@geology.sdsu.edu

Table of Contents

Cover Page	1
Table of Contents	2
Summary	3
Introduction	3
Regional Geologic Setting	5
Description of the Dogwood Site	5
Trench Stratigraphy	6
Evidence For Surface Ruptures	7
Lake and Earthquake Chronology	8
Discussion	9
Conclusions	11
Data and Resources	12
Acknowledgements	12
References Cited	13
Tables	17
Figures	24
Appendix of Event Evidence	42

SUMMARY

We continued the development of a long record of earthquakes on the Imperial fault at Mesquite Basin, Imperial Valley, southern California. We extended our 500-year chronology of surface ruptures back to 1200-1400 years, the timeframe over which Lake Cahuilla occupied the Salton depression. We document evidence for up to 17 surface ruptures in this time period, the most recent of which are the 1940 and 1979 Imperial Valley earthquake ruptures. The average recurrence interval for surface rupturing events is about 80 years, albeit with a large coefficient of variation of 0.84 suggesting non-periodic behavior. We tested the hypothesis of a connection between lake and earthquake cycles; however, our data indicate that the connection is either very weak or nonexistent as many of the ruptures occurred during dry periods between lakes. On the other hand, we found a strong correlation between the earthquake chronologies in the southern San Andreas fault and the rupture history on the northern Imperial fault, suggesting surface rupture at the southernmost portion of San Andreas fault may have triggered surface slip on the northern Imperial fault, or visa versa.

Based on our previous 3D work on several buried channels, slip at the Dogwood site does not appear characteristic, as slip ranges from 0.2 to 1.5 m per event. We excavated a long trench parallel to the fault to search for additional buried channels to resolve lateral slip. We found no coherent channels below the ones that we had already excavated, so we have displacement for only the past six surface ruptures. Nevertheless, in combination with the timing evidence of the 17 surface ruptures, one explanation for the apparent lack of periodicity and non-uniform slip is that some Imperial ruptures involve the entire fault and represent complete stress drop events, whereas others are complex ruptures with only partial failure of the fault, resulting in significantly variability in timing and displacement.

INTRODUCTION

The Imperial fault is a northwest-striking, dextral fault located in the Salton Trough, an area in which the pattern of seismicity has been interpreted to represent rifting and transform faulting (Sharp, 1982a). The Imperial, along with the San Jacinto and Elsinore faults, comprise the onshore San Andreas fault system in southern California, and together they accommodate a significant proportion of the North American-Pacific plate-boundary motion (Hill et al., 1990). Geodetic studies indicate that the rate across this transform boundary is approximately 50.4 ± 3.4 mm/yr at the mouth of the Gulf of California (Antonelis et al., 1999), of which 40-45 mm/yr is believed to be accommodated by the Imperial fault itself (DeMets et al., 1994). The 70-km long Imperial fault crosses the U.S.-Mexico Border and terminates to the south at a releasing step-over to the Cerro Prieto fault. To the north, the fault transfers slip to the San Andreas fault via the Brawley Seismic Zone, which extends north of Mesquite basin to the Salton Sea (Figure 1). The fault was not recognized until the 1940 M_L 7.1 earthquake caused an end-to-end rupture of the fault, propagating mostly to the southeast (Buwalda and Richter, 1941; Richter, 1958). The 1940 earthquake is believed to have nucleated along the northern third of the fault in or just south of Mesquite Basin (Figure 2) (Buwalda and Richter, 1941; Doser and Kanamori, 1986; Doser, 1990), and the associated surface displacement was less than a meter along the northernmost 25 km of the rupture. To the south, the displacements rapidly increased to ~6 m south of Heber dunes, were about 5 m in the area of the international border, and were ~2.7 m at Tamaulipas in Baja California. The rupture terminated near the town of Saltillo at the step-over between the Imperial and Cerro Prieto faults (Sharp, 1982b; Thomas and Rockwell, 1996; Meltzner, 2006).

Thirty-nine years later, surface rupture recurred on the fault in an M_L 6.6 earthquake (Chavez et al, 1982; Sharp, 1982b; Archuletta, 1984), which was felt from Las Vegas, Nevada, to the Pacific Ocean (Johnson et al., 1982). The rupture nucleated south of the International Border and propagated unilaterally to the northwest (Figure 2). For this earthquake, surface rupture was

only produced along the northernmost 30 km of the fault, from south of Heber Dunes to a point about 3 km south of Brawley, California (Fuis, 1982; Harsh, 1982; Sharp, 1982b), much shorter than the 1940 rupture length (Sharp, 1982b). However, the observed slip on the northwest section of the fault resembled that of the 1940 rupture (Sharp, 1982b; Sieh, 1996). The coseismic dextral slip recorded after the earthquake was about 20 cm at the Dogwood paleoseismic site, 37 cm near County Highway S-80, and then increased steadily southward to about 62 cm at Heber Road, 1 km from the south end of the surface rupture (Crook, 1982). Surface faulting also occurred simultaneously along the Brawley fault, and surface rupture was observed along the Superstition Hills fault and the southernmost segment of the San Andreas fault (Fuis, 1982; Sieh, 1982). Although no ground breakage was discovered along the Coyote Creek fault, a resurvey of an array across the fault revealed an unexpectedly large offset since the previous survey (Fuis, 1982). Besides the two well-known historic surface ruptures, mainshocks with at least modified Mercalli intensity VII (MMVII) occurred in the region in 1906, 1915, 1917 and 1927 (Beal, 1915; Townley and Allen, 1939; Toppozada et al, 1978; Johnson and Hill, 1982), all of which may have been associated with the Imperial fault (Johnson and Hill, 1982). In addition, the Imperial fault is characterized by a component of aseismic creep (Goulty et al, 1978; Cohn et al, 1982, Johnson and Hill, 1982). Creep episodes with 1 to 2 cm of measured displacement occurred at approximately two-year intervals on the central segment of the Imperial fault (Goulty et al, 1978) for the 12 years prior to the 1979 earthquake (Cohn et al, 1982), and some after-slip has almost certainly occurred at the Dogwood site as nearby roads and canals show recent cracking and right-lateral oblique slip.

The effects of the 1940 and 1979 events in this seismically active region were widely documented in historical records (Buwulda and Richter, 1941; Toppozada et al., 1978; Johnson and Hill, 1982), by mapping (Sharp, 1980; 1982a; 1982b) and with seismic instruments (Chavez et al., 1982; Crook et al. 1982; Johnson et al., 1982). However, information on the long-term rupture history of this plate boundary fault is sparse, with only a few paleoseismic investigations having been completed for this fault (Sharp 1980; 1982a; 1982b; Thomas and Rockwell, 1996; Meltzner and Rockwell, 2011 in review). In their study near the International Border, Thomas and Rockwell (1996) found evidence for an older paleoearthquake of undetermined slip magnitude occurring during the waning stages of the Lake Cahuilla highstand approximately 300 years ago, which is similar to what Sharp (1980) concluded from a study on the north side of the border, located about 75 m from the Thomas and Rockwell (1996) study. Meltzner and Rockwell (2011 in review) excavated trenches in Mesquite basin at Harris Road and east of Dogwood Road, naming the latter site the Dogwood site. In their study, they determined displacement and timing for the past six surface ruptures from trench exposures and channel deflections, all of which have occurred in the past ~500 years, including the 1979 and 1940 surface ruptures for which there are direct observations of displacement (Sharp, 1982b).

In this study, we continued to work at the Dogwood site by excavating 10 new trenches and lengthening two existing trenches (Figure 3) to extend the record of late Holocene surface ruptures to ~1300 years. Our primary goals are to better understand the behavior and rupture patterns of this plate-boundary strike-slip fault and to improve earthquake forecast models.

Rupture behavior underpins most forecast models, and the Imperial fault has been cited as an example for some models. For instance, Sieh (1996) proposed the slip-patch model for the northern Imperial fault in which the northern segment is a patch that has its own characteristic repeating slip, and that the small offsets observed in 1940 and 1979 events are typical for this segment. If correct, Sieh's (1996) model predicts a recurrence rate of 39-73 years for the northern Imperial fault. In contrast, Meltzner and Rockwell (2011 in review) determined about a 100-year average recurrence interval for the northern Imperial fault at the Dogwood site, with most of the slip events being larger than that which occurred in 1940 or 1979. They argue that because the 1940 rupture started in the north near the juncture of the Imperial and Brawley faults, and because the rupture grew southward to 5-6 m in the border region, that the northern low-slip section

simply re-ruptured in 1979 as a result of stress loading from the 1940 event. Paleoseismic work by Thomas and Rockwell (1996) at the International Border revealed only two events in the past ~300 years, yielding a short-term average recurrence interval of ~250 years on the central segment of the Imperial fault, broadly consistent with either model.

In this paper, we develop new data on the timing of past surface ruptures on the northern Imperial fault. We include a brief discussion on the regional geologic setting, a description of the Dogwood site and its stratigraphy, the lake chronology model that was used to estimate ages of paleo-surface ruptures, and a brief description of evidence for surface ruptures. For a complete detailed description of evidence of each rupture from each trench exposure, see Appendix A in the electronic supplement to this article." We conclude with a discussion on the recurrence interval and earthquake patterns of the northern Imperial fault.

REGIONAL GEOLOGIC SETTING

The Imperial Valley is part of a linear structural and topographic depression that extends roughly 1400 km through southern California and Mexico to the southern end of the Gulf of California (Sharp, 1982a). The Salton Trough, a complexly folded, faulted, and down-warped graben-like structure located at the northern part of this linear depression, is an extension of the Gulf of California but has been separated from the gulf by the buildup of the deltaic cone of the Colorado River (Sharp, 1982a). The Salton Trough, which surface elevations of as much as 90 m below sea level, is filled with as much as 6 km of sedimentary deposits in the central Imperial Valley (Tarbet, 1951; Fuis et al., 1982), most of which were derived from the Colorado River basin (Merriam and Bandy, 1965; Muffler and Doe, 1968). During late Quaternary time, the Salton Trough north of the delta evolved into a desert basin when flow of seawater from the gulf to the south was blocked by the deltaic cone (Sharp, 1982a). During the past 1200-1300 years, the Colorado River has switched from its present southward course to the Gulf of California and flowed northward into the Salton Trough at least five times (Gurrola and Rockwell, 1996). The floodwaters of the Colorado River inundated the sub-sea level portions of the Coachella and Imperial Valleys to episodically form ancient Lake Cahuilla, an ephemeral freshwater lake that had a maximum highstand elevation of between 9 and 13 m above modern sea level (Stanley, 1963, 1966; Thomas, 1963; Van de Kamp, 1973; Sharp, 1982a; Waters, 1983; Sieh, 1986; Sieh and Williams, 1990; Rockwell and Sieh, 1994; Gurrola and Rockwell, 1996; Thomas and Rockwell, 1996; Orgil, 2001). Because of the hot, arid climate, Lake Cahuilla can desiccate in as short as a 60 to 70 year period once the Colorado River resumes its course to the Gulf of California (Sieh and Williams, 1990). Although five lake highstands have been recognized in the past 1200 years at different sites along the shoreline, it is possible that during some periods of time, the lake did not completely desiccated between the highstands or was only partially filled by the Colorado River (Meltzner et al, 2006). There is no known historical or geologic evidence for any lakes larger than the present Salton Sea since the ca. A.D. 1700 lake, although the limited historical data may suggest a short-lived partial filling of Lake Cahuilla between about 1680 and 1825 (Blake, 1854, 1915; Barrows, 1900; Cory, 1913; Modesto and Mount, 1980; Sieh and Williams, 1990).

DESCRIPTION OF THE DOGWOOD SITE

The Dogwood site lies approximately 27 m below sea level, well below the ancient Lake Cahuilla shoreline at about 12 m above modern sea level. It is located near the southern border of the city of Brawley, north of the city of El Centro, California, at precisely 32.860356° N and 115.534478° W (Google Earth). The overall strike of the fault is northwest and the primary sense of slip is right-lateral, with a minor extensional dip-slip component (downthrown side on the east) in Mesquite basin. The fault scarp at the surface is well expressed at this site and coincides with the major fault zone in all of the fault-perpendicular trenches.

The Dogwood site is an ideal location for paleoseismic work on the Imperial fault because it is structurally simple in this area, with a single rupture surface that transitions northward into a zone of transpression (Figure 4). Furthermore, local down-warping has allowed for an area where sediment has deeply accumulated and erosion appears to have been minimal, resulting in a complete record of lacustrine depositional events (Figure 5). In addition, despite the heavy agricultural activity in this region, this property has not been developed for agricultural or other use, resulting in one of the only virgin sections of land along the length of the Imperial fault.

TRENCH STRATIGRAPHY

The lacustrine sub-aqueous deposits exposed in trenches at the Dogwood site and its vicinity are associated with Lake Cahuilla and range from coarser-grained deltaic and fluvial sand to finer-grained lacustrine clay (Meltzner, 2006). The deltaic sediments are likely derived from the Colorado River during a period of inundation of Lake Cahuilla, as the site is near the New River delta. We also recognize the presence of fluvial deposits which originated from small channels that incised the sub-horizontal bedded lacustrine strata. The downthrown side of the fault is composed of late Holocene sediments, including the deposits from the most recent Lake Cahuilla highstand, and possibly up to seven lake highstands to a depth of 6 m. The upthrown block contains older, middle to late Holocene sediments, which predate the entire section exposed in the hanging wall. Therefore, we only discuss the stratigraphy in detail for the hanging wall, as that is the section that contains the evidence of past surface ruptures.

About 6 meters of stratigraphic section of the hanging wall was exposed in the various trenches that were excavated to different depths (Figure 6). The extension of Meltzner and Rockwell's (2011 in review) T2 trench revealed a localized structural depression where the accumulated sediments are thicker than in other trenches, allowing for the preservation of the best stratigraphic record at the site (Figure 7). Therefore, we decided to explore and excavate new fault-perpendicular trenches, the T9 and T4Deep trenches, at the axis of the syncline to better understand the relationship between the fault and the stratigraphy. The strata were logged onto digital photography and interpreted in terms of the origin of the various sediment packages. For instance, well-bedded, laminated clayey/silty strata were interpreted as lacustrine/deltaic in origin, whereas channeled sediments filled by sand with or without crossbeds and blocks of reworked lacustrine strata were interpreted as fluvial flow in small channels that incised the lacustrine strata during dry periods. A third primary deposit is interpreted as sand-blow (liquefaction) deposits based on their well-sorted nature, the presence of foreset beds that seem to radiate from a point source in some cases, and from their non-tabular form.

From the observations of periods of fluvial incisions, which we interpret as periods of sub-aerial exposure during a hiatus in lake deposition, along with other observations of (minimal) sub-aerial exposure such as the presence of oxidation or root casts, we divided the stratigraphic section into seven lake phases (A to G), the most recent six of which correlate to those identified in the Lake Cahuilla chronology model developed by Meltzner and Rockwell (2011 in review); the oldest Lake G is absent in their model due to insufficient age data from older sediments. The lake phases are labeled in letters in the order of increasing age. Because this site is more than 30 meters below the highstand shoreline of the lake, lacustrine sediments may represent periods of time when the basin was only partially full; deltaic sediments represent a period of lake recession; and sub-aerial intervals represented by fluvial deposition imply that the entire lake basin desiccated to below -31 m elevation. We further sub-divided units based on continuity of major strata, and with the aid of the fault-parallel trenches, correlated all strata throughout all trenches at the site. Stratigraphic units were numbered in the order of increasing stratigraphic depth. For detailed descriptions of each unit, please refer to the generalized stratigraphic column as shown in Figure 6.

EVIDENCE FOR SURFACE RUPTURES

Common paleoseismic indicators that were used to identify the ground or lake bottom surface (event horizons) at the time of past surface ruptures include the upward termination of fault strands (UT), the presence of fissure fills capped by unbroken stratigraphy (FF), the presence of sand blow (SB) deposits that apparently ejected to a surface, the occurrence of angular unconformities (AU), buried scarps (Sc) and associated colluvial wedges (CW) or scarp-derived debris (Db), the presence of liquefaction pipes (LP), and the downward growth of displacement (DG). We have made detailed descriptions of the evidence for each event, including annotated photographs, which are included in the appendix. For this paper, we provide a few examples here to illustrate the types of data that are used in our analysis. We refer the reader to the appendix for the complete description of evidence of each event.

Figure 8 shows several indicators and their relative positions that define the event horizon for Event 8. A fissure fill is bounded by two fault splays that terminate upward, and at the same horizon, a clean, well-sorted sand unit, interpreted as a sand blow, was deposited nearly horizontally on the paleo-surface, forming an angular unconformity with the strata below. Similarly, Figure 9 shows clear evidence for Event 3 in which a series of fault splays all terminate upward at the same horizon. These faults are also associated with a fissure fill that contains broken lithic fragments which have fallen into fissures when the ground opened up. The same figure also shows the location of the event horizon and the associated evidence for Event 4, including upward fault truncation and the presence of a colluvial wedge, a wedge of colluvial debris that is formed adjacent to near-vertical fault scarp soon after the surface rupture event (McCalpin and Nelson, 1996). The presence of a sand-blow deposit is strong evidence for past strong ground shaking, and if associated directly with a fault trace, likely indicates rupture on that fault. However, sometimes the nature of a sand-blow deposit may not be interpreted with certainty, therefore, the presence of additional paleoseismic indicators is necessary to correctly identify an event horizon. In Figure 10, on top of the interpreted sand-blow deposit that was marked with "SB", the exposure revealed an apparent upward termination of a single fault splay and a clear angular unconformity between Units 505-550 and Unit 580 which marks the event horizon for Event 13. Numerous other examples are found in the event evidence that is detailed in the appendix.

To better qualify the likelihood of occurrence of a past earthquake, we devised a rating scheme of the paleoseismic indicators for each event horizon. The scheme is somewhat similar to the one developed by Scharer et al. (2007) for the San Andreas fault. However, the fundamental approach in our rating scheme is somewhat different in that we had done preliminary interpretation of event evidence and the apparent likelihood of the corresponding event horizons in the field, in contrast to the approach by Scharer et al. (2007) where they ranked the quality of all evidence of ground deformation, including individual splays in a fault zone. As opposed to the rating scheme which Scharer et al. (2007) used as a primary tool for interpretation, the rating scheme we present here serves as a supplementary instrument that allows us to re-analyze the evidence for events in a more objective and quantitative way.

Each event indicator receives a rating of 1 to 4, with 1 being the weakest and 4 being the strongest (Table 1). For example, a distinct angular unconformity is a strong line of evidence hence it has a rating of 4. Other strong paleoseismic indicators with a rating of 4 that suggest the occurrence of a surface rupture without much ambiguity include the presence of a scarp and associated colluvial wedge or scarp-derived debris, and fissure fills associated with faults rupturing to the surface. On the contrary, weak evidence such as downward growth of vertical separation or upward termination of minor cracks have the lowest rating of 1 due to the ambiguity in interpretation, as they might be the result of a fault splay dying out upward. Sand blows receive a rating of either 2 or 4, depending on the level of certainty for the nature of the deposit. If there is strong evidence supporting the deposit being a sand blow, the paleoseismic indicator receives a rating of 4, otherwise it only receives a rating of 2.

Upward truncation of faults and liquefaction pipes are the two indicators that may require more vigilance in rating designation (1 to 4) as they are rated based on density, location, and for fault splays, whether they are associated with fissure fills. If the fault splays all terminate at the same stratigraphic level with fissure fills in between, this indicator of upward truncation of faults will receive a rating of 4. Liquefaction pipes can also be a strong line of evidence for a surface rupture when a large number of pipes terminate at the same level, but not when only a few were observed. (For a simpler computation, a network of fault splays is considered as one observation of upward fault truncation rather than each individual splay. Yet they are listed as two separate observations if they are considerably far apart, even in the same trench exposure.)

The frequency (F) of these observations is another factor to determine the likelihood of an event. In this method, the value of F is calculated by dividing the number of exposures where the indicator was observed (E_o) by the number of exposures where the indicator *should be* observed (E_t), i.e. the exposures that contain the strata which should express evidence for the event. Finally, the rating of each observation (R) is multiplied by the frequency (F) for the R*F value, which indicates the likelihood of a paleoearthquake. The higher the R*F value, the more likely the event occurred (Figure 11).

Using this scheme, there are still potential problems that suggest that we may under-rate some events. For instance, Event 4 received a relatively low R*F value but its occurrence is nearly certain as this event produced lateral slip on a buried channel (Meltzner and Rockwell, 2011 in review). Among all 17 events, almost all events receive an R*F value higher than 1 except for Events 4, 8.5, 8.7 and 9. From the analysis of the paleoseismic indicators, these events could be interpreted as unlikely or as events with small displacement, which coincides with our preliminary field interpretation for the likelihood of each event.

There are other limitations in this rating scheme. First, the R*F value may be inflated for older events due to the limited number of trench exposures available (a low E_t value) because they are exposed only in the deeper section. Second, although the presence of colluvial wedges or scarp-derived debris associated with a scarp serves as a strong indicator with a high rating, a low R*F value may be assigned due to the localized nature of their formation, thereby limiting the chance of exposure in trenches (a low E_o value). Third, some events with strong evidence may have low average R*F values because of low sedimentation rate, bioturbation of stratigraphy, or transpression along the fault that, in some trench exposures, increases the ambiguity of strata correlation and the exact location of the paleoseismic indicators. This makes rating upward fault terminations (UT) and liquefaction pipes (LP) more difficult because the rating (1 to 4) highly depends on where these features terminate and whether they all terminate at the same stratigraphic level.

LAKE AND EARTHQUAKE CHRONOLOGY

The ages of sediments at the Dogwood site is constrained by ^{14}C analysis on detrital charcoal using accelerator mass spectrometry (AMS) techniques. Pieces of detrital charcoal that were found embedded within the strata were collected and cleaned with deionized water, and those pieces that weighed at least 1 mg after cleaning were submitted to the CAMS facility at UC Irvine. The radiocarbon ages were then placed in stratigraphic order in OxCal (Bronk-Ramsey, 1995) and calibrated to the AD timescale.

To correctly interpret the meaning of the ages, one must understand that nature and source of the detrital charcoal collected at a site. There are only a few possibilities for the sources of charcoal in the Imperial Valley. The detrital charcoal might have been transported from afar, resulted from a nearby range or forest fires, or have been derived from cooking fires by the indigenous people of the area, the Cahuilla Indians. The sparse vegetation pattern in this arid climate would not be enough to fuel range and forest fires, so we discount the likelihood of this possibility. Most of the charcoal fragments were found in clusters rather than being evenly

distributed in the strata, which argues against them being transported from afar. That leaves local fires by Native Americans as the most likely source for most or all of the charcoal fragments.

The limitation in this ^{14}C analysis includes a possibly large inherited age of the charcoal pieces that come from the burning of wood by the Indians. First, ^{14}C dates record the date of wood growth, however, the Indians were likely to burn dry, old wood which makes the detrital charcoal useful only for providing a maximum age constraint. Second, there may have been a delay between the burning of wood and the transport of charcoal to the deposition site, resulting in older apparent ages of the burned wood than the actual age of the host sediment. This is likely the case for all samples that were recovered from lacustrine sediments, as wood doe not grow or burn under water. Third, wood only grows during the drying period between lakes, therefore the charcoal found in the host lake sediments can only at best give the age of the drying period immediately prior to a lake highstand.

Using these concepts, and holding to the assumptions mentioned above, Meltzner and Rockwell (2011 in review) developed and are still in the process of refining the chronology model of Lake Cahuilla. Over the past few years, they collected over 300 samples and submitted over 180 detrital charcoal and peat samples from the Lake Cahuilla strata at different localities in the Imperial Valley for ^{14}C analysis. About 50 of these ^{14}C dates in BP years (four from this study and a total of 27 from the Dogwood site) that carry a relatively low inheritance were chosen and calibrated into calendar years by the OxCal 4.1 software which uses the standard calibration curves from dendrochronology and coral data (Bronk-Ramsey, 1995). The calendar ages are expressed as probability distributions that are often irregular and multimodal but can be tightened by adding other chronological information such as stratigraphic ordering and historical constraints (Lienkaemper and Ramsey, 2009). As a result, by taking into account of all the age constraints entered into the model, a sequence of lake highstands and the chronology of Lake Cahuilla were generated (Figure 12). For details of OxCal, please refer to Bronk-Ramsey (1995) and Lienkaemper and Ramsey (2009). For details of the lake chronology model of Lake Cahuilla, please refer to Meltzner and Rockwell (2011 in review).

Based on the Lake Cahuilla chronology, a chronology of paleo-events in the Imperial Valley can be developed as we have determined where each event horizon is located stratigraphically in the Lake Cahuilla sequence. Take Event 3 as an example, which occurred during the highstand of Lake A as recorded in the stratigraphy. Instead of having OxCal to calculate the age of the lake as done in the lake chronology model, we want to determine the age of Event 3 that is constrained by the younger ^{14}C ages and strata in the upper sequence and older ^{14}C ages and strata in the lower sequence. Due to the limited number of charcoal samples collected in the older, deeper section, ages for older events are not as well constrained as those for Event 7 and younger. It is therefore critical to collect more charcoal samples from the lower section to refine both the lake and paleoearthquake chronology models.

DISCUSSION

Recurrence Interval

For the record of the past 1300 years, there have been up to 17 events that have occurred at the Dogwood site on the northern Imperial fault (Figure 13). Using all 17 events yields a recurrence interval for rupture along the northern Imperial fault of about 80 years on average. However, the standard deviation is large at about 68 years and the data have a coefficient of variation of 0.844, suggesting non-episodic earthquake behavior. If the three less likely events (Events 8.5, 8.7 and 9) are excluded in the calculation, the recurrence interval increases to about 100 years on average but the recurrence statistics still argue for irregular recurrence. Regardless of the time frame considered and the inclusion or exclusion of the less likely or low-slip events, this study concludes that the Imperial fault has an average recurrence interval of 100 years or less and has produce irregular earthquakes.

Sieh (1996) proposed the slip-patch model for the northern Imperial fault in which the northern segment is a patch that has its own characteristic repeating slip and that the small offsets as observed in 1940 and 1979 events are typical for this segment, resulting in an estimation of 39-73 years for the average recurrence interval on the northern Imperial fault. This shorter average recurrence interval compared to what we found in this study could be a result of the lack of a longer paleoseismic record in Sieh's study. After all, his estimation was solely based on the occurrence of the two most recent ruptures that happened in the twentieth century. On the other hand, the paleoseismic work by Thomas and Rockwell (1996) at the International Border revealed only two events in the past ~300 years, giving an average recurrence interval of about 250 years (ca 1690 to 1940) on the central segment of the Imperial fault, contrasting with the shorter recurrence interval of 80 years that we determined in this study. The discrepancy is largely the result of a short record of earthquakes at the Border site. In the earlier study at the Dogwood site by Meltzner and Rockwell (2011 in review), the resolution of six events for the past ~500 years yielded an average recurrence interval of ~100 years on the northern Imperial fault, which does not deviate significantly from the estimation in this study (~80 years), when we consider the average recurrence interval in a time frame (1300 years) more than twice as long as theirs (500 years).

Slip Per Event

Meltzner and Rockwell (2011 in review) concluded that slip per event at the Dogwood site ranges from 0.15 to 1.5 m, with an average of 0.83 m (Figure 14). They also determined total slip to be about 5 m over the past 500 years, yielding an average slip rate of approximately 11 mm/year at the northern Imperial fault. If we use this slip rate and the average recurrence interval estimated in this study (80 years), the slip per event along the northern Imperial fault would be slightly less than a meter, which does not differ much from the average slip per event that Meltzner and Rockwell (2011 in review) estimated.

Triggered Seismicity by Lake Loading

The cluster of earthquakes events 11, 12 and 13, which occurred during the filling of Lake F (AD 850-950), has prompted us to explore the possibility of a connection between earthquake cycle and lake cycle. Studies on reservoir- and lake-triggered seismicity suggest that earthquakes are most likely to be triggered during a time of substantial water level change, either soon after the initiation of filling of a lake or a reservoir, or shortly after the drop of water level, or a combination of both (Simpson et al., 1988; Gupta, 2005; Luttrell et al., 2007; Philibosian et al., 2011). The filling of Lake Cahuilla would have caused a stress perturbation and potentially affected the timing of rupture on the Imperial fault in three different ways: (1) the direct effect of water loading would increase the normal stress on the fault plane and thus inhibit failure (Philibosian et al., 2011), (2) the pore pressure would increase when water is free to percolate to seismogenic depth and thus promote failure (Simpson et al., 1988; Luttrell et al., 2007; Philibosian et al., 2011), and (3) the bending of lithosphere near the shoreline due to viscoelastic deformation would cause horizontal extension or compression, inhibiting or promoting failure depending on the location of the fault relative to the lithosphere's inflection points (Luttrell et al., 2007; Philibosian et al., 2011). Given that these effects likely occur during or soon after lake filling, one would expect to see a correlation between the changes in lake levels and the surface ruptures on the Imperial fault.

From our study, eight of the 17 events occurred during dry periods between lake phases; four events happened during deep-water deposition during a lake highstand when the water level should have been constant, or nearly so; and only five events occurred during possible changes in water level, either during the filling of a lake or when the lake started to desiccate. Thus, if there is a correlation between filling episodes and earthquakes on the Imperial fault, it does not appear to be strong.

Luttrell et al. (2007) modeled the stress changes that would have been produced by Lake Cahuilla on the southern San Andreas fault and concluded that the magnitude of Coulomb stress

change is about 10 times smaller than stress released by a typical earthquake. Therefore, the lake level changes are likely to make only a significant difference to faults that are already close to failure (Luttrell et al., 2007; Philibosian et al., 2011). In addition, due to the large uncertainty in both lake and earthquake chronologies that we have at this point of the study, it is difficult to draw solid conclusions about a connection between lake and earthquake cycles on the northern Imperial fault.

Triggered Slip by the Southern San Andreas Fault

In contrast, there appears to be a strong correlation in the earthquake chronology between the Indio (Sieh, 1986) and Coachella (Philibosian et al. 2011) paleoseismic sites on the southernmost portion of the San Andreas fault and our study area on the northern Imperial fault. All four events at Indio and all seven events at Coachella show a general strong correlation to the events at the Dogwood site (Figure 15). The most recent events at Indio (Ind-1) and at Coachella (Coa-1) on the southern San Andreas fault occurred around AD 1690 which is the age of Event 4 on the northern Imperial fault. In addition, Coa-7 on the San Andreas fault and Event 10 both occurred ca. AD 930. There are also weakly correlated pairs, such as E9 and Ind-4 where the apparent age difference can be as large as 50 years. However, the same event on the northern Imperial shows a good correlation with Coa-6 at Coachella (Figure 15). In the same sense, the age difference for another weakly correlated pair of events, E7 and Coa-3, is about 40 years, but the age of E7 shows a good match with that of Ind-2 at Indio (Figure 15). These observations indicate that we are probably near the limit of discrete dating of individual paleo-events from site to site because the Indio and Coachella events almost certainly represent the same major earthquakes as the sites are so close. Nevertheless, the earthquakes chronologies in Coachella and Indio on the southern San Andreas fault can be correlated easily to some of the events on the northern Imperial fault, although not all of the events at the Dogwood site are recorded in the earthquake chronology of the southern San Andreas. This observation suggests that rupture on the southernmost portion of the San Andreas fault might have triggered surface slip on the northern Imperial fault, but not vice versa, especially when the rupture propagation on the southern San Andreas was directed mostly to the southeast. This implication has a significant influence on our earthquake forecast model. If the southern San Andreas ruptures in the near future, after a 300-year quiescence, it may sufficiently load the Imperial fault to cause it to re-rupture after only a few decades of accrued elastic loading after the 1979 earthquake.

CONCLUSION

We conducted this paleoseismic study on the northern Imperial fault at the Dogwood site in Mesquite Basin, southern California, to extend the record of late Holocene surface ruptures to better understand the behavior of this plate boundary strike-slip fault. Event horizons in 12 trench exposures were identified within the Lake Cahuilla stratigraphy using the standard paleoseismic indicators such as angular unconformity, fissure fill and upward truncation of faults. By using the lake chronology model that Meltzner and Rockwell (2011 in review) developed for Lake Cahuilla in the Imperial Valley, we developed an earthquake chronology of the northern Imperial fault. Our study has revealed evidence for up to 17 events in the past 1300 years, yielding an average recurrence interval of about 80 years, albeit with a large standard deviation and coefficient of variation. We tested the hypothesis of a connection between lake and earthquake cycles, however, our data suggest that the connection is either very weak or non-existent as the majority of the ruptures occurred during dry periods between lakes. On the other hand, we do find a strong correlation between the earthquake chronologies determined for the southern San Andreas fault and the rupture history on the northern Imperial fault, suggesting surface rupture at the southernmost portion of San Andreas fault may have triggered earthquakes on the northern Imperial fault.

DATA AND RESOURCES

All data used in this paper came from our original research or from published sources listed in the references.

ACKNOWLEDGEMENTS

We are grateful for the help we received that has made this project possible. We thank the landowner for permission to excavate on his property and Jim Little for the backhoe operation. Field assistants including Paula Figueiredo, Gayatri Marliyani, Petra Štěpančíková, Nissa Morton, Barrett Salisbury, Mike Buga, Eulàlia Masana and Katie Anderson offered much help in the exposure preparation. This project was funded by the National Earthquake Hazards Reduction Program (NEHRP).

REFERENCES

Antonelis, K., D. J. Johnson, M. M. Miller, and R. Palmer (1999). GPS determination of current Pacific–North American plate motion. *Geology* **27**, 299-302.

Archuleta, R.J. (1984). A faulting model for the 1979 Imperial Valley earthquake, *J. Geophys. Res.* **89**, 4559-4585.

Barrows, D. P. (1900). The Colorado Desert, *Natl. Geogr. Mag.* **11**, 337-351.

Beal, C. H. (1915). The earthquake in the Imperial Valley, California, June 22, 1915, *Bull. Seism. Soc. Am.* **5**, 130-149.

Blake, W. P. (1854). Ancient lake in the Colorado Desert, *Am. J. Sci. (second series)* **17**, 435-438.

Blake, W. P. (1915). Sketch of the region at the head of the Gulf of California, in *The Imperial Valley and the Salton Sink*, H. T. Cory (Editor), J. J. Newbegin, San Francisco, California, 1-35.

Bronk-Ramsey, C. (1995). Radiocarbon calibration and analysis of stratigraphy: the OxCal program, Radiocarbon **37**, 425–430.

Buwalda, J. P., & C. F. Richter (1941). Imperial Valley earthquake of May 18, 1940. *Bul.l Geol. Soc. Am.*, **52**, 1942-1943.

Chavez, D., J. Gonzales, A. Reyes, M. Medina, C. Duarte, J. N. Brune, F. L. Verson, III, R. Simons, L. K. Hutton, P. T. German, and C. E. Johnson. (1982). Mainshock location and magnitude determination using combined U.S. and Mexican data, in *The Imperial Valley, California, Earthquake, October 15, 1979, U.S. Geol. Surv. Profess. Pap. 1254*, 51-54.

Cohn, S. N., C. R. Allen, R. Gilman, & N. R. Goulty. (1982). Preearthquake and postearthquake creep on the Imperial fault and the Brawley fault zone, in *The Imperial Valley, California, Earthquake, October 15, 1979, U.S. Geol. Surv. Profess. Pap. 1254*, 161-167.

Cory, H. T. (1913). Irrigation and river control in the Colorado River Delta, *Trans. ASCE* **76**, 1204-1453, paper no. 1270. Reprinted in Cory, H. T. (1915), *The Imperial Valley and the Salton Sink*, J.J. Newbegin, San Francisco, California, 452 pp.

Crook, C. N., R. G. Mason, and P. R. Wood (1982). Geodetic Measurements of Horizontal Deformation on the Imperial Fault, in *The Imperial Valley, California, Earthquake, October 15, 1979, U.S. Geol. Surv. Profess. Pap. 1254*, 183-191.

DeMets, C., R. G. Gordon, D. F. Argus, and S. Stein. (1994). Effects of recent revisions to the geomagnetic reversal time scale on estimates of current plate motions, *Geophys. Res. Lett.* **21**, 2191-2194.

Doser, D.I. (1990). Source characteristics of earthquakes along the southern San Jacinto and Imperial fault zones (1937 to 1954), *Bull. Seism. Soc. Am.* **80**, 1099-1117.

Doser, D.I. and H. Kanamori (1986). Spatial and temporal variations in seismicity in the Imperial Valley (1902–1984), *Bull. Seism. Soc. Am.* **76**, 421-438.

Fuis, G. S., W. D. Mooney, J. H. Healey, G. A. McMechan, and W. J. Lutter (1982). Crustal structure of the Imperial Valley region, in *The Imperial Valley, California, Earthquake, October 15, 1979, U.S. Geol. Surv. Profess. Pap. 1254*, 25-50.

Google Inc. (2011). Google Earth (Version 6.0.3.2197) [Software]. Available from http://www.google.com/earth/index.html.

Goulty, N. R., R. O. Burford, C. R. Allen, R. Gilman, C. E. Johnson, and R. P. Keller (1978). Large creep events on the Imperial fault, California, *Bull. Seism. Soc. Am.* **68**, 517-521.

Gupta, H. K. (2005). Artificial water reservoir-triggered earthquakes with special emphasis at Koyna, *Curr Sci* **88**, 1628-1631.

Gurrola, L. D., and T. K. Rockwell (1996). Timing and slip for prehistoric earthquakes on the Superstition Mountain fault, Imperial Valley, southern California, *J. Geophys. Res.* **101**, 5977-5985.

Harsh, P. W. (1982). Distribution of afterslip along the Imperial fault, in *The Imperial Valley, California Earthquake of October 15, 1979, U.S. Geol. Surv. Profess. Pap. 1254*, 193-203.

Hill, D. P., J. P. Eaton, and L. M. Jones (1990). Seismicity: 1980-1986, in *Wallace, R.E., ed. The San Andreas Fault System, U.S. Geol. Surv. Profess. Pap. 1515*, 114-151.

Johnson, C. E., and D. P. Hill (1982). Seismicity of the Imperial Valley, in *The Imperial Valley, California Earthquake of October 15, 1979, U.S. Geol. Surv. Profess. Pap. 1254*, 15-23.

Johnson, C. E., C. Rojahn, and R. V. Sharp (1982). Introduction, in *The Imperial Valley, California Earthquake of October 15, 1979, U.S. Geol. Surv. Profess. Pap. 1254*, 1-4.

Lienkaemper, J. J., and C. B. Ramsey (2009). OxCal: Versatile Tool for Developing Paleoearthquake Chronologies – A Primer, *Seismol Res Lett* **80**, 431-434.

Luttrell, K., D. Sandwell, B. Smith-Konter, B. Bills, and Y. Bock (2007). Modulation of the earthquake cycle at the southern San Andreas fault by lake loading, *J. Geophys. Res.* **112**, B08411, doi:10.1029/2006JB004752.

McCalpin, J. P., and A. R. Nelson (1996). Introduction to Paleoseismology, in *Paleoseismology*, Academic Press, San Diego, 20.

McCalpin, J. P., T. K. Rockwell, and Ray J. Weldon II (1996). Paleoseismology of Strike-Slip Tectonic Environments, in *Paleoseismology*, Academic Press, San Diego, 271-329.

Meltzner, A. J. (2006). Characterization of the long-term behavior of the Imperial and Brawley faults, Imperial Valley, California, M. S. Thesis, San Diego State University, San Diego, CA, 40 pp.

Meltzner, A. J., T. K. Rockwell, L. A. Owen (2006). Recent and Long-Term Behavior of the Brawley Fault Zone, Imperial Valley, California: An Escalation in Slip Rate?, *Bull. Seism. Soc. Am.* **96**, 2304-2328.

Meltzner, A. J., and T. K. Rockwell (2011 in review). Unpublished data as of this moment but their paper will be published by the end of 2011.

Merriam, R., and O. L. Bandy (1965). *Source of upper Cenozoic sediments in Colorado delta region, J. Sediment. Petrol.* **35**, 911-916.

Modesto, R. and G. Mount (1980). *Not for Innocent Ears: Spiritual Traditions of a Desert Cahuilla Medicine Woman*, Sweetlight Books, Arcata, CA, 120 pp.

Muffler, L. J. P., and Doe, B. R. (1968). Composition and mean age of detritus of the Colorado River delta in the Salton Trough, southeastern California, *J. Sediment. Petrol.* **38**, 384-399.

Obermeier, S. F. (1996). Using Liquefaction-Induced Features for Paleoseismic Analysis, in *Paleoseismology*, Academic Press, San Diego, 331-396.

Philibosian, B., T. Fumal, and R. Weldon (2011). San Andreas Fault Chronology and Lake Cahuilla History at Coachella, Californi, *Bull. Seism. Soc. Am.* **101**, 13-38.

Reimer, P. J., M. G. L. Baillie, E. Bard, A. Bayliss, J. W. Beck, P. G. Blackwell, C. Bronk Ramsey, C. E. Buck, G. S. Burr, R. L. Edwards, M. Friedrich, P. M. Grootes, T. P. Guilderson, I. Hajdas, T. J. Heaton, A. G. Hogg, K. A. Hughen, K. F. Kaiser, B. Kromer, F. G. McCormac, S. W. Manning, R. W. Reimer, D. A. Richards, J. R. Southon, S. Talamo, C. S. M. Turney, J. van der Plicht, and C. E. Weyhenmeyer (2009). IntCal09 and Marine09 radiocarbon age calibration curves, 0-50,000 years cal BP, *Radiocarbon* **51**, 1111-1150.

Rymer, M.J., V.E. Langenheim, and E. Hauksson (2002). The Hector Mine, California, earthquake of 16 October 1999: Introduction to the special issue, *Bull. Seism. Soc. Am.* **92**, 1147-1153.

Richter, C. F. (1958). Elementary seismology: San Francisco. W. H. Freeman, 768.

Rockwell, T. K., and Sieh (1994). Correlation of large earthquakes using regional lacustrine stratigraphy, examples from the Salton Trough, California, *Geol. Soc. Am. Abstr. Programs* **26**, A-239.

Scharer, K. M., R. J. Weldon II, T. E. Fumal, and G. P. Biasi (2007). Paleoearthquakes on the Southern San Andreas Fault, Wrightwood, California, 3000 to 1500 B.C.: A New Method for Evaluating Paleoseismic Evidence and Earthquake Horizons, *Bull. Seism. Soc. Am.* **97**, 1054-1093.

Sharp, R. V. (1980). 1940 and Prehistoric earthquake displacements on the Imperial fault, Imperial and Mexicali Valleys, California and Mexico, in *California Seismic Safety Commission Symposium Proceedings, The Human Settlements on the San Andreas Fault,* Calif. Seismic Safety Comm., Sacramento, 68-81.

Sharp, R. V. (1982a). Tectonic setting of the Imperial Valley region, in *The Imperial Valley, California Earthquake of October 15, 1979, U.S. Geol. Surv. Profess. Pap. 1254*, 5-14.

Sharp, R. V. (1982b). Comparison of 1979 surface faulting with earlier displacements in the Imperial Valley, in *The Imperial Valley, California Earthquake of October 15, 1979, U.S. Geol. Surv. Profess. Pap. 1254*, 213-221.

Sieh, K. E. (1982). Slip along the San Andreas Fault associated with the earthquake,in *The Imperial Valley, California Earthquake of October 15, 1979, U.S. Geol. Surv. Profess. Pap. 1254*, 155-159.

Sieh, K. E. (1986). Slip rate across the San Andreas and prehistoric earthquakes at Indio, California, *EOS Trans. AGU* **67**, 1200.

Sieh, K. (1996). The repetition of large-earthquake ruptures, *Proc. Natl. Acad. Sci. USA* **93**, 3764-3771.

Sieh, K. E., and P. L. Williams (1990). Behavior of the southernmost San Andreas fault during the past 300 years, *J. Geophys. Res.* **95**, 6629-6645.

Simpson, D. W., W. S. Leith, and C. H. Scholz (1988). Two Types of Reservoir-Induced Seismicity, *Bull. Seism. Soc. Am.* **78**, 2025-2040.

Stanley, G. M. (1963). Prehistoric lakes in the Salton Sea Basin, *Spec. Pap. Geol. Soc. Am.* **73**, 249-250.

Stanley, G. M. (1966). Deformation of Pleistocene Lake Cahuilla shoreline, Salton Basin, California, *Spec. Pap. Geol. Soc. Am.* **87**, 165 pp.

Stuiver, M. and H. A. Polach (1977). Discussion: reporting of C-14 data, *Radiocarbon* **19**, 355-363.

Tarbet, L. A. (1951). Imperial Valley, California, [sec. 13], in *Possible future petroleum provinces of North America*, *Am. Assoc. Petrol. Geol. Bull.* **35**, 260-263.

Thomas, A. P., and T. K. Rockwell (1996). A 300- to 550-year history of sip on the Imperial fault near the U.S.- Mexico border: Missing slip at the Imperial fault bottleneck, *Journal of Geophysical Research* **101**, 5987-5997.

Thomas, R. G. (1963). The late Pleistocene 150-foot fresh water beachline of the Salton Sea area, *S. Calif. Acad. Sci. Bull.* **62**, 9-17.

Toppozada, T. R., D. L. Parke, and C. T. Higgins (1978). Seismicity of California 1900-1931, *California Division of Mines and Geology Special Report 135*, 39.

Townley, S. D., and M. W. Allen (1939). Descriptive catalog of earthquakes of the Pacific coast of the United States, 1769 to 1928, *Bull. Seism. Soc. Am.* **29**, 1-297.

Van de Kamp, P. C. (1973). Holocene continental sedimentation in the Salton Basin, California: a reconnaissance, *Geol. Soc. Am. Bull.* **84**, 827-848.

Waters, M. R. (1983). Late Holocene lacustrine stratigraphy and archaeology of ancient Lake Cahuilla, California, *Quat. Res.* **19**, 373-387.

Table 1: Rating Scheme of Paleoseismic Indicators

Event ID	Stratigra-phic location	Horizon color	Trench	Type of event indicator	Rating of indicator (R)	No. of exposures with indicator present (E_o)	No. of exposures where indicators should be present theoretically (E_t)	Frequency (F) E_o/E_t	R*F	Average R*F for the event	Comments
1*	n/a	n/a	T1-NW	RS	4	9	9	1.00	4.00		rupture to ground surface
1*	n/a	n/a	T3A-NW	RS	4	9	9	1.00	4.00		rupture to ground surface
1*	n/a	n/a	T3A-SE	RS	4	9	9	1.00	4.00		rupture to ground surface
1*	n/a	n/a	T3B-NW	RS	4	9	9	1.00	4.00		rupture to ground surface
1*	n/a	n/a	T4-NW	RS	4	9	9	1.00	4.00	**4.00**	rupture to ground surface
1*	n/a	n/a	T4-SE	RS	4	9	9	1.00	4.00		rupture to ground surface
1*	n/a	n/a	T9A-SE	RS	4	9	9	1.00	4.00		rupture capped by thin layer of spoil or fill
1*	n/a	n/a	T9B-SE	RS	4	9	9	1.00	4.00		rupture capped by thin layer of spoil or fill
1*	n/a	n/a	T9C-SE	RS	4	9	9	1.00	4.00		rupture capped by thin layer of spoil or fill
1*	n/a	n/a	n/a	DC	n/a	n/a	n/a	n/a	n/a		60-cm deflection of modern rill, coseismic and after-slip for Events 1&2
2*	LF	dark pink	T4-NW	FF	4	3	9	0.33	1.33		fissure associated with 8 splays of fault terminating upward
2*	LF	dark pink	T9B-SE	FF	4	3	9	0.33	1.33		fissure associated with 8 splays of fault terminating upward
2*	LF	dark pink	T9C-SE	FF	4	3	9	0.33	1.33		fissure associated with 10 splays of fault terminating upward
2*	LF	dark pink	T4-NW	UT	4	3	9	0.33	1.33	**1.33**	fissure associated with 8 splays of fault terminating upward
2*	LF	dark pink	T9B-SE	UT	4	3	9	0.33	1.33		fissure associated with 8 splays of fault terminating upward
2*	LF	dark pink	T9C-SE	UT	4	3	9	0.33	1.33		fissure associated with 10 splays of fault terminating upward
2*	LF	dark pink	n/a	DC	4	n/a	n/a	n/a	n/a		60-cm deflection of modern rill, coseismic and after-slip for Events 1&2
3	base of 200	teal	T4-NW	FF	4	3	9	0.33	1.33		fissure associated with 4 splays of fault terminating upward
3	base of 200	teal	T4-SE	FF	4	3	9	0.33	1.33		fissure associated with 12 splays of fault terminating upward
3	base of 200	teal	T9B-SE	FF	4	3	9	0.33	1.33		fissure associated with 7 splays of fault terminating upward
3	base of 200	teal	T4-NW	UT	4	3	9	0.33	1.33	**1.33**	fissure associated with 4 splays of fault terminating upward
3	base of 200	teal	T4-SE	UT	4	3	9	0.33	1.33		fissure associated with 12 splays of fault terminating upward
3	base of 200	teal	T9B-SE	UT	4	3	9	0.33	1.33		fissure associated with 7 splays of fault terminating upward
3	base of 201	teal	T2,T5A,B &C	OC	4	n/a	n/a	n/a	n/a		beheaded channel measured to be 1.4 m from feeder channel
4	top of 300	purple	T9B-SE	CW	4	1	9	0.11	0.44		
4	top of 300	purple	T4-SE	FF	4	2	9	0.22	0.89		fissure associated with only 1 fault terminating upward
4	top of 300	purple	T9B-SE	Sc	4	1	9	0.11	0.44		
4	top of 300	purple	T4-SE	UT	4	3	9	0.33	1.33	**0.70**	single splay but associated with fissure fill
4	top of 300	purple	T9C-SE	FF	2	2	9	0.22	0.44		FF below composite horizon of Events 4, 5 & 6

Table 1: Rating Scheme of Paleoseismic Indicators

Event ID	Stratigra-phic location	Horizon color	Trench	Type of event indicator	Rating of indicator (R)	No. of exposures with indicator present (E_o)	No. of exposures where indicators should be present theoretically (E_t)	Frequency (F) E_o/E_t	R*F	Average R*F for the event	Comments
4	top of 300	purple	T9C-SE	UT	2	3	9	0.33	0.67		UT at composite horizon of Events 4, 5 & 6
4	top of 300	purple	T9B-SE	UT	2	3	9	0.33	0.67		UT at composite horizon of Events 4, 5 & 6
5 and 6	bottom of 305	yellow	T4-SE	AU	4	3	9	0.33	1.33		
	top of 333	yellow	T9B-SE	AU	4	3	9	0.33	1.33		
5 and 6	bottom of 305	yellow	T9C-SE	AU	4	3	9	0.33	1.33		
	top of 333	yellow	T4-SE	FF	4	4	9	0.44	1.78		
5 and 6	bottom of 305	yellow	T4-NW	FF	4	4	9	0.44	1.78		
	top of 333	yellow	T9B-SE	FF	4	4	9	0.44	1.78		
5 and 6	bottom of 305	yellow	T9C-SE	FF	4	4	9	0.44	1.78		
	top of 333	yellow	T4-NW	UT	4	5	9	0.56	2.22	**1.68**	associated with fissure fill
5 and 6	bottom of 305	yellow	T4-SE	UT	4	5	9	0.56	2.22		associated with fissure fill
	top of 333	yellow	T9A-SE	UT	4	5	9	0.56	2.22		associated with fissure fill
5 and 6	bottom of 305	yellow	T9B-SE	UT	4	5	9	0.56	2.22		associated with fissure fill
	top of 333	yellow	T9C-SE	UT	4	5	9	0.56	2.22		associated with fissure fill
5 and 6	bottom of 305	yellow	T9B-SE	LP	3	2	9	0.22	0.67		4 pipes just terminate below the horizon
	top of 333	yellow	T9C-SE	LP	3	2	9	0.22	0.67		4 pipes just terminate below the horizon
5 and 6	bottom of 305	yellow	T2,T5A,B &C	OC	n/a	n/a	n/a	n/a	n/a		1.4 and 1.5 slip for E5 & E6 respectively, beheaded buried channels
	top of 333	yellow									
7	top of 360	blue	T3A-SE	AU	4	4	7	0.57	2.29		
7	top of 360	blue	T9A-SE	AU	4	4	7	0.57	2.29		
7	top of 360	blue	T9B-SE	AU	4	4	7	0.57	2.29		
7	top of 360	blue	T9C-SE	AU	4	4	7	0.57	2.29		
7	top of 360	blue	T3A-SE	FF	4	3	7	0.43	1.71		associated with abundant fault splays
7	top of 360	blue	T9B-SE	FF	4	3	7	0.43	1.71	**2.03**	associated with dense network of fault splays
7	top of 360	blue	T9C-SE	FF	4	3	7	0.43	1.71		associated with dense network of fault splays
7	top of 360	blue	T3A-SE	UT	4	4	7	0.57	2.29		dense network of splays associated with fissure fill
7	top of 360	blue	T9B-SE	UT	4	4	7	0.57	2.29		dense network of splays associated with fissure fill
7	top of 360	blue	T9C-SE	UT	4	4	7	0.57	2.29		a few splays associated with fissure fill

Table 1: Rating Scheme of Paleoseismic Indicators

Event ID	Stratigra-phic location	Horizon color	Trench	Type of event indicator	Rating of indicator (R)	No. of exposures with indicator present (E_o)	No. of exposures where indicators should be present theoretically (E_t)	Frequency (F) E_o/E_t	R*F	Average R*F for the event	Comments
7	top of 360	blue	T9A-SE	UT	2	4	7	0.57	1.14		fissure fill not observed with fault splays
8	top of 400	magenta	T3A-SE	AU	4	1	10	0.10	0.40		
8	top of 400	magenta	T9B-SE	Db	4	1	10	0.10	0.40		scarp-derived debris flow
8	top of 400	magenta	T3A-SE	FF	4	1	10	0.10	0.40		associated with a few fault splays
8	top of 400	magenta	T3B-NW	SB	4	6	10	0.60	2.40		
8	top of 400	magenta	T4Deep-NW-A	SB	4	6	10	0.60	2.40		
8	top of 400	magenta	T4Deep-NW-B	SB	4	6	10	0.60	2.40		
8	top of 400	magenta	T4Deep-NW-C	SB	4	6	10	0.60	2.40		
8	top of 400	magenta	T4Deep-SE-A	SB	4	6	10	0.60	2.40		
8	top of 400	magenta	T4Deep-SE-B	SB	4	6	10	0.60	2.40		
8	top of 400	magenta	T3A-SE	UT	4	6	10	0.60	2.40	**1.62**	associated with fissure fill
8	top of 400	magenta	T4Deep-NW-A	UT	2	4	10	0.40	0.80		single fault; massive sand might have obscured any vertical separation caused by fault, if any
8	top of 400	magenta	T4Deep-NW-B	UT	2	4	10	0.40	0.80		single fault; massive sand might have obscured any vertical separation caused by fault, if any
8	top of 400	magenta	T4Deep-NW-C	UT	2	4	10	0.40	0.80		single fault; massive sand might have obscured any vertical separation caused by fault, if any
8	top of 400	magenta	T4Deep-SE-B	UT	2	4	10	0.40	0.80		single fault; massive sand might have obscured any vertical separation caused by fault, if any
8	top of 400	magenta	T4Deep-NW-A	LP	4	5	10	0.50	2.00		dense network of LP connected to paleosurface
8	top of 400	magenta	T4Deep-NW-B	LP	4	5	10	0.50	2.00		dense network of LP connected to paleosurface
8	top of 400	magenta	T4Deep-NW-C	LP	4	5	10	0.50	2.00		dense network of LP connected to paleosurface
8	top of 400	magenta	T4Deep-SE-A	LP	4	5	10	0.50	2.00		dense network of LP connected to paleosurface
8	top of 400	magenta	T4Deep-SE-B	LP	3	5	10	0.50	1.50		dense network of LP, but not connected to paleosurface
8.5	base of 410	brown	T4Deep-SE-B	UT	2	1	8	0.13	0.25		Only 1 fault terminates exactly at the horizon, 2 other faults terminate lower, but offset is obvious
8.5	base of 410	brown	T4Deep-SE-B	UT	2	1	8	0.13	0.25	**0.21**	LP obscuring stratigraphy and trace of fault
8.5	base of 410	brown	T4Deep-SE-A	DG	1	1	8	0.13	0.13		DG generally is not an unambiguous indicator for a single seismic event
8.7	base of 424	dark green	T4Deep-NW-A	UT	2	2	8	0.25	0.50		Clear UT but only on single fault
8.7	base of 424	dark green	T4Deep-NW-B	UT	1	2	8	0.25	0.25	**0.38**	single fault UT and strata above are not well bedded enough to see any possible offset

Table 1: Rating Scheme of Paleoseismic Indicators

Event ID	Stratigra-phic location	Horizon color	Trench	Type of event indicator	Rating of indicator (R)	No. of exposures with indicator present (E_o)	No. of exposures where indicators should be present theoretically (E_t)	Frequency (F) E_o/E_t	R*F	Average R*F for the event	Comments
9	base of 430	yellow-green	T4Deep-SE-A	SB	2	2	9	0.22	0.44		uncertain whether it is a SB because of clayey content
9	base of 430	yellow-green	T4Deep-SE-B	SB	2	2	9	0.22	0.44		uncertain whether it is a SB because of clayey content
9	base of 430	yellow-green	T4Deep-SE-B	UT	2	1	9	0.11	0.22	**0.49**	just one single fault, but offset and UT are obvious
9	base of 430	yellow-green	T4Deep-NW-A	LP	3	2	9	0.22	0.67		several LP broke up clay beds into blocks; highly possible that they terminate at the event horizon
9	base of 430	yellow-green	T4Deep-NW-B	LP	3	2	9	0.22	0.67		several LP broke up clay beds into blocks; highly possible that they terminate at the event horizon
10	base of 480	cyan	T4Deep-NW-A	SB	2	5	9	0.56	1.11		CH with E11; isolated clay clasts ripped off from LP vent wall and deposited at the bottom of SB ^
10	base of 480	cyan	T4Deep-NW-B	SB	2	5	9	0.56	1.11		CH with E11; isolated clay clasts ripped off from LP vent wall and deposited at the bottom of SB ^
10	base of 480	cyan	T4Deep-NW-C	SB	2	5	9	0.56	1.11		isolated clay clasts ripped off from LP vent wall and deposited at the bottom of SB ^
10	base of 480	cyan	T4Deep-SE-A	SB	2	5	9	0.56	1.11		absence of isolated clay clasts
10	base of 480	cyan	T4Deep-SE-B	SB	2	5	9	0.56	1.11	**0.78**	absence of isolated clay clasts
10	base of 480	cyan	T3A-NW	Sc	2	1	9	0.11	0.22		scarp for CH ^
10	base of 480	cyan	T1-NW	UT	1.5	2	9	0.22	0.33		CH with E11; UT of 4 fault splays but units older than Unit 500 are not well correlated ^
10	base of 480	cyan	T3A-NW	UT	0.5	2	9	0.22	0.11		CH with E11; only 1 single fault was terminated, and it was not exactly at the horizon ^
11	top of 500b/500	apple green	T4Deep-SE-A	Db	4	2	9	0.22	0.89		
11	top of 500b/500	apple green	T4Deep-SE-B	Db	4	2	9	0.22	0.89		
11	top of 500b/500	apple green	T4Deep-NW-A	SB	2	3	9	0.33	0.67		CH with E10; isolated clay clasts ripped off from LP vent wall and deposited at the bottom of SB ^
11	top of 500b/500	apple green	T4Deep-NW-B	SB	2	3	9	0.33	0.67		CH with E10; isolated clay clasts ripped off from LP vent wall and deposited at the bottom of SB ^
11	top of 500b/500	apple green	T4Deep-NW-C	SB	2	3	9	0.33	0.67		CH with E10; isolated clay clasts ripped off from LP vent wall and deposited at the bottom of SB ^
11	top of 500b/500	apple green	T4Deep-SE-A	Sc	4	3	9	0.33	1.33	**0.76**	
11	top of 500b/500	apple green	T4Deep-SE-B	Sc	4	3	9	0.33	1.33		
11	top of 500b/500	apple green	T3A-NW	Sc	2	3	9	0.33	0.67		CH with E10 ^
11	top of 500b/500	apple green	T1-NW	UT	1.5	2	9	0.22	0.33		CH with E10; UT of 4 fault splays but units older than Unit 500 are not well correlated ^
11	top of 500b/500	apple green	T3A-NW	UT	0.5	2	9	0.22	0.11		CH with E10; only 1 single fault was terminated, and it was not exactly at the horizon ^
12	top of 505-550	orange	T3B-NW	AU	4	1	8	0.13	0.50		

Table 1: Rating Scheme of Paleoseismic Indicators

Event ID	Stratigra-phic location	Horizon color	Trench	Type of event indicator	Rating of indicator (R)	No. of exposures with indicator present (E_o)	No. of exposures where indicators should be present theoretically (E_t)	Frequency (F) E_o/E_t	R*F	Average R*F for the event	Comments
12	top of 505-550	orange	T3B-NW	FF	4	1	8	0.13	0.50		
12	top of 505-550	orange	T4Deep-NW-A	SB	4	5	8	0.63	2.50		SB with vent
12	top of 505-550	orange	T4Deep-NW-B	SB	4	5	8	0.63	2.50		SB with vent
12	top of 505-550	orange	T4Deep-NW-C	SB	4	5	8	0.63	2.50	**1.20**	SB with vent
12	top of 505-550	orange	T4Deep-SE-A	SB	2	5	8	0.63	1.25		likely to be the same SB as the one exposed in T4Deep-NW, but uncertainty remains
12	top of 505-550	orange	T4Deep-SE-B	SB	2	5	8	0.63	1.25		likely to be the same SB as the one exposed in T4Deep-NW, but uncertainty remains
12	top of 505-550	orange	T4Deep-NW-C	Sc?	2	1	8	0.13	0.25		
12	top of 505-550	orange	T3B-NW	UT	2	2	8	0.25	0.50		only 4 splays of fault with 1 terminating exactly at the horizon
12	top of 505-550	orange	T4Deep-SE-B	UT	1	2	8	0.25	0.25		only 2 splays of fault, away from main fault zone
13	top of 580	dark blue	T4Deep-NW-C	AU	4	1	2	0.50	2.00		
13	top of 580	dark blue	T4Deep-NW-C	SB	4	1	2	0.50	2.00	**1.50**	SB with vent
13	top of 580	dark blue	T4Deep-NW-C	UT	1	1	2	0.50	0.50		only a single splay
14	top of 600	light pink	T1-NW	AU	4	1	1	1.00	4.00		Unambiguous angular unconformity
14	top of 600	light pink	T1-NW	LP	4	1	1	1.00	4.00	**4.00**	LP with vent connect to paleosurface
15	top of 700	buff	T1-NW	UT	2	1	1	1.00	2.00	**2.00**	difficult to trace faults above event horizon (if any) upward into overlying massive clay

Events 1* and 2* are the 1979 and 1940 historical earthquakes respectively.

For upward termination of faults (UT), a network of fault splays is considered as one observation rather than the individual splay. They are considered as two separate observations if they are far apart substantially in the same exposure. Rating of UT depends on the density of fault splays, whether they are associated with any fissure fill, and whether they all terminate at the same stratigraphic level. Rating of liquefaction pipes (LP) shares a similar set of criteria.

^For Events 10 and 11, the same indicators for the composite horizon of Events 10/11 are tabulated twice to account for both events. However, the rating of each observation is reduced by half to account for the ambiguity of horizon designation to these indicators.

AU = Angular Unconformity
CH = Composite Horizon
CW = Colluvial Wedge
Db = Scarp-derived Debris

DC = Deflected Channels
DG = Downward Growth of displacement
FF = Fissure Fill
LF = Localized Flood deposits

LP = Liquefaction Pipes
OC = Offset Channels
RS = Rupture to Surface
SB = Sand Blow

Sc = Scarp
UT = Upward Termination of faults

Table 2. Radiocarbon Dates from Dogwood Site

Sample (1)	Stratigraphic Unit (2)	Uncalibrated ^{14}C Age, Years B.P. (4)	Calibrated Calendric 2σ Max-Min Date Range (5)	% (6)
IFD-T2-C61	205	130 ± 15	AD 1681 - 1939	95.3
IFD-T5-C78	271-279	3095 ± 15	1419 - 1315 BC	95.4
IFD-T2-C67	306	320 ± 15	AD 1496 - 1643	95.4
IFD-T2-C30	310-314	795 ± 50	AD 1057 - 1289	95.4
IFD-T2-C25	310-314	670 ± 15	AD 1280 - 1385	95.4
IFD-T2-C24	310-314	670 ± 15	AD 1280 - 1385	95.4
IFD-T2-C23	310-314	655 ± 15	AD 1285 - 1388	95.4
IFD-T5-C72	315-319	825 ± 15	AD 1180 - 1260	95.4
IFD-T5-C73	315-319	630 ± 15	AD 1293 - 1393	95.4
IFD-T5-C75	315-319	605 ± 15	AD 1301 - 1401	95.4
IFD-T5-C86	315-319	615 ± 25	AD 1295 - 1400	95.4
IFD-T5-C87	315-319	680 ± 15	AD 1277 - 1383	95.4
IFD-T5-C68	333	650 ± 15	AD 1286 - 1390	95.4
IFD-T2-C21	336	640 ± 15	AD 1289 - 1391	95.4
IFD-T2-C36	342	380 ± 15	AD 1449 - 1618	95.4
IFD-T2-C37	342	2265 ± 15	394 - 233 BC	95.4
IFD-T2-C44	342/344	655 ± 15	AD 1285 - 1388	95.4
IFD-T2-C20	342/344	630 ± 15	AD 1293 - 1393	95.4
IFD-T2-C49	346	655 ± 15	AD 1285 - 1388	95.4
IFD-T5-C79	348-358	630 ± 15	AD 1293 - 1393	95.4
IFD-T5-C80	348-358	615 ± 15	AD 1297 - 1398	95.4
IFD-T5-C84	348-358	625 ± 15	AD 1294 - 1394	95.4
IFD-T2-C14	349-358	1125 ± 15	AD 888 - 973	95.4
IFD-T2-C11	349-358	610 ± 15	AD 1298 - 1400	95.4
IFD-T2-C45	354/356	625 ± 15	AD 1294 - 1394	95.4
IFD-T2-C47	356	605 ± 15	AD 1301 - 1401	95.4
*IFD-C-320	361	640 ± 30	AD 1283 - 1396	95.4
IFD-T3-C51	366/367	2545 ± 15	796 - 593 BC	95.5
*IFD-C-181	375	1495 ± 30	AD 443 - 643	95.4
*IFD-C-180	375	660 ± 25	AD 1279 - 1391	95.4
IFD-T3-C50	380	2715 ± 25	909 - 812 BC	95.4
IFD-T3-C42	390	1515 ± 15	AD 469 - 603	95.4
*IFD-C-140	390	1010 ± 20	AD 986 - 1040	95.4
^IFD-T3-S1	390	1665 ± 15	AD 342 - 422	95.4
IFD-T3-C41	400	1180 ± 15	AD 778 - 892	95.4
IFD-T3-C40	400	2570 ± 15	800 - 675 BC	95.4
*IFD-C-330	400	2860 ± 25	1122 - 935 BC	95.4
*IFD-C-350	410	2980 ± 25	1306 - 1126 BC	95.4
*IFD-C-368	410	2540 ± 15	795 - 568 BC	95.3
*IFD-C-336	410	2200 ± 50	391 - 116 BC	95.4
*IFD-C-345	425	2655 ± 15	830 - 798 BC	95.4
*IFD-C-374	425	3005 ± 20	1374 - 1132 BC	95.4
*IFD-C-338	425	3020 ± 35	1392 - 1131 BC	95.5

Table 2. Radiocarbon Dates from Dogwood Site

Sample (1)	Stratigraphic Unit (2)	Uncalibrated ^{14}C Age, Years B.P. (4)	Calibrated Calendric 2σ Max-Min Date Range (5)	% (6)
*IFD-C-412	427a	845 ± 15	AD 1161 - 1252	95.4
*IFD-C409b	427a	1175 ± 15	AD 777 - 933	95.4
IFD-T3-C66	480/500	1200 ± 15	AD 777 - 882	95.4
*IFD-C-200	500	2275 ± 25	399 - 214 BC	95.4
*IFD-C-362	503	2330 ± 15	406 - 386 BC	95.4
*IFD-C-390	505-550	2190 ± 110	510 BC - AD 54	95.4
*IFD-C-394b	505-550	2115 ± 15	197 - 60 BC	95.4
*IFD-C-398	505-550	2035 ± 15	92 BC - AD 20	95.4
*IFD-C-139	550	2555 ± 20	801 - 593 BC	95.3
*IFD-C-404	550-580	2100 ± 90	372 BC - AD 59	95.4
*IFD-C-406b	550-580	1965 ± 15	75 BC - 1 AD	95.4
*IFD-C-407	550-580	2280 ± 15	399 - 237 BC	95.4
*IFD-C-163	580	2345 ± 20	484 - 382 BC	95.4
*IFD-C-402	580	2550 ± 45	808 - 538 BC	95.4

(1) * These are charcoal samples that were collected in this study from 2010 to 2011, the rest were collected by Meltzner and Rockwell (2011 in review) in 2008.
^ Shell fragments were collected by Meltzner and Rockwell (2011 in review).

(2) Stratigraphic units are numbered such that higher-numbered units are older than lower-numbered units.

(3) All results have been corrected for isotopic fractionation according to the conventions of Stuiver and Polach (1977), with $\delta^{13}C$ values measured on prepared graphite using the AMS spectrometer.

(4) The quoted ^{14}C age is in radiocarbon years using the Libby half life of 5568 years and is following the conventions of Stuiver and Polach (1977).

(5) Calendric dates were obtained through OxCal using the IntCal 09 calibration curve by Reimer et al. (2009).

(6) Probability area under normal distribution curve

Figure 1. Aerial photo showing major structures in southern California, including the San Andreas, Imperial and Cerro Prieto faults, the Brawley Fault Zone and the Brawley Seismic Zone (Meltzner, 2006, modified from Rymer et al, 2002).

Figure 2. Simplified fault map and recent seismicity of the southern part of the Salton Trough, also showing the location of the Dogwood site in this study. Surface ruptures indicated for the 1892 (M 7.25), 1934 (M_L 7.1), 1940 (M_L 7.1), 1968 (M_L 6.4), 1979 (M_L 6.6) and 1987 (M_S 6.2 and 6.6) earthquakes (modified from Thomas and Rockwell, 1996).

Figure 3. Trench location map showing trenches opened in this study (yellow) and those opened by Meltzner and Rockwell, in review (pink) (modified from Meltzner and Rockwell, 2011 in review).

Figure 4. Satellite image showing the trace of Imperial fault and the site location (modified from Meltzner and Rockwell, 2011 in review).

Figure 5. Two logs (T9B-SE and T4Deep-SE) stacked together showing the remarkable stratigraphy and the event horizons that were identified in both exposures.

Figure 6. Generalized stratigraphic column of trench stratigraphy, also showing where each event horizon is located stratigraphically.

Figure 7. Beds dipping in opposite directions to form a synform, exposed in the original trench T2 excavated in 2008 and its extension excavated in 2010.

Figure 8. Cropped image from trench log of T3A-SE, showing the paleoseismic indicators used to identify the event horizon for Event 8, including angular unconformity between Units 390 and 400, fissure fill and fault splays that were truncated at the horizon and capped by Unit 390.

Figure 9. Cropped image from trench log of T9B-SE, showing the paleoseismic indicators used to identify the event horizon for Events 3 and 4 including upward fault truncation, presence of a fissure fill (Event 3) and a colluvial wedge (Event 4).

Figure 10. Cropped image from trench log of T4Deep-NW-C, showing the paleoseismic indicators used to identify the event horizon for Event 13 including upward truncation of a single fault splay, a sand-blow deposit, and an angular unconformity between Units 505-550 and 580 as the strongest line of evidence.

Figure 11. Plot of average R*F values for each possible event (a total of 17). The higher the R*F value an event has, the more likely it occurred. The Events 4, 8.5, 8.7 and 9 appear to be the outliers of low values in this analysis, suggesting a lower likelihood of occurrence or low-slip events. However, the occurrence of Event 4 was assured in the study by Meltzner and Rockwell (2011 in review), therefore, only Events 8.5, 8.7 and 9 seem less likely based on this analysis.

Figure 12. Chronology model of Lake Cahuilla developed by Meltzner and Rockwell (2011 in review).

Figure 13. Earthquake calendar ages obtained from OxCal. The higher the probability density, the better constrained the ages are. The height of a peak does not give any information about the likelihood of a paleoearthquake.

Figure 14. Slip per event and cumulative displacement for the most recent six surface ruptures resolved at the Dogwood Site on the northern Imperial fault by Meltzner and Rockwell in 2008 (2011 in review).

Figure 15. Earthquake chronologies from paleoseismic sites on the southern San Andreas fault and the northern Imperial fault. The possible earthquakes Coa-3 and Coa-6, and the less likely events E8.5, E8.7 and E9 are shown in gray text. Correlations of events at the three paleoseismic sites are highlighted in pink. Sources for chronologies at Indio and Coachella are listed in the text.

Table 1. List of paleoseismic indicators used to identify each event, their ratings (R), the number of trench exposures with the indicators observed (E_o) , the number of exposures where the indicators should be present theoretically (E_t), the frequency (F), the RF value for each indicator and the average RF value for one event.

Table 2. Radiocarbon ages derived from detrital charcoal samples and shell fragments.

Appendix. Detailed descriptions with annotated photographs of evidence for each event.

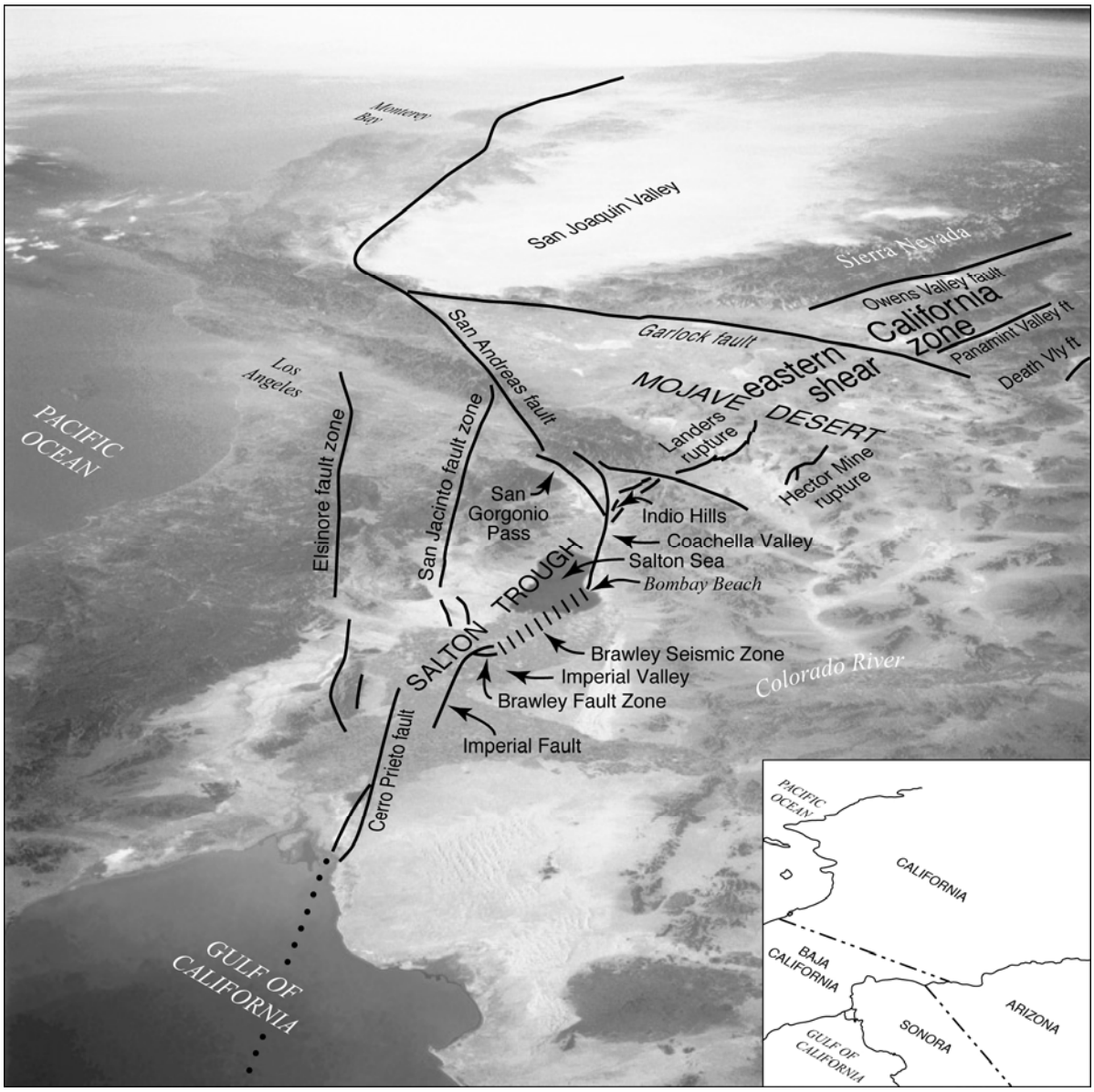
Monterey Bay
San Joaquin Valley
Sierra Nevada
Owens Valley fault
California zone
Panamint Valley ft
Death Vly ft
Garlock fault
San Andreas fault
eastern shear
MOJAVE DESERT
Landers rupture
Hector Mine rupture
Los Angeles
PACIFIC OCEAN
Elsinore fault zone
San Jacinto fault zone
San Gorgonio Pass
Indio Hills
Coachella Valley
Salton Sea
Bombay Beach
SALTON TROUGH
Brawley Seismic Zone
Imperial Valley
Brawley Fault Zone
Imperial Fault
Colorado River
Cerro Prieto fault
GULF OF CALIFORNIA
PACIFIC OCEAN
CALIFORNIA
BAJA CALIFORNIA
ARIZONA
SONORA
GULF OF CALIFORNIA

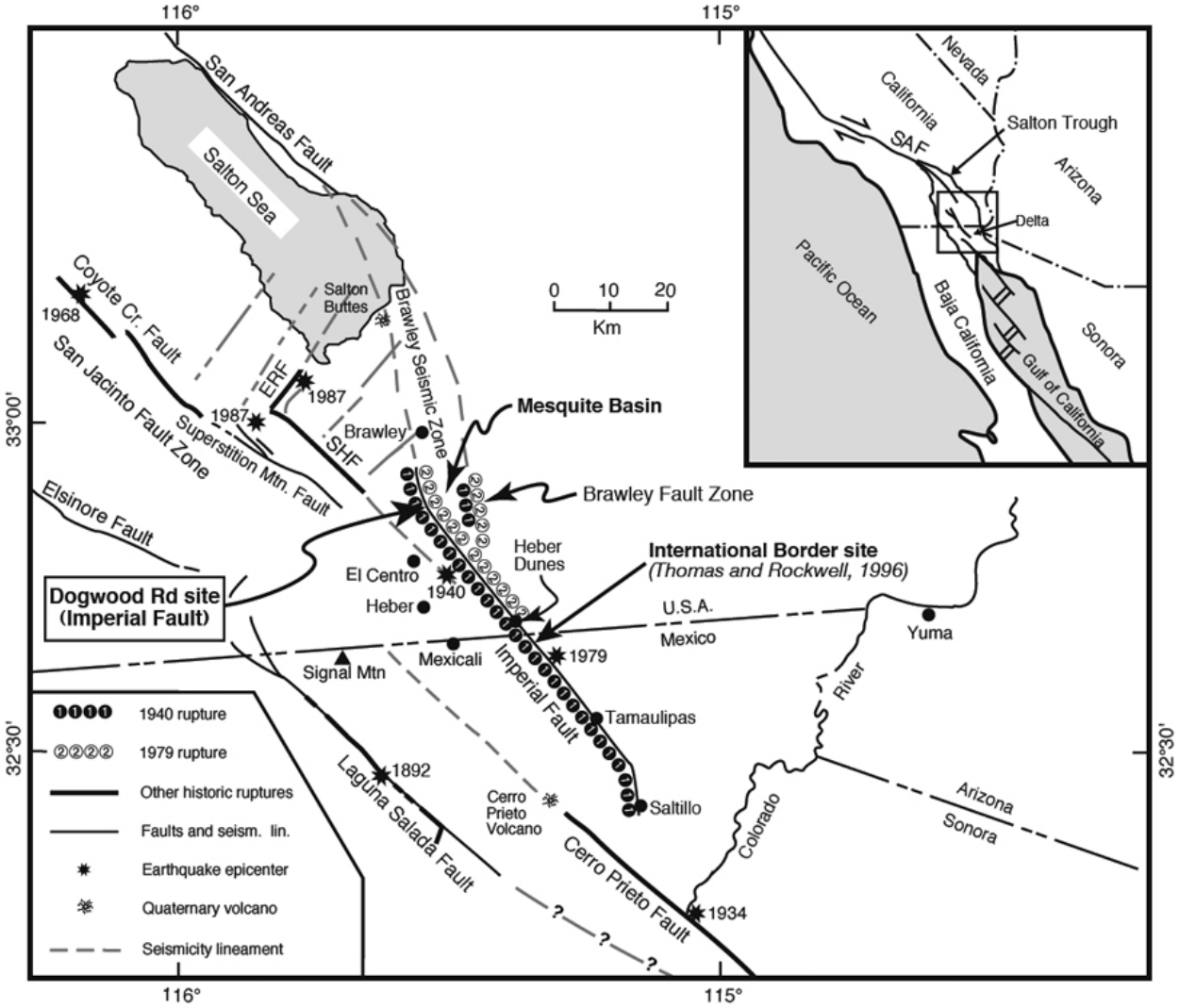
116°
115°
33°00'
32°30'
San Andreas Fault
Salton Sea
Salton Buttes
Coyote Cr. Fault
1968
San Jacinto Fault Zone
1987
1987
ERF
SHF
Superstition Mtn. Fault
Brawley Seismic Zone
Brawley
Mesquite Basin
Brawley Fault Zone
Elsinore Fault
Dogwood Rd site
(Imperial Fault)
El Centro
1940
Heber
Heber Dunes
International Border site
(Thomas and Rockwell, 1996)
U.S.A.
Mexico
Yuma
Mexicali
Signal Mtn
1979
Imperial Fault
Tamaulipas
River
Colorado
Arizona
Sonora
1892
Laguna Salada Fault
Cerro Prieto Volcano
Saltillo
Cerro Prieto Fault
1934
0 10 20
Km
1940 rupture
1979 rupture
Other historic ruptures
Faults and seism. lin.
Earthquake epicenter
Quaternary volcano
Seismicity lineament
Nevada
California
SAF
Salton Trough
Arizona
Delta
Pacific Ocean
Baja California
Gulf of California
Sonora

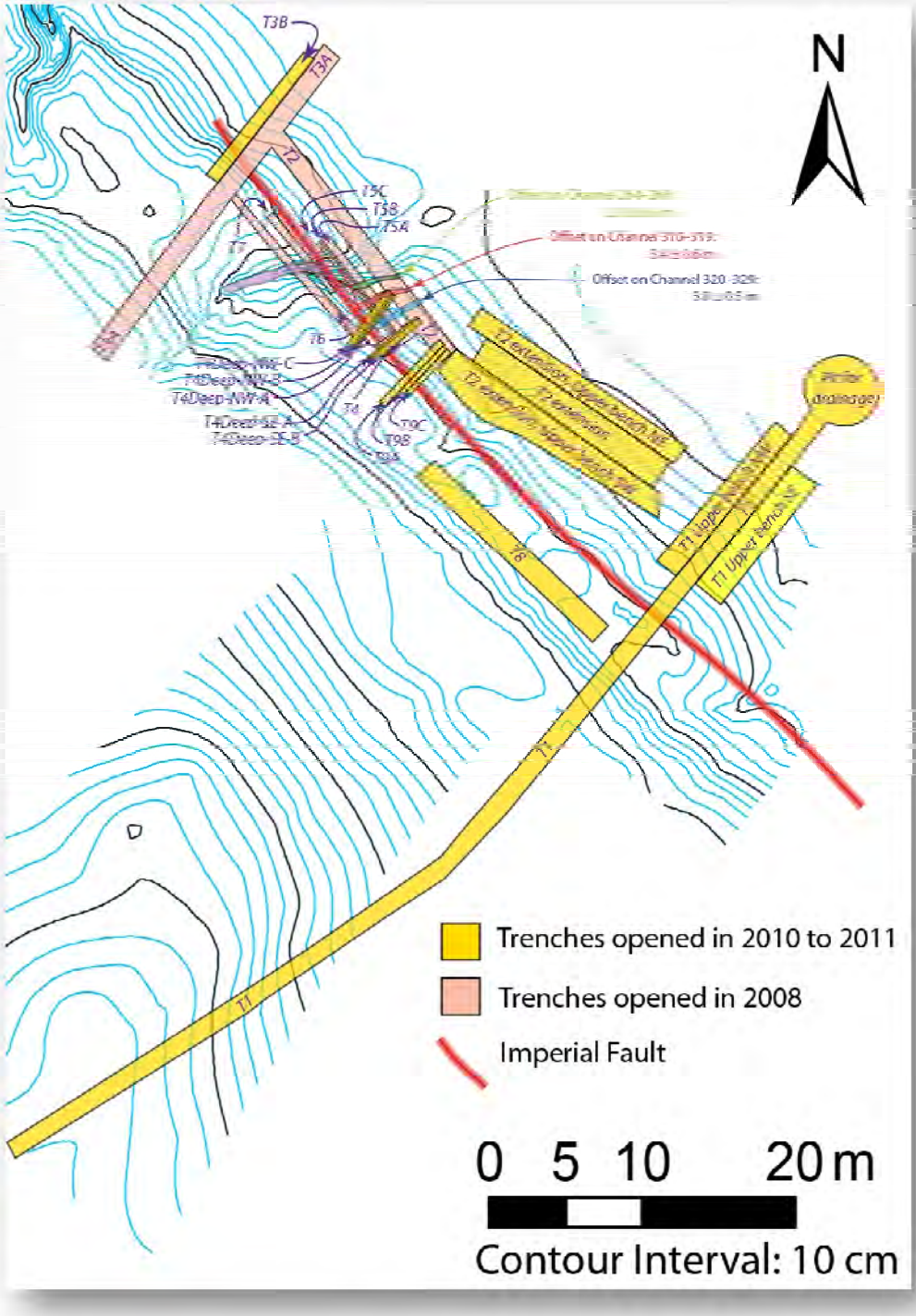
N
T3B
T3A
T2
T5C
T5B
T5A
T7
T6
T4Deep-NW-C
T4Deep-NW-B
T4Deep-NW-A
T4Deep-SE-A
T4Deep-SE-B
T4
T9C
T9B
T9A
T8
T1
Offset on Channel 320-328:
Trenches opened in 2010 to 2011
Trenches opened in 2008
Imperial Fault
0 5 10 20 m
Contour Interval: 10 cm

N
Dogwood Road
0
1 km
1 mi

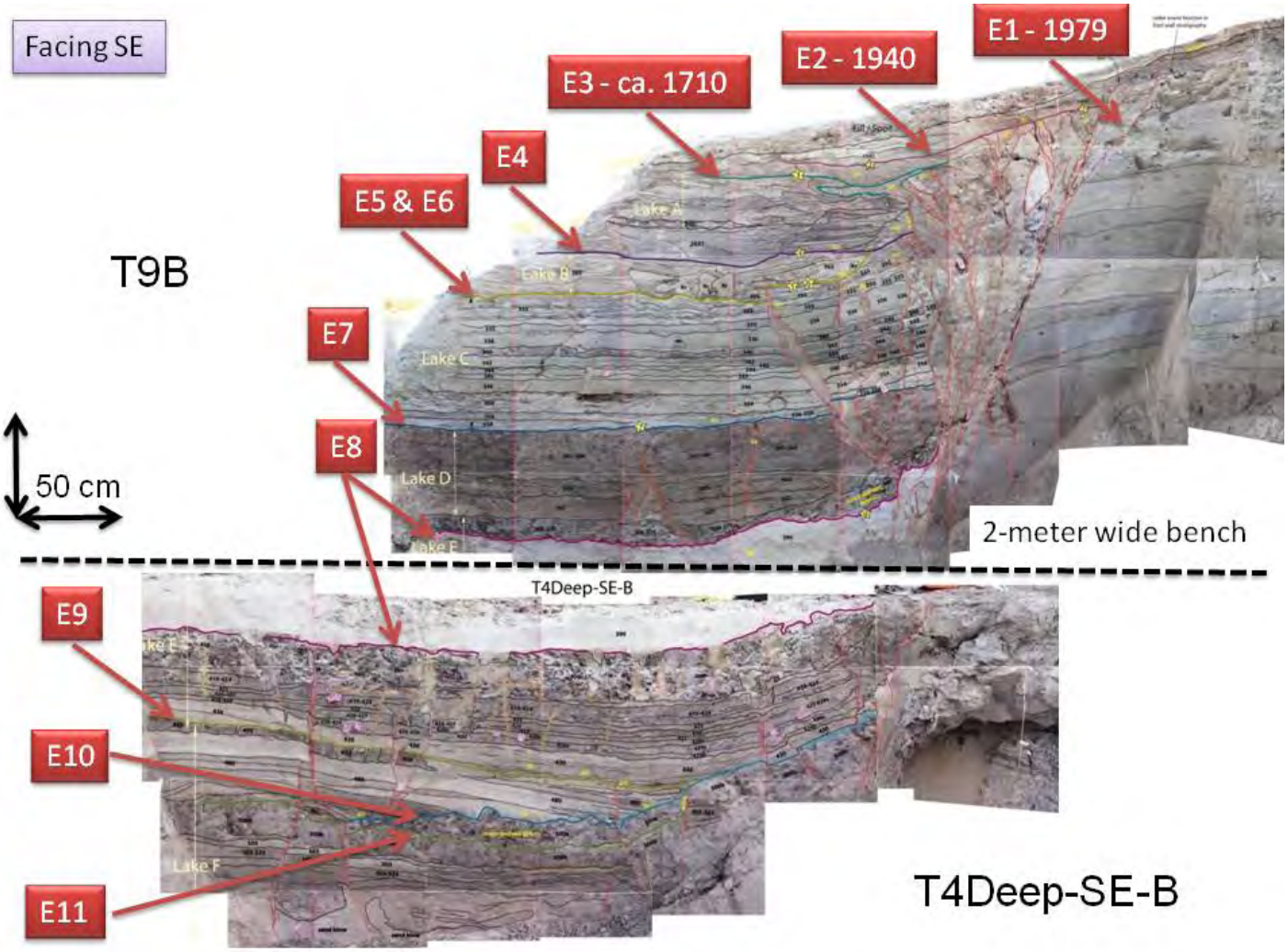
Facing SE
E1 - 1979
E2 - 1940
E3 - ca. 1710
E4
E5 & E6
E7
E8
T9B
Lake A
Lake B
Lake C
Lake D
Lake E
Lake F
50 cm
2-meter wide bench
T4Deep-SE-B
E9
E10
E11
T4Deep-SE-B

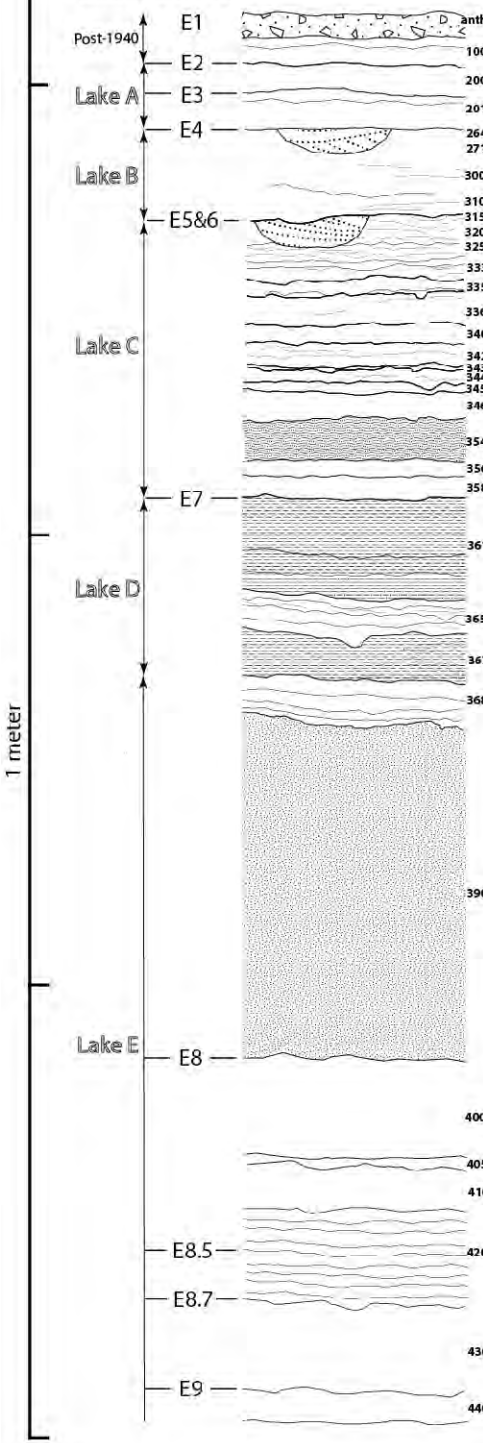

Lake	Event	Units	Lithology	Deposition Environment
Post-1940	E1	anthropogenic fill	massive silty sand with chunks of clay; voids filled with salt crystals from dessication	
	E2	100	bedded light tan clay and silty sand in limited exposures; poorly correlated	localized flood deposits from storms
Lake A	E3	200	massive brown clay and bedded silty sand	lacustrine; last lake highstand in ca 1720
		201-208	predominantly massive brown clay with poorly bedded sandy silt at the base	deltaic to lacustrine
	E4	264-268 271-279	cross-bedded medium sand and laminations of clay and silt	channel incision after lake dessication
Lake B		300-306	laminar brown clay and tan silt	deltaic to lacustrine
	E5&6	310-314 315-319 320-324 325-329	cross-bedded medium sand and laminar clay and silt	channel incision after lake dessication
		333	wavy, parallel contacts between interbedded white-tan silt and bluish gray clay	deltaic to lacustrine; toward the end of lake highstand
		335	silty clay differentiated by color; Unit 336 contains burrows	
		336		
Lake C		340	grayish clay; contains burrows	
		342	laminar silt and clay; ripple marks in Unit 342	deltaic
		343	silty clay	
		344	light gray laminar silt and clay	
		345		
		346-348	silty clay	
		354	wavy, discontinuous laminations of grayish clay and white-tan silt	
		356	silt with planar continuous laminations of clay	deltaic
	E7	358	silt with wavy discontinuous laminations of clay	
Lake D		361-364	5 to 10-cm interbedded clay of different shades of gray	lacustrine
		365	5-cm interbedded gray clay and brownish gray silty clay	deltaic
		367	brownish gray silty clay	deltaic
		368-375	thin beds of clay distinguished by color, interbedded with laminar silty clay	lacustrine
		390	very well-sorted white-tan sand with foreset beds dipping in different directions in in different exposures	sand blow coming out probably from a large but unknown vent
Lake E	E8	400	blocky brown clay with 1-cm lamination of silt; pervasive liquefaction pipes in T4Deep trenches	lacustrine
		405	white-tan clayey silt up to a few cm in limited exposures	
		410	massive grayish clay	lacustrine
	E8.5	420-427a	interbedded brownish silty clay distinguished by silt content and shades of brown; each bed is only up to a few cm thick	deltaic
	E8.7	430	white-tan fine sand with wavy, discontinuous (in fault-perpendicular trenches) or planar, continuous (in fault-parallel trenches) laminations of brownish clay	sand blow
	E9	440?	white-tan fine sand with planar, continuous laminations of clay, only in limited exposures; higher clay content than Unit 430	

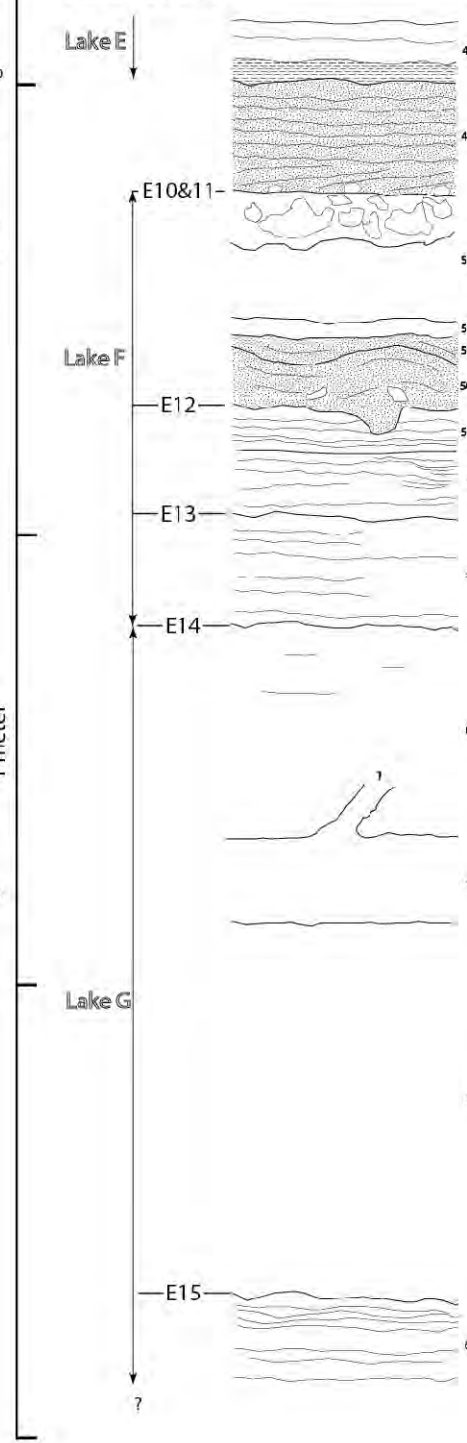

Lake	Event	Units	Lithology	Deposition Environment
Lake E		450-453	laminations of silt and clay near upper contact; thin bed of brown clay at the base; not all exposures have all Units 450-453; package highly penetrated by liquefaction pipes in the scale of mm; units disappear closer to fault in T4Deep trenches	deltaic
	E10&11	480	white-tan fine sand with planar, continuous laminations of clay; laminations gently dipping closer to the base; isolated clasts of clay at the base which have very similar color and texture to Unit 500, likely to be rip-up clasts from sand blow vent	sand blow
		(a)		
		500	brown massive clay; overlain by a scarp-derived clayey debris in T4Deep-SE exposures where unit is split into 500a and 500b but not in other trenches	lacustrine
		(b)		
Lake F		501	massive clay with a deeper shade of brown	lacustrine
		502	lenticular grayish white sand with laminations of clay, could be associated with Unit 503	sand blow
	E12	503	slightly clayey fine sand with fine clay laminations and chunks of clay; sand blow vent is clearly exposed in T4Deep-NW	sand blow
		505-525	interbedded brown clay and white-tan silt; bedding is not clear in T4Deep exposures	deltaic
	E13	550	interbedded and laminated brown clay and white-tan silt; bedding is not clear in T4Deep exposures	deltaic
		580	interbedded clay and silt laterally graded into clay with minimal silty laminations in T2 and T1 trenches; bedding is not clear in T4Deep exposures where correlation is not certain because of limited exposure in deepest part of trench	deltaic
	E14	600	mostly grayish massive, blocky clay with very few thin laminations of clay in different shades of gray and brown; unit is only exposed in T1	lacustrine
		630	white-tan clayey silt and sand; unit has similar texture and color to the pipe at the upper contact; could be a liquefiable unit connected to a liquefaction pipe that penetrates through Unit 600 to the paleosurface which marks the event horizon for E14; only exposed in T1	sill?
Lake G		680	grayish massive clay, very similar with Unit 600 in terms of color and texture; only exposed in T1	lacustrine
	E15	690	laminated silty clay in different shades of brown; only exposed in T1	deltaic

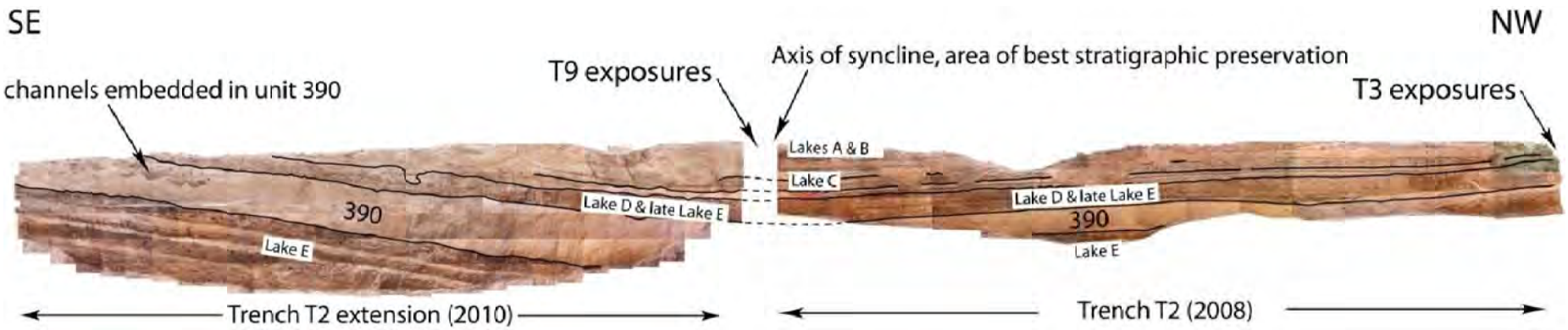
SE
NW
channels embedded in unit 390
T9 exposures
Axis of syncline, area of best stratigraphic preservation
T3 exposures
Lakes A & B
Lake C
Lake D & late Lake E
390
Lake E
Lake D & late Lake E
390
Lake E
Trench T2 extension (2010)
Trench T2 (2008)

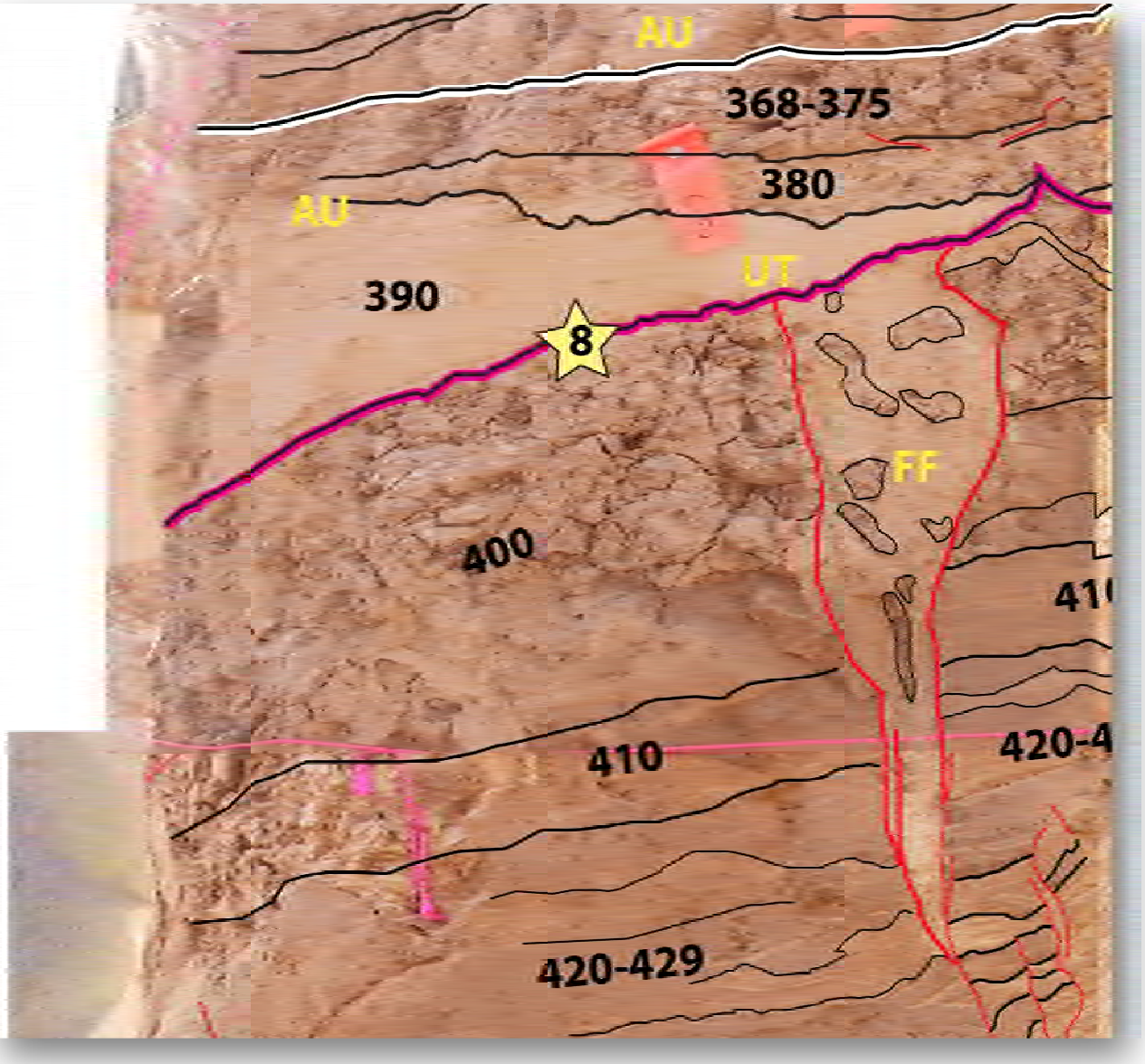
AU
368-375
380
AU
390
UT
8
FF
400
410
420-4
410
420-429

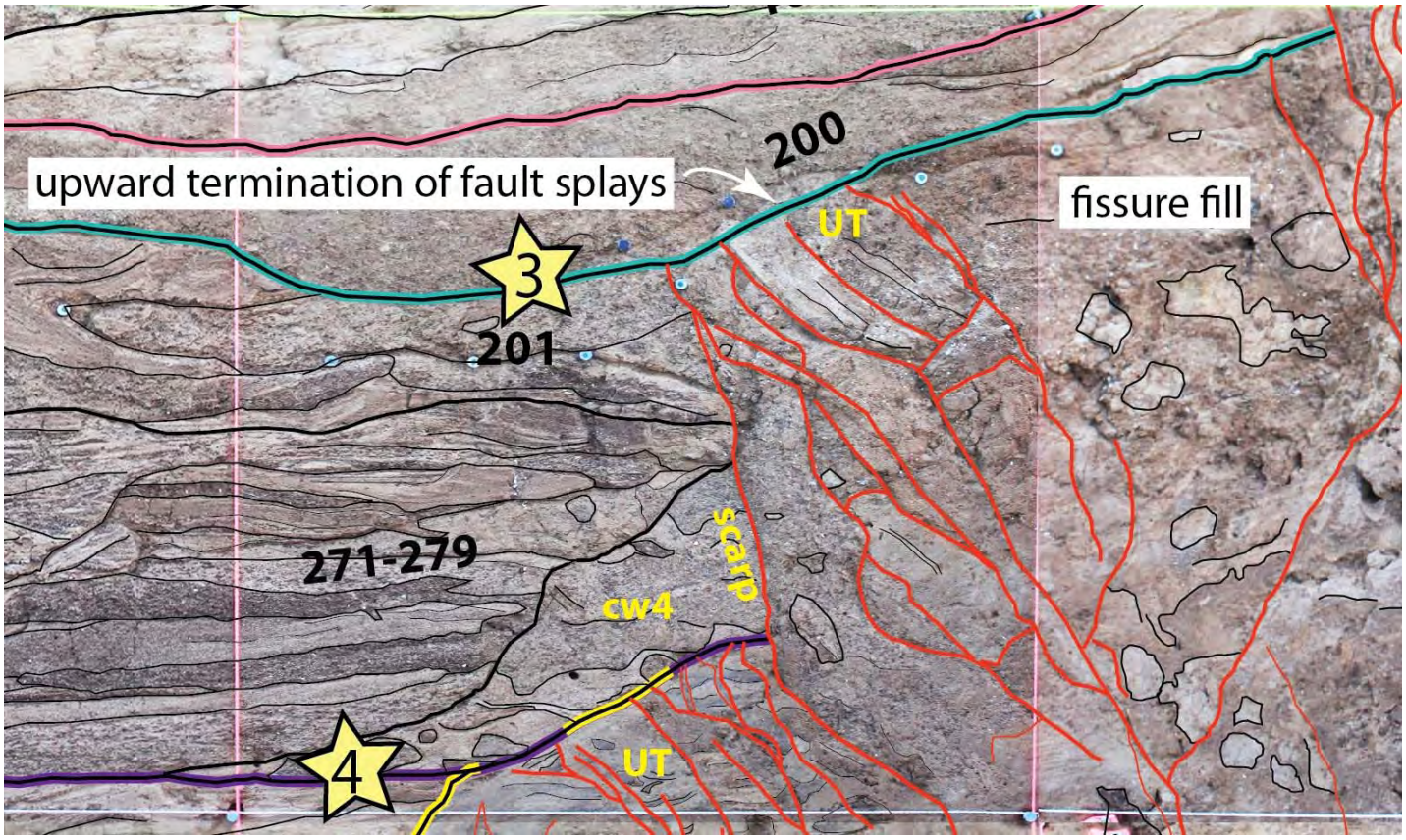
upward termination of fault splays
200
fissure fill
UT
3
201
271-279
scarp
cw4
4
UT

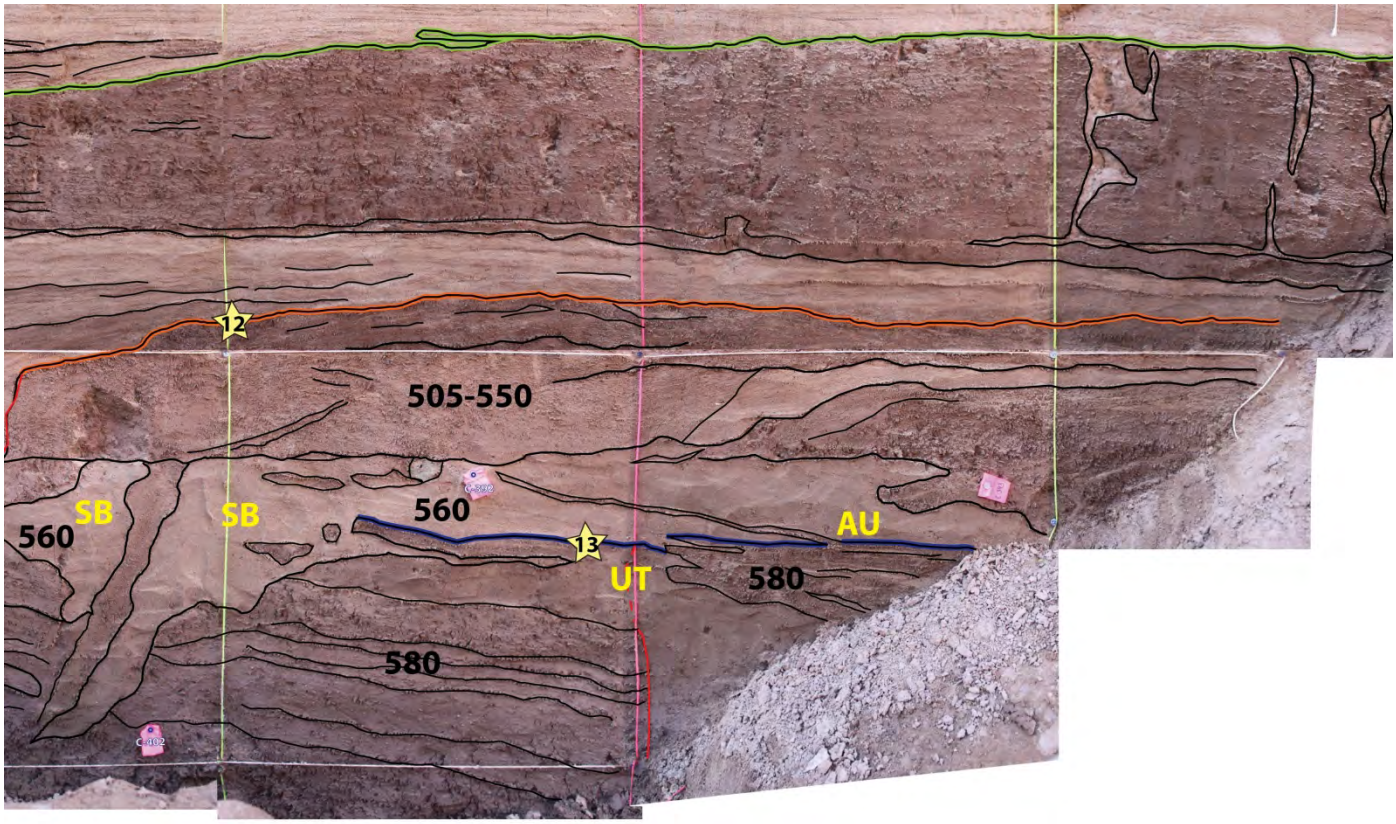
12
505-550
SB
560
SB
560
13
AU
UT
580
580

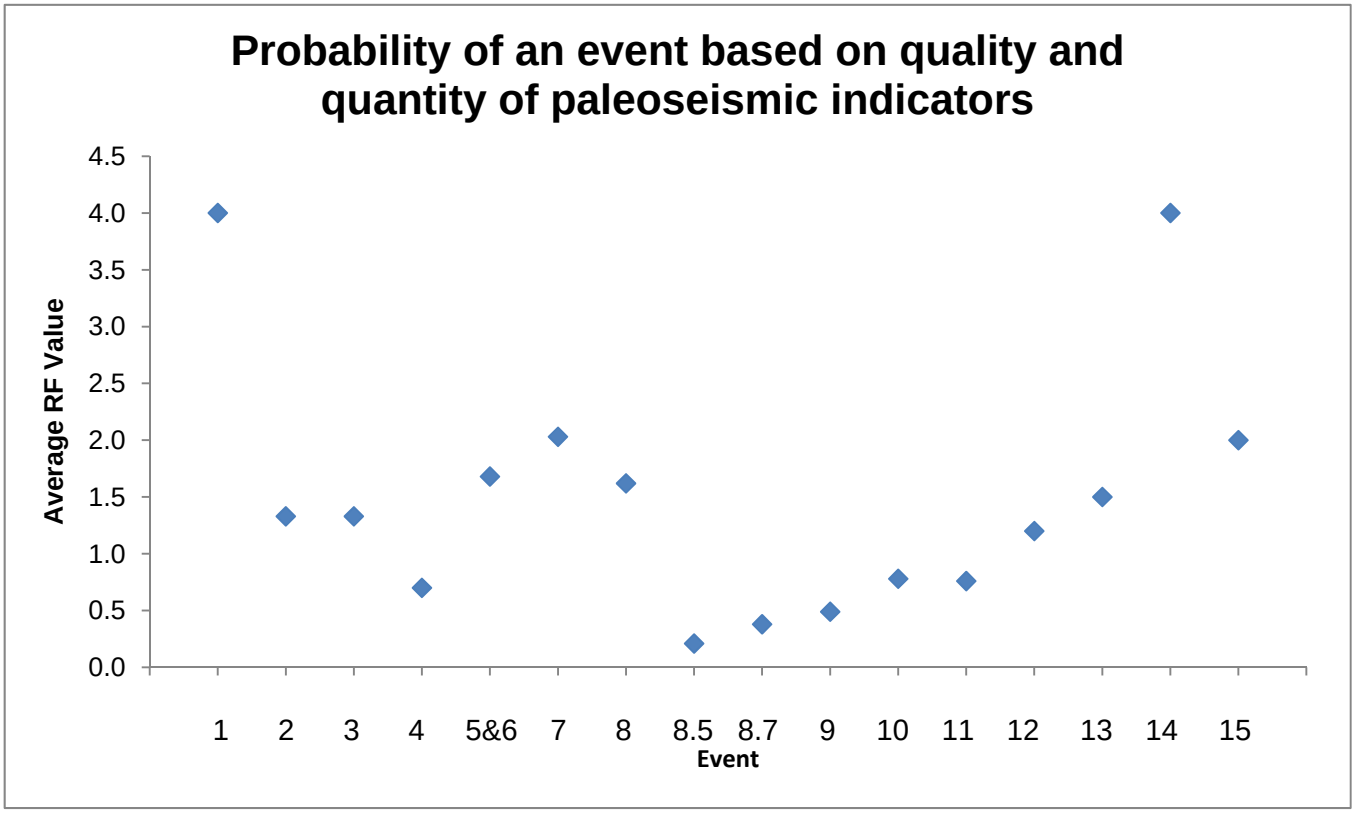
Probability of an event based on quality and quantity of paleoseismic indicators
Average RF Value
4.5
4.0
3.5
3.0
2.5
2.0
1.5
1.0
0.5
0.0
1
2
3
4
5&6
7
8
8.5
8.7
9
10
11
12
13
14
15
Event

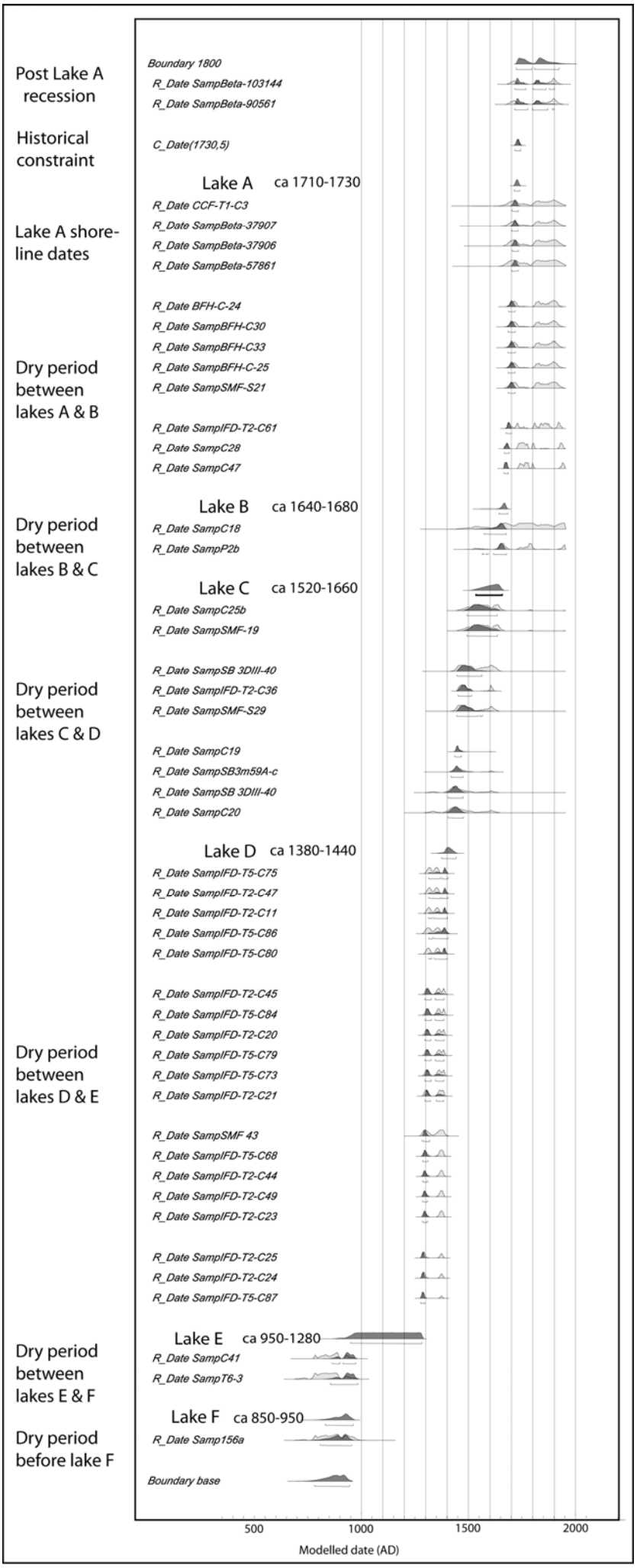
Post Lake A recession
Historical constraint
Lake A shore-line dates
Dry period between lakes A & B
Dry period between lakes B & C
Dry period between lakes C & D
Dry period between lakes D & E
Dry period between lakes E & F
Dry period before lake F
Boundary 1800
R_Date SampBeta-103144
R_Date SampBeta-90561
C_Date(1730,5)
Lake A ca 1710-1730
R_Date CCF-T1-C3
R_Date SampBeta-37907
R_Date SampBeta-37906
R_Date SampBeta-57861
R_Date BFH-C-24
R_Date SampBFH-C30
R_Date SampBFH-C33
R_Date SampBFH-C-25
R_Date SampSMF-S21
R_Date SampIFD-T2-C61
R_Date SampC28
R_Date SampC47
Lake B ca 1640-1680
R_Date SampC18
R_Date SampP2b
Lake C ca 1520-1660
R_Date SampC25b
R_Date SampSMF-19
R_Date SampSB 3DIII-40
R_Date SampIFD-T2-C36
R_Date SampSMF-S29
R_Date SampC19
R_Date SampSB3m59A-c
R_Date SampSB 3DIII-40
R_Date SampC20
Lake D ca 1380-1440
R_Date SampIFD-T5-C75
R_Date SampIFD-T2-C47
R_Date SampIFD-T2-C11
R_Date SampIFD-T5-C86
R_Date SampIFD-T5-C80
R_Date SampIFD-T2-C45
R_Date SampIFD-T5-C84
R_Date SampIFD-T2-C20
R_Date SampIFD-T5-C79
R_Date SampIFD-T5-C73
R_Date SampIFD-T2-C21
R_Date SampSMF 43
R_Date SampIFD-T5-C68
R_Date SampIFD-T2-C44
R_Date SampIFD-T2-C49
R_Date SampIFD-T2-C23
R_Date SampIFD-T2-C25
R_Date SampIFD-T2-C24
R_Date SampIFD-T5-C87
Lake E ca 950-1280
R_Date SampC41
R_Date SampT6-3
Lake F ca 850-950
R_Date Samp156a
Boundary base
500
1000
1500
2000
Modelled date (AD)

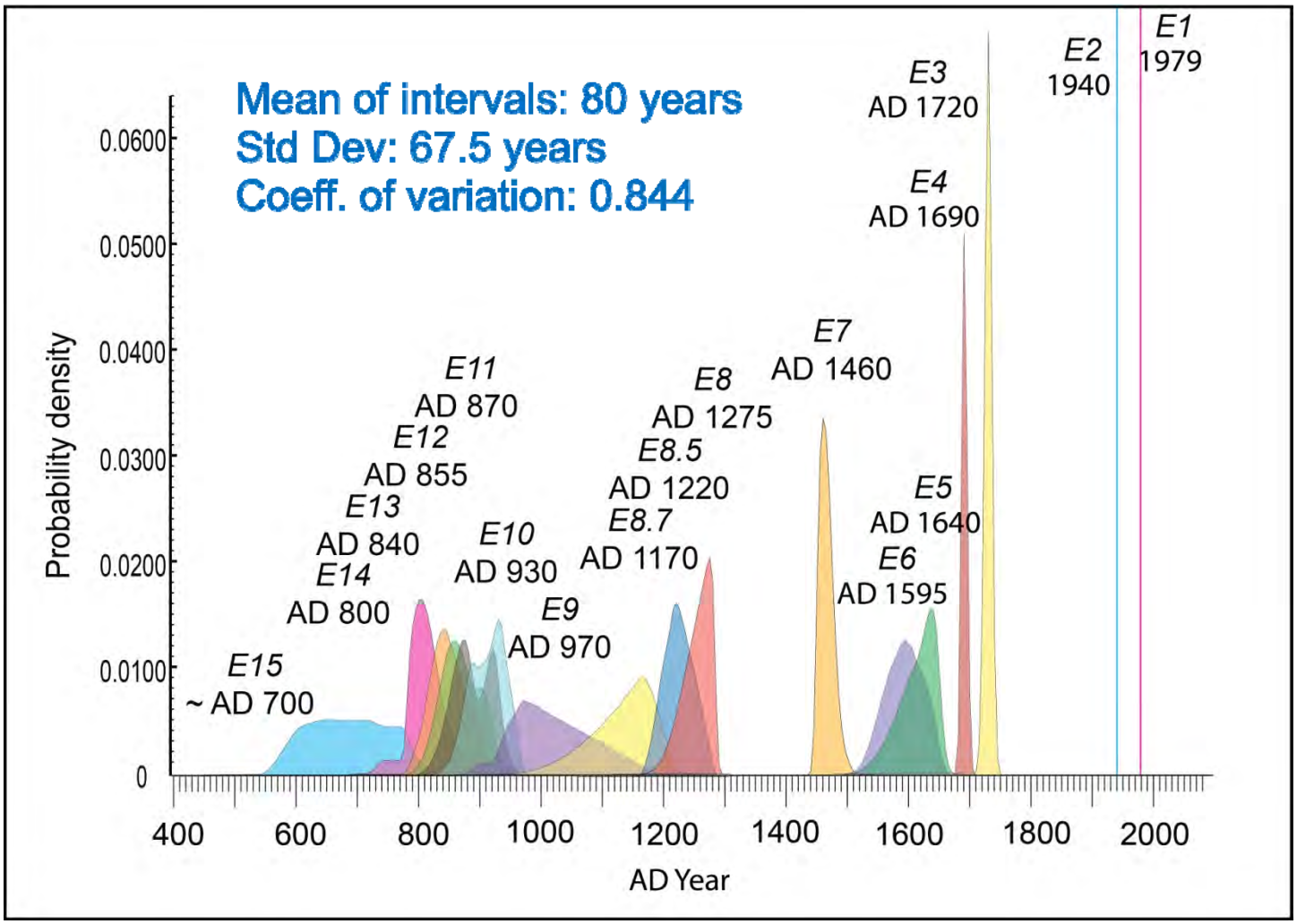
Mean of intervals: 80 years
Std Dev: 67.5 years
Coeff. of variation: 0.844
Probability density
0.0600
0.0500
0.0400
0.0300
0.0200
0.0100
0
400
600
800
1000
1200
1400
1600
1800
2000
AD Year
E15
~ AD 700
E14
AD 800
E13
AD 840
E12
AD 855
E11
AD 870
E10
AD 930
E9
AD 970
E8.7
AD 1170
E8.5
AD 1220
E8
AD 1275
E7
AD 1460
E6
AD 1595
E5
AD 1640
E4
AD 1690
E3
AD 1720
E2
1940
E1
1979

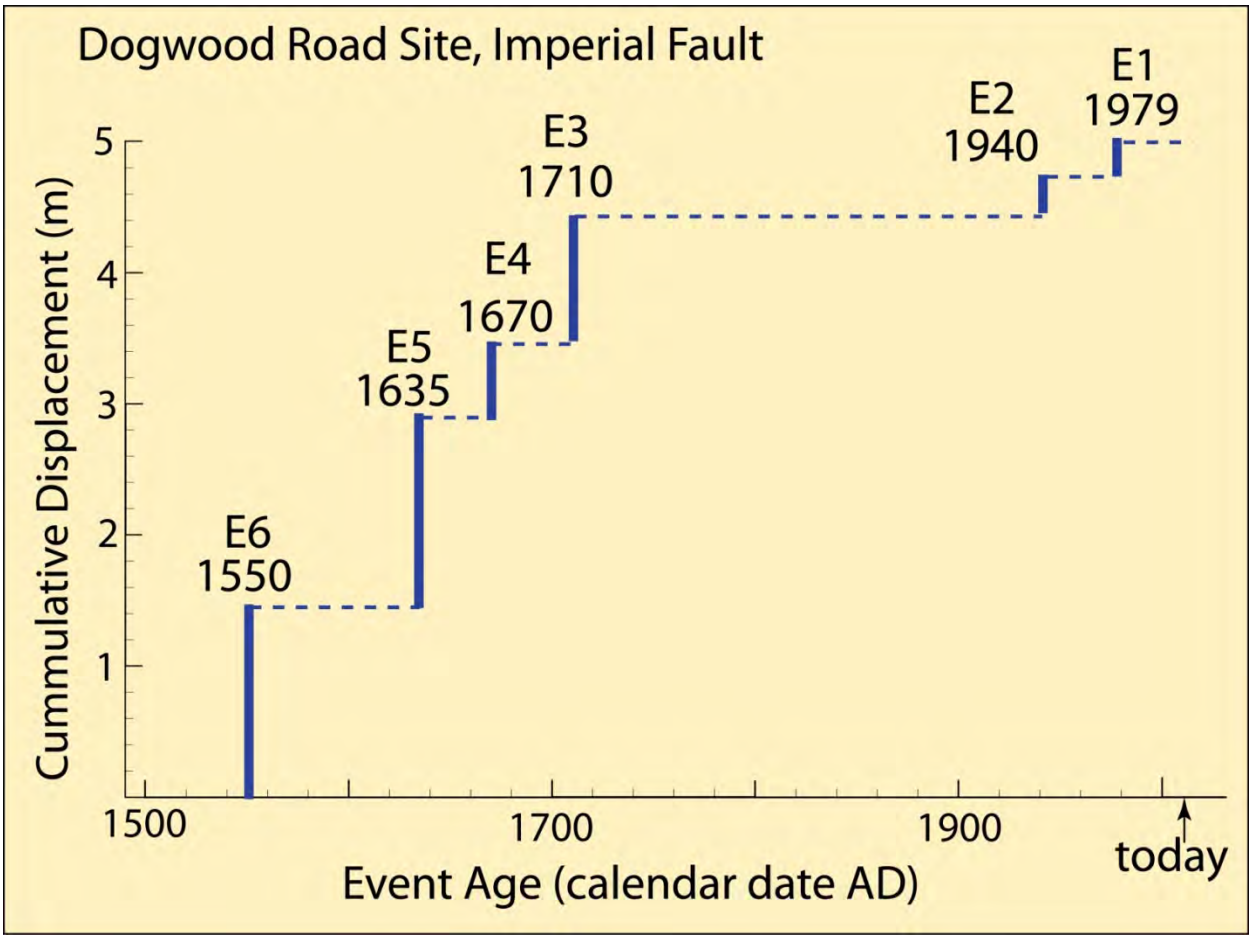
Dogwood Road Site, Imperial Fault
E1
1979
E2
1940
E3
1710
E4
1670
E5
1635
E6
1550
Cummulative Displacement (m)
5
4
3
2
1
1500
1700
1900
today
Event Age (calendar date AD)

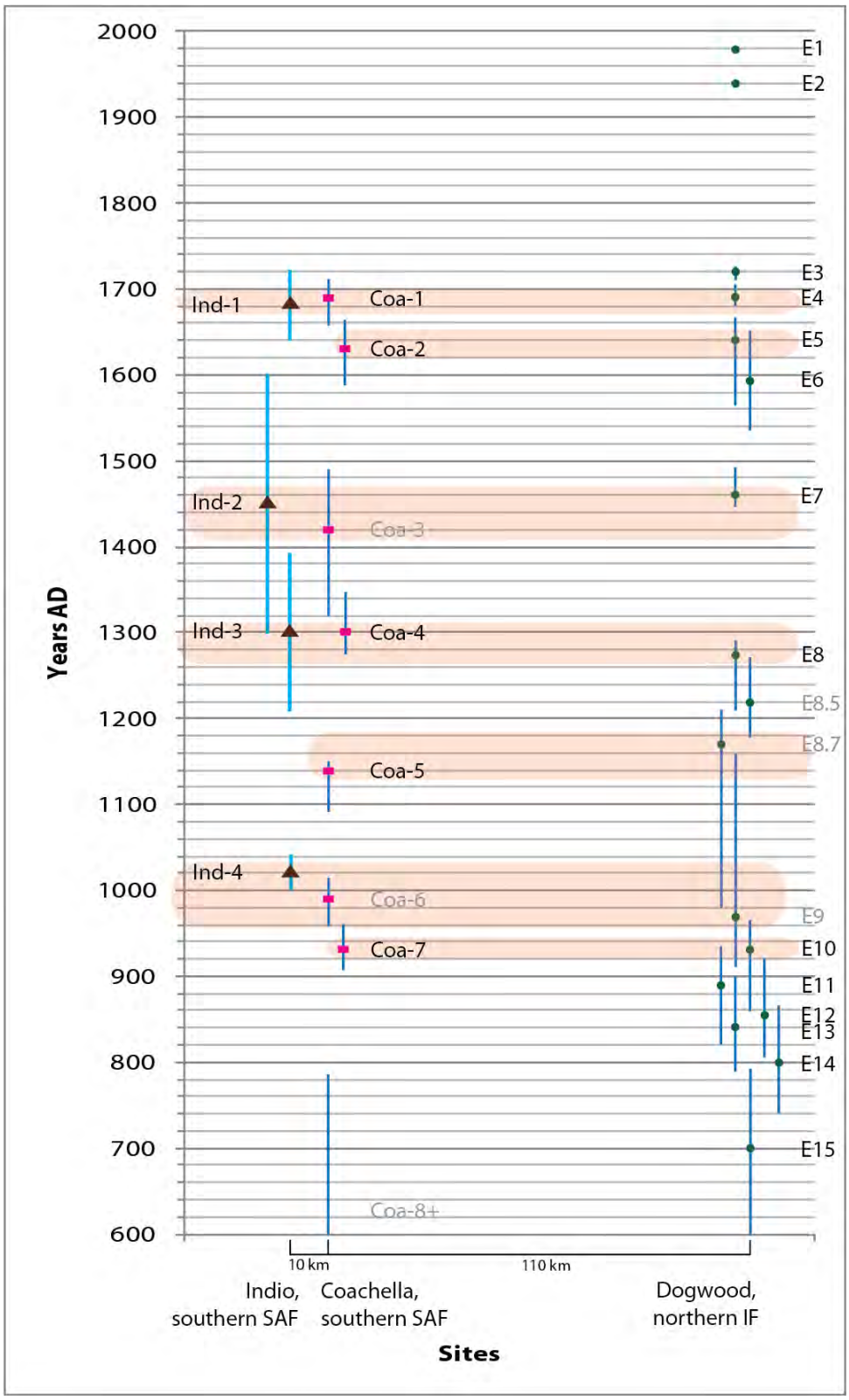
2000
1900
1800
1700
1600
1500
1400
1300
1200
1100
1000
900
800
700
600
Years AD
Ind-1
Ind-2
Ind-3
Ind-4
Coa-1
Coa-2
Coa-3
Coa-4
Coa-5
Coa-6
Coa-7
Coa-8+
E1
E2
E3
E4
E5
E6
E7
E8
E8.5
E8.7
E9
E10
E11
E12
E13
E14
E15
10 km
110 km
Indio, southern SAF
Coachella, southern SAF
Dogwood, northern IF
Sites

APPENDIX 1

Evidence For Surface Rupturing Events at the Dogwood Site, Imperial Fault

Event 1

Event 1 is the most recent event recorded in the stratigraphy of the site and is attributed to the widely documented 1979 M_L 6.6 earthquake in the Imperial Valley (Cohn et al., 1982; Chavez et al., 1982; Harsh, 1982; Sharp, 1982a; Sharp, 1982b; Archuletta, 1984). Displacement in this event at this site was measured after the earthquake as about 20 cm, but Meltzner and Rockwell (2011 in review) estimated that deflected channels suggest about 30 cm in 1979, which includes 30 years of after-slip. The fault ruptured to the ground surface, and evidence for this rupture was observed in the T1-NW exposure, all T3 and T9 exposures and both faces of T4.

In trench T1-NW, T3A-NW/SE and T3B-NW, fault rupturing to the ground surface was observed.

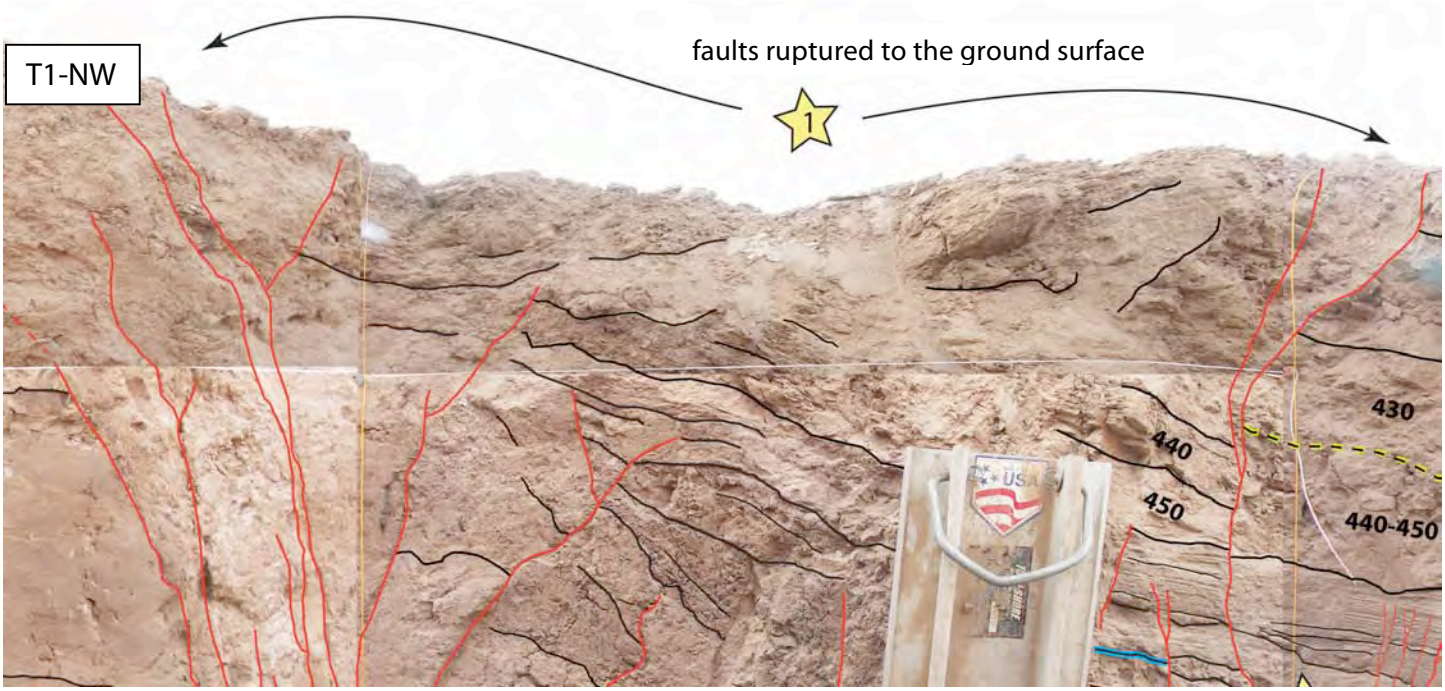

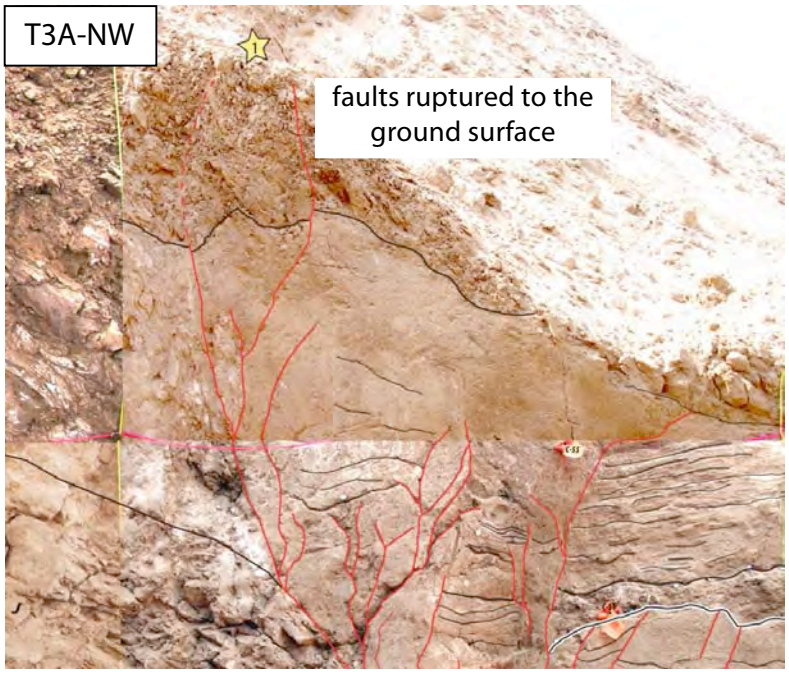

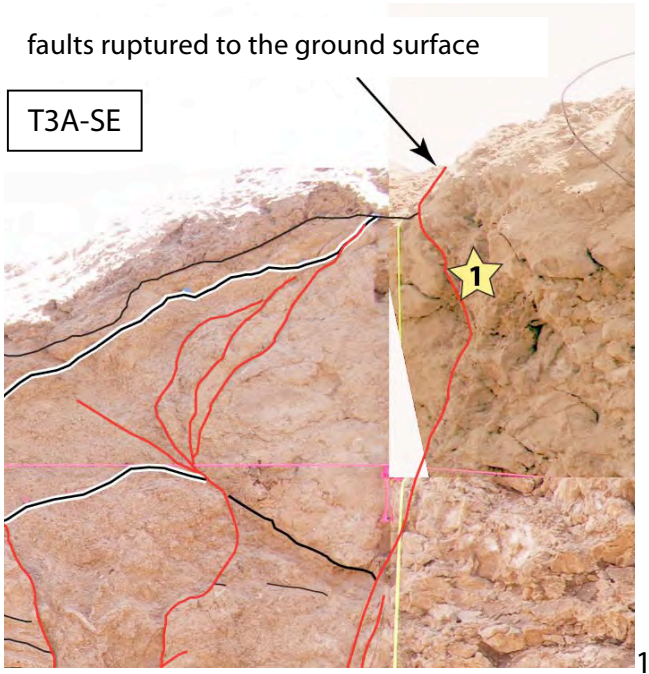

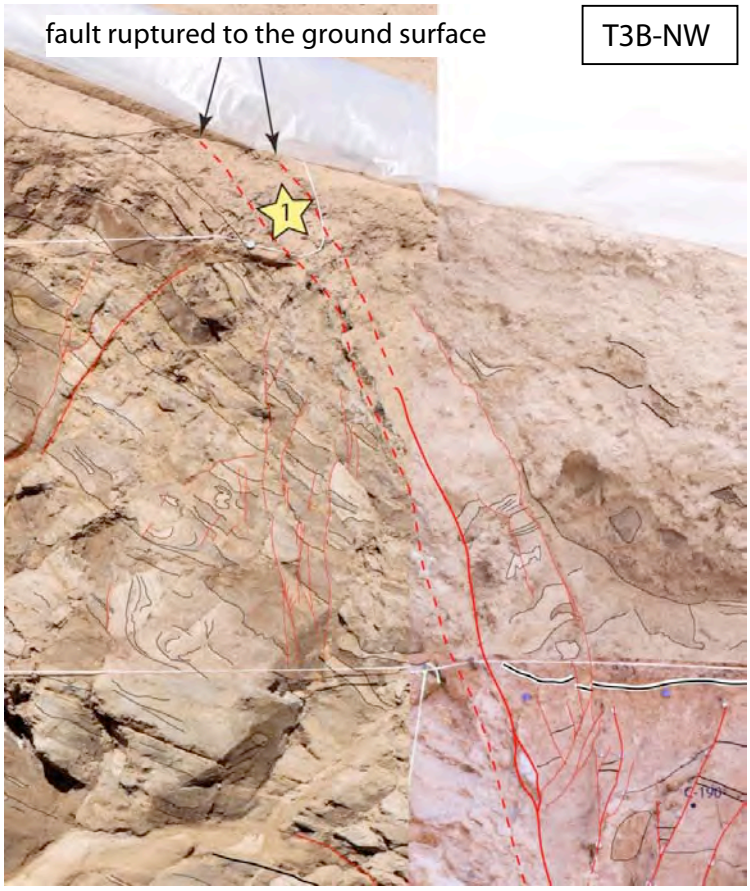

A series of fault splays ruptured to the ground surface as seen in trench T4-SE. In trench T4-NW, some fault splays (dashed lines) ruptured to the ground surface and some splays (solid lines) are capped by a 5-cm layer of spoil at the top.

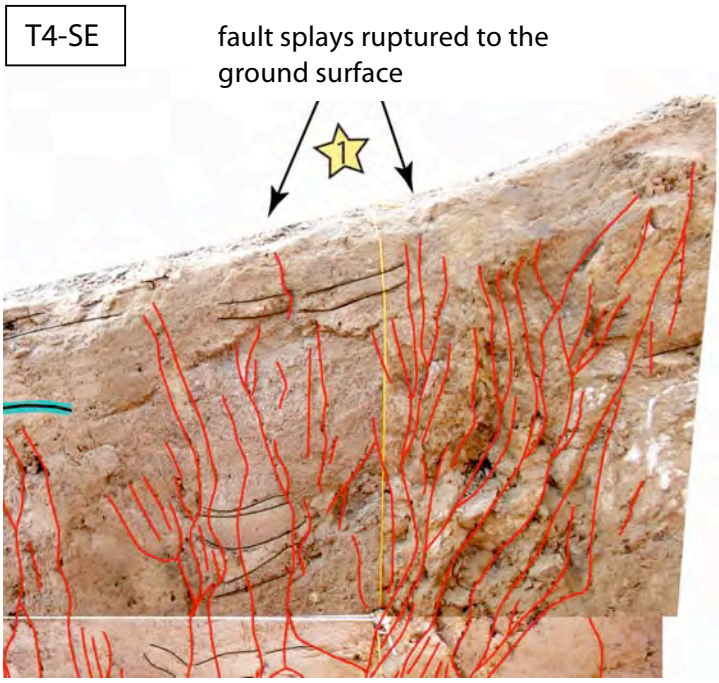

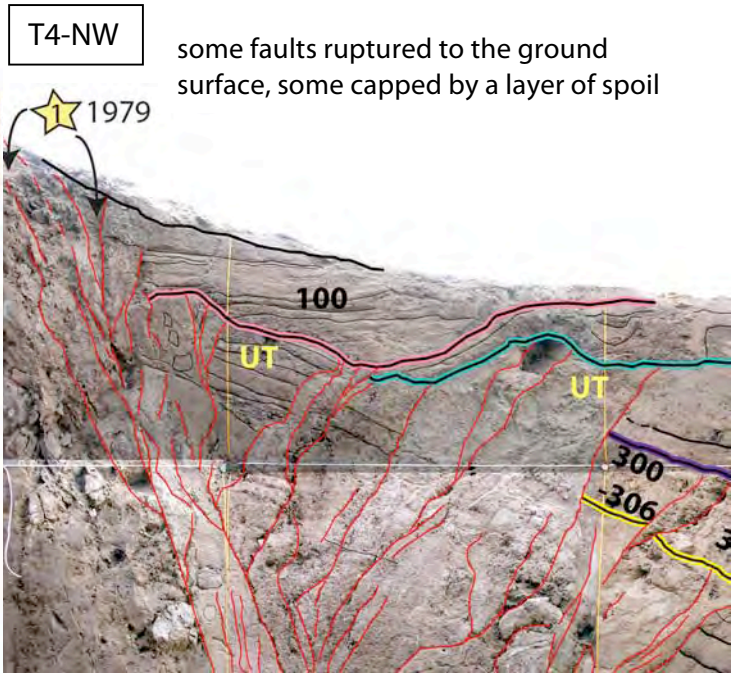

The rupture is capped by a layer of fill or spoil as exposed in T9A-SE, T9B-SE and T9C-SE. The scarp at the ground surface is preserved and is shown in the exposures.

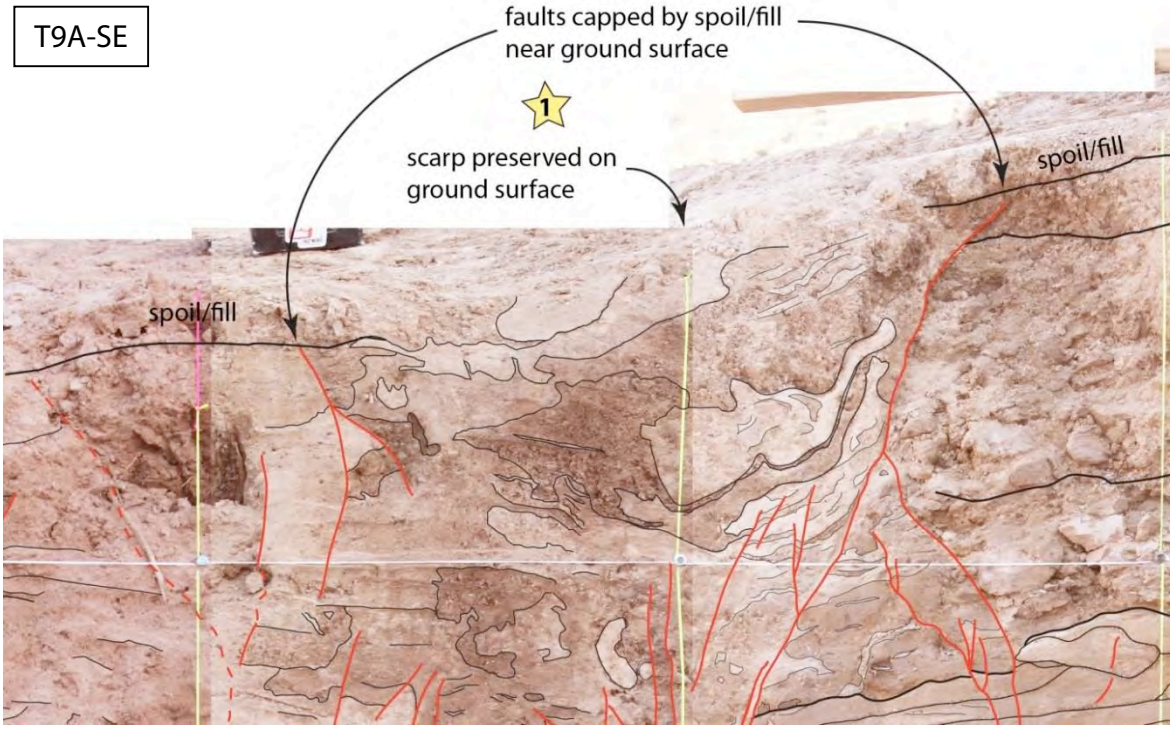

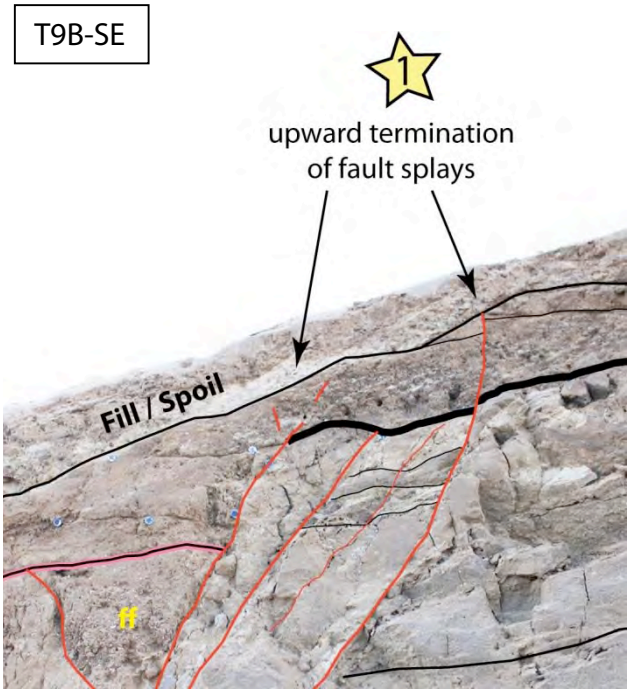

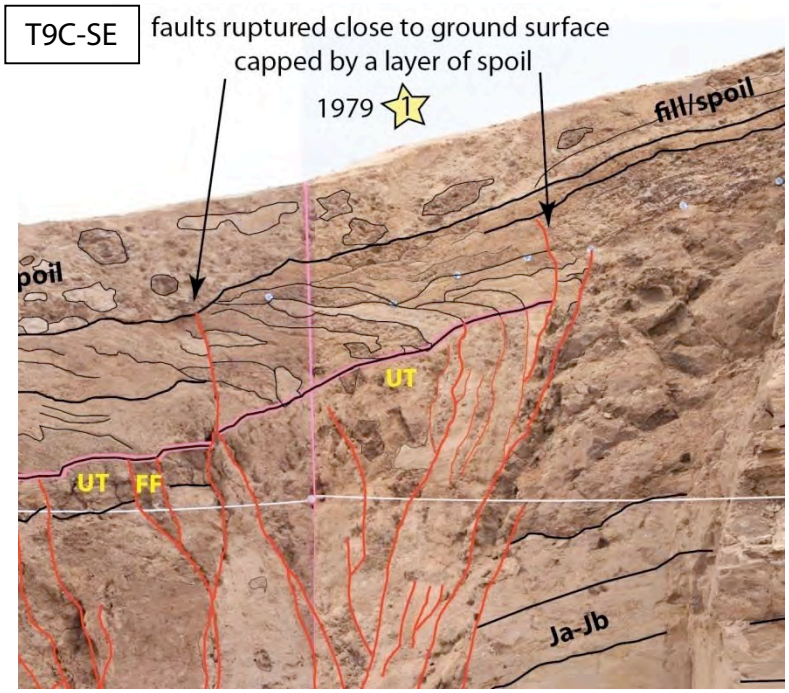

Event 2

Event 2 is interpreted as the penultimate historical earthquake on this fault in 1940, which had a magnitude of M_L 7.1 (Buwalda and Richter, 1941; Richter, 1958). By measuring deflected channels, Meltzner and Rockwell (2011 in review) estimated slip to be about 30 cm, including co-seismic plus after-slip. The event occurred after the most recent highstand of Lake Cahuilla, as the corresponding event horizon caps the youngest lake deposit, Unit 200, as seen in T9B-SE. The 5-cm layer of silt and fine sand deposited (Unit LF)on top of the horizon could have originated from a localized flooding episode during the winter season in wet years; these strata do not correlate among the different trench exposures.

Evidence for Event 2 is clearly exposed in trenches T4-NW, T9B-SE and T9C-SE, and is likely present in other trenches but is difficult to distinguish from events 1 or 3. In T4-NW, faults splays and fissure fills terminate at the paleosurface, capped by the localized flood deposits. In T9B-SE, evidence for this event includes the upward termination of fault splays and a few fissure fills that are all capped by the localized flood deposits. The fissure fills consist of loose sand and silt and broken fragments of dark clay. These same features were observed in the next cut T9C-SE, which is about 20 cm behind Cut B.

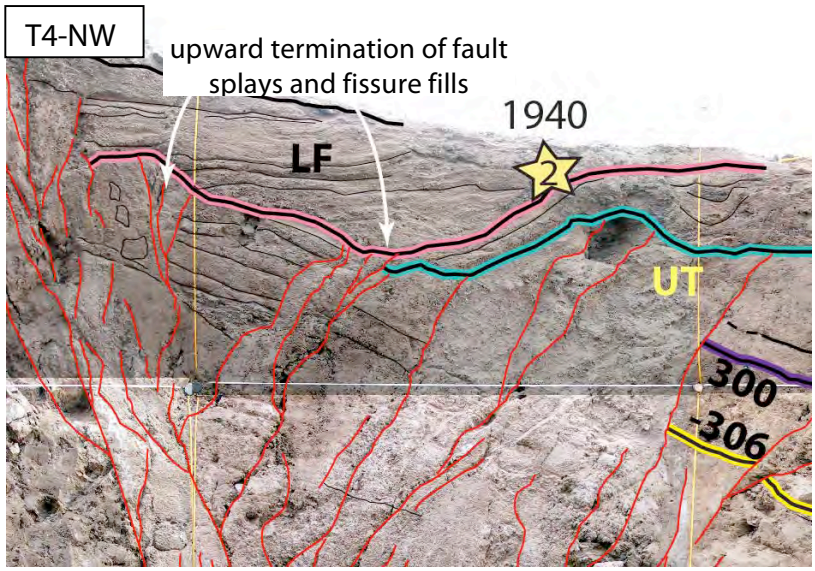

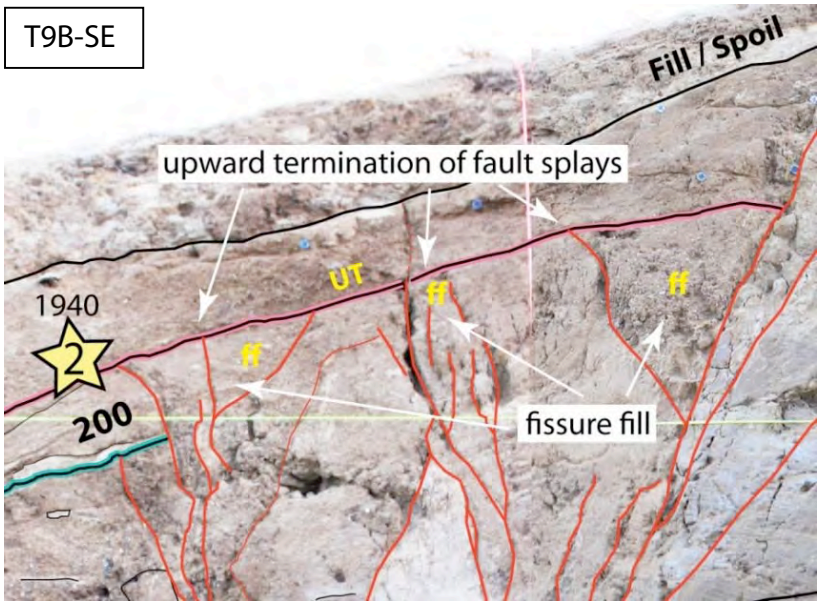

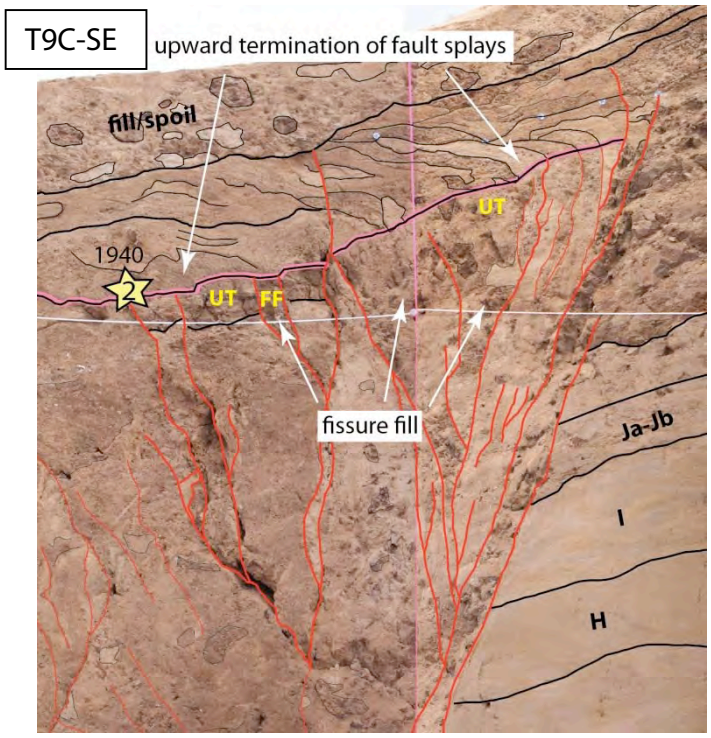

Event 3

Event 3 occurred during the most recent lake filling episode, between the deposition of two distinct lake units 200 and 201 in the stratigraphy. Meltzner and Rockwell (2011 in review) identified buried beheaded channels in several fault-parallel trenches and determined the displacement to be ~1 m by measuring the distance from its modern feeder channel. Evidence for this event is also clearly exposed in trenches T4-NW, T4-SE and T9B-SE, but is not so clear in other cuts of the T9 trenches. In trench T4-NW, fault splays terminate upward and are capped by Unit 200. This feature was also observed in another exposure in trench T9B-SE, in addition to the fissure fill that consists of broken fragments of hardened silty clay.

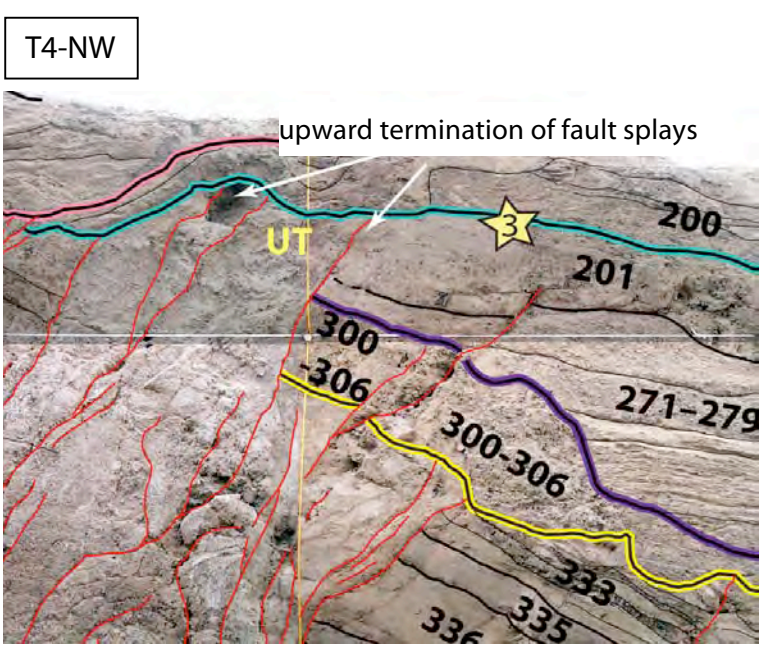

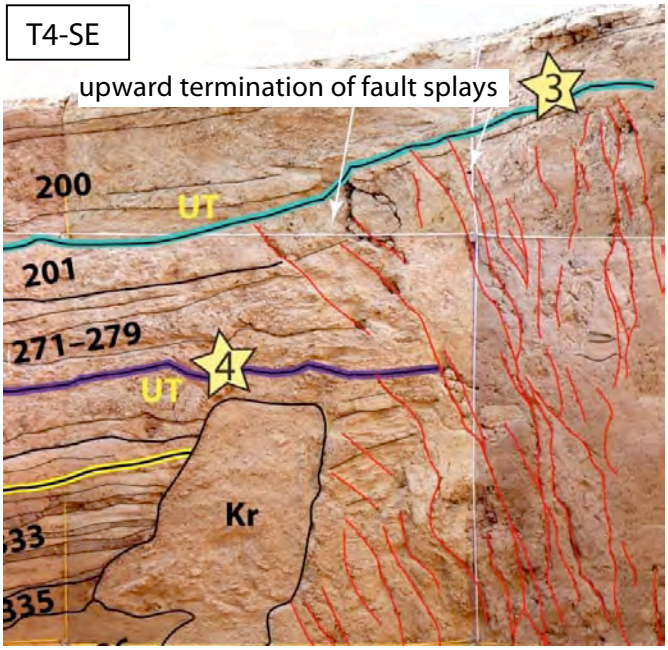

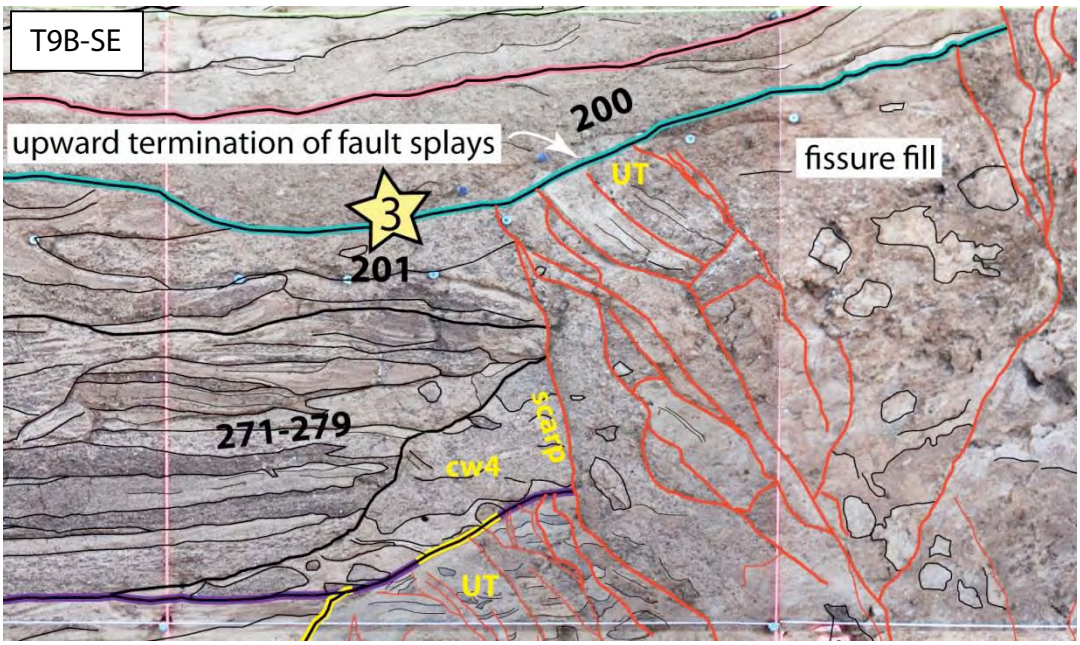

Event 4

The event horizon of Event 4 was found below the channel deposits Unit 271-279 and above the lacustrine deposits Units 300-305 (Lake B) and Unit 333 (Lake C). Hence, we deduce that Event 4 occurred at the beginning of a dry period after the filling episode of Lake B. Meltzner and Rockwell (2011 in review) documented slip for this event to be ~60 cm by studying offset buried channels.

Evidence for this event was observed in 3 different exposures. In trench T4-SE, a series of fault splays terminate at the paleosurface capped by the channel deposits Units 271-279. In trench T9B-SE, the base of the colluvial wedge marks the paleosurface of Event 4. The wedge consists of unstratified mixture of fine sand, silt and fragments of clay which resemble the material on the upthrown block adjacent to the scarp that also fills the fissures to the right. Furthermore, splays of fault terminate at the horizon below the wedge. Part of the horizon for Event 4 overlaps with that for Events 5 and 6, and details of which will be discussed in the next section. The upward termination of these fault splays are also observed in the subsequent cut (~20 cm behind) in trench T9C-SE; fine sand and silt fill the fissures.

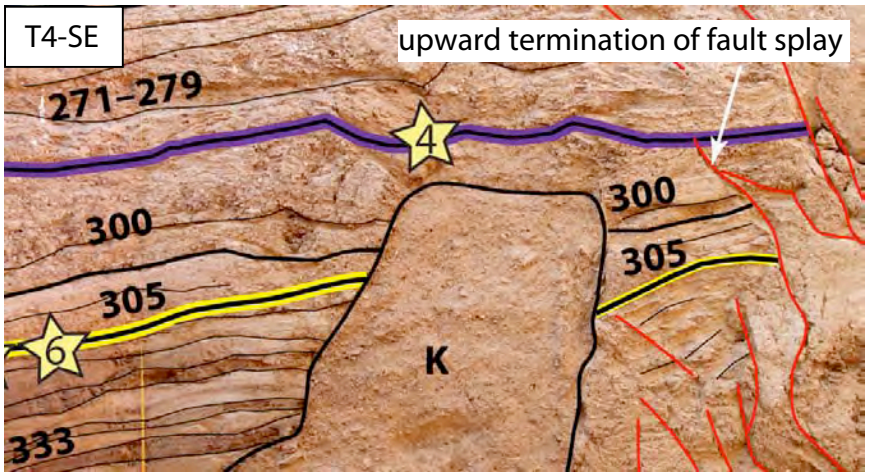

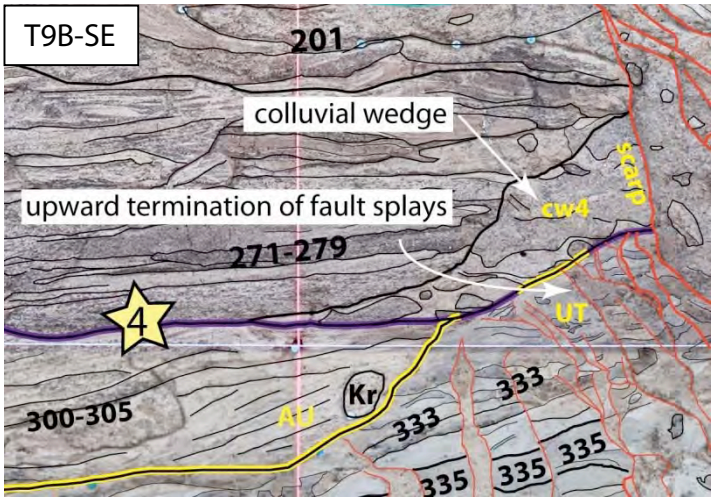

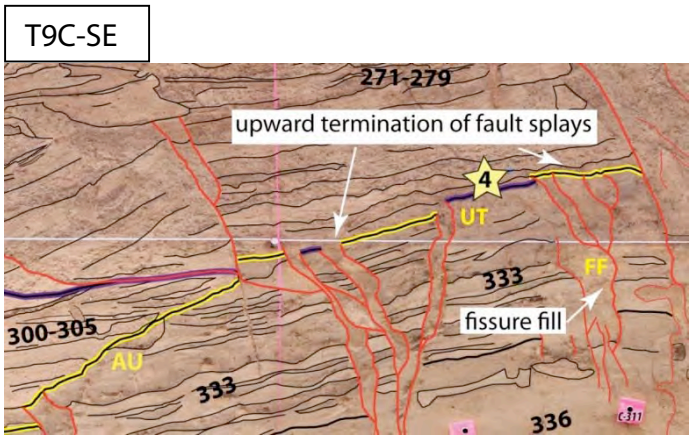

Events 5 / 6

Events 5 and 6 occurred at essentially the same stratigraphic horizon, at the top of Unit 333 and the base of Units 300-306, the dry period between Lakes B and C, and are therefore difficult to distinguish as two separate events in most exposures. However, Meltzner and Rockwell (2011 in review) determined displacement discretely to be ~1.5 m for each of these events by measuring offset channels in 3-D subsurface exposures, so their occurrence is assured. These two events share the same event horizon possibly due to the low deposition rate during the dry period after Lake C. For this couplet of events, evidence is discussed together. Evidence for events 5/6 was found in 5 different exposures.

In trench T4-NW and SE, evidence for Events 5 and 6 is present between Units 305/306 and 333. In both exposures of the same trench, fault splays terminate upward at the horizon capped by lacustrine deposits Units 300-305/306 (Lake B). In the SE exposure, the interbedded clay and silt in Unit 333 (Lake C) was deformed and was capped by the undeformed, horizontally bedded lacustrine deposits of Lake B forming an angular unconformity.

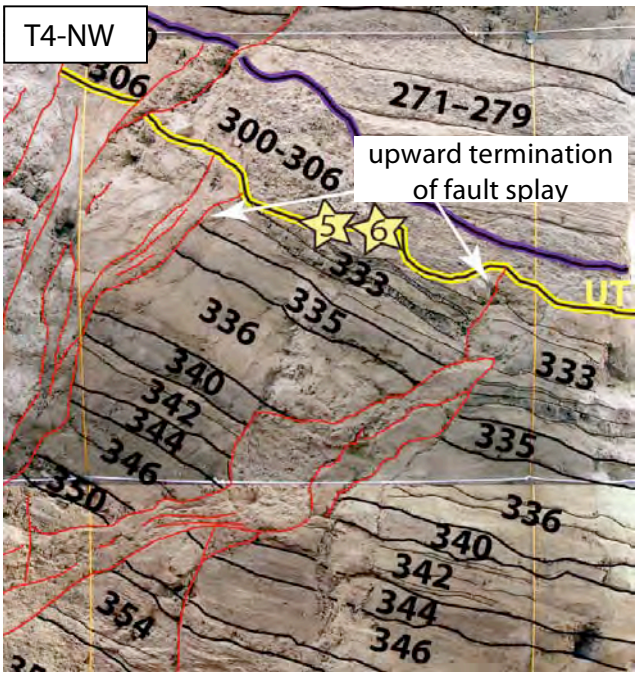

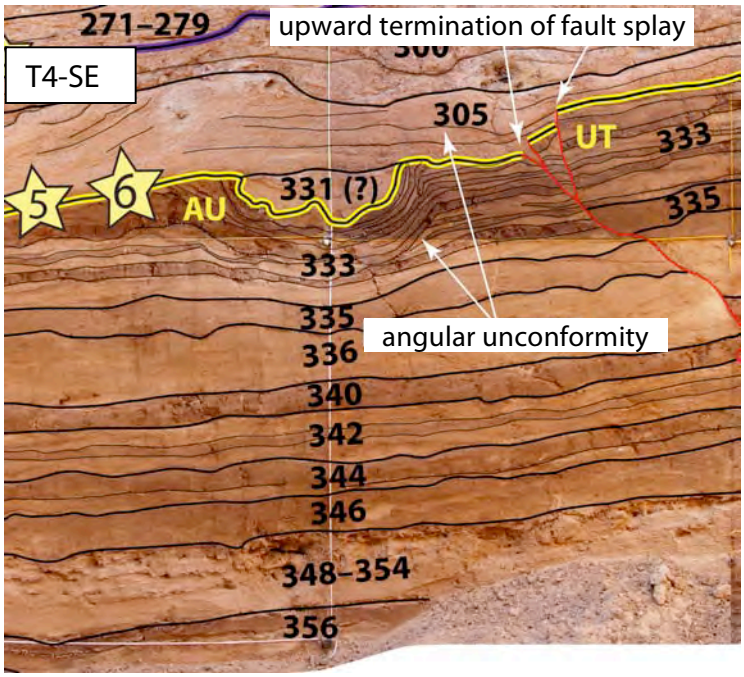

In trench T9-SE, all three cuts display evidence for Events 5/6. Part of the horizon of Events 5/6 (yellow) that is closer to the main fault zone to the right overlaps with that of Event 4 (purple). One possible explanation is that the lacustrine deposits of Lake B (Units 300-306) were removed by subaerial erosion during the dry period between Lake B and the next lake. Regardless, termination of fault splays was observed both at the tripled composite horizon of Events 4 /5/6 (line with alternating purple and yellow colors) and just the horizon of Events 5/6 (yellow) further away from the main fault zone, as exposed in T9C-SE and T9B-SE.

In trench T9B-SE, in addition to the upward termination of fault splays, a series of liquefaction pipes filled with fine sand also terminate at the same paleosurface. Fissure fills consisting of loose sand and clay fragments were observed closer to the main fault zone. The lacustrine beds of Lake C (Units 333 and below) were deformed and warped and were capped by nearly horizontal younger lacustrine beds (Units 300-305) and fluvial deposits (Units 271-279). The same features were also observed in the subsequent cut that is ~20 cm behind (T9C-SE).

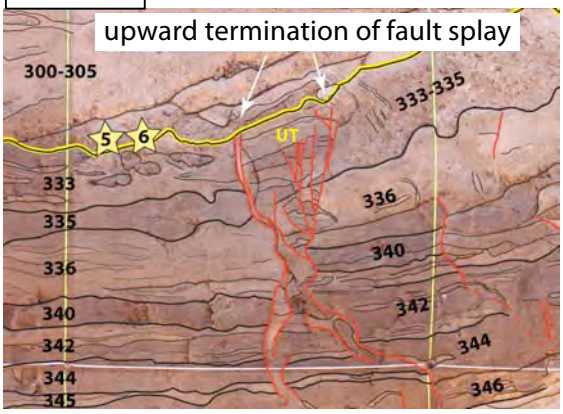

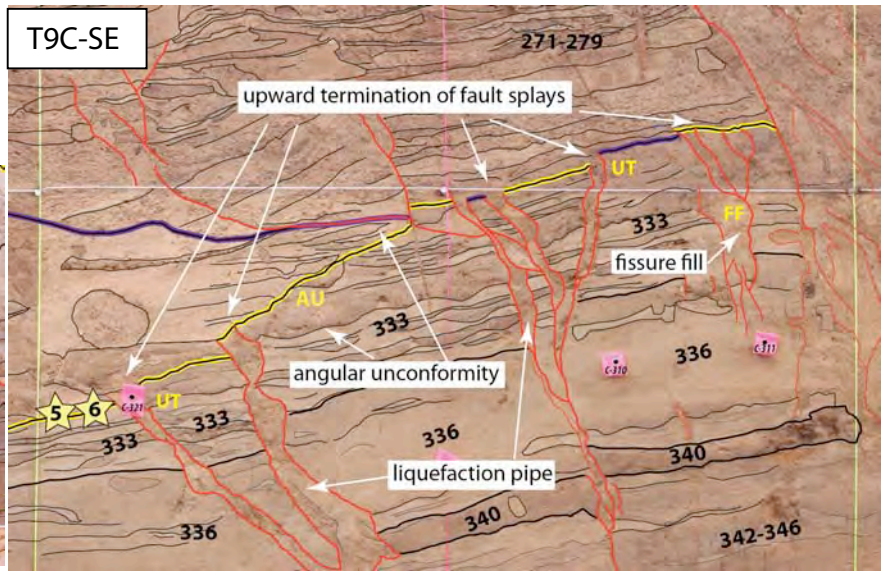

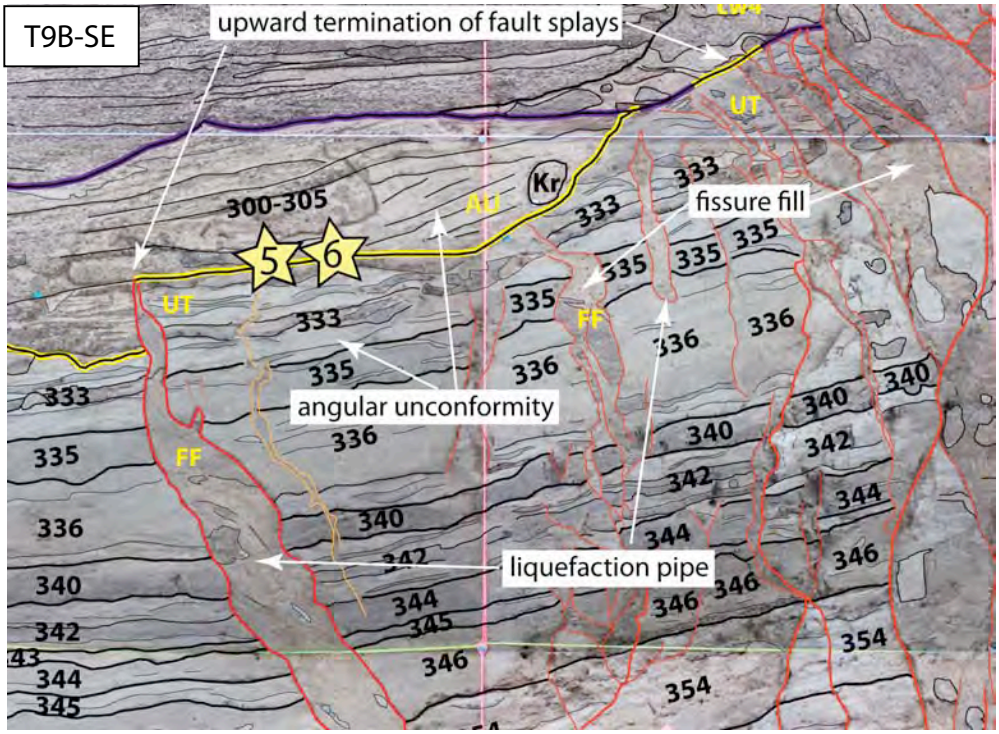

Event 7

Slip per event was only resolved for the first six events, as far as Meltzner and Rockwell (2011 in review) have documented; we could not find any additional buried channels that may correspond to Event 7 and older. Therefore, only evidence for each event will be discussed in the following.

Evidence for Event 7 was observed in 3 different exposures. In trench T3A-SE, a clear angular unconformity is present between the tilted, lower lacustrine deposits of Lake C (Units 348-358) and the deformed lacustrine beds of Lake D (Units 360-365) that are slightly dipping in the opposite direction, denoting the horizon of Event 7 which happened during the dry period between Lakes C and D. In addition, splays of fault and a fissure filled with loose, well-sorted, fine sand were capped by the younger strata, Units 348-358.

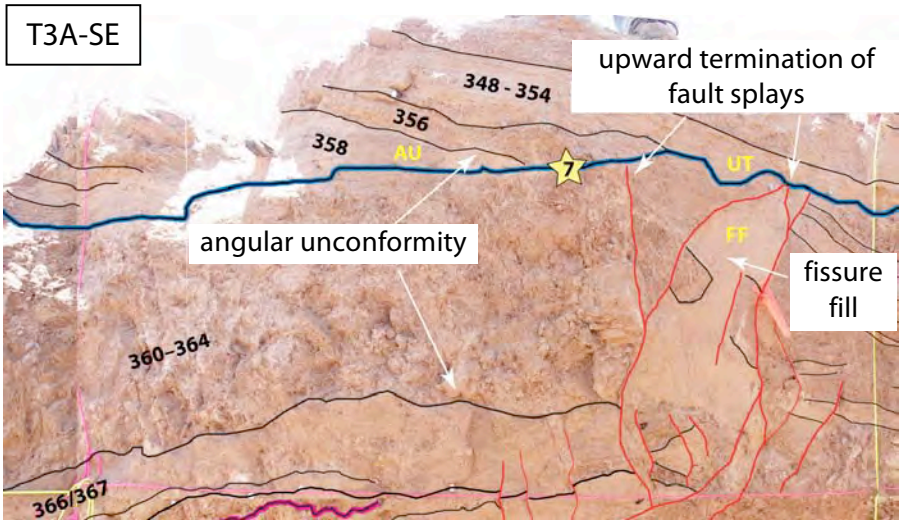

In trench T9C-SE, splays of fault in a 1-meter wide zone all terminate at the same stratigraphic horizon between Units 356-358 and Units 361-364, marking the paleosurface of Event 7. Some of the fissures were filled with silt, fine sand and clay fragments. These same features were also observed in the previous cut (~20 cm in front) in trench T9B-SE. In addition, the nearly horizontal beds of Units 356-358 and the slightly tilted beds of Units 361-364 form an angular unconformity that is indicative of the occurrence of Event 7.

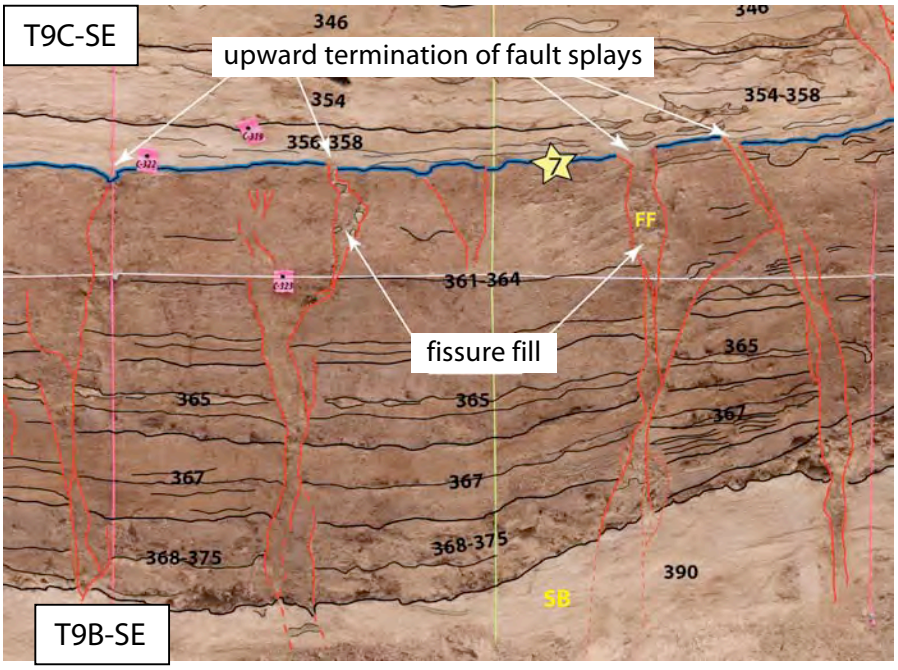

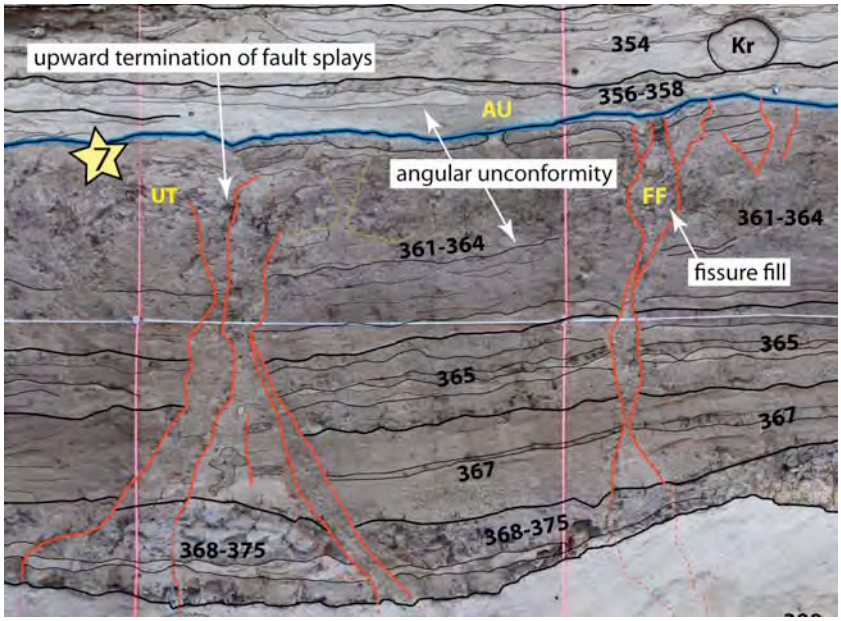

Event 8

Event 8 occurred stratigraphically at the base of Units 390/395 and the top of Unit 400, a clayey unit that represents the filling episode of Lake E. Evidence for this event is widespread throughout the trench site including a sand blow (Unit 390) exposed in multiple trenches which can be up to 2 m in thickness as seen in trench T2-Extension-SW.

Unit 390 was initially interpreted as a fluvial/deltaic deposit due to its sandy texture before the new trenches were excavated in 2010 and 2011. However, after further studying and understanding the stratigraphy of the site, we interpret Unit 390 is of seismogenic origin, and the argument is presented in the following.

Unit 390 is a very well-sorted, fine sand with pervasive foreset beds. The thickness of such unit in various exposures ranges from 30 cm to 2 m. Other possible origins have been considered, including deltaic and eolian. (1) Despite the pervasive foreset beds, Unit 390 is not likely to be of eolian origin but is rather derived locally because the foreset beds are dipping in different directions in various trench exposures. For example, in trenches T2-SW and T2-Extension-SW, the foreset beds are dipping in opposite directions, to the SE and to the NW respectively, and in T4Deep-NW-A the foreset beds are dipping to the NE. Therefore, Unit 390 is likely to be derived locally rather than by eolian deposition. (2) It is not likely to be a deltaic deposit because it is distinctly bounded by two clean clay units at the top and bottom with no grading upward or downward. Unit 390 was likely to be deposited during the filling episode of Lake E, suggesting a subaqueous environment at the paleosurface. In addition, the presence of an irregular, wavy contact between the lacustrine clay (Units 368-375) and Unit 390 as exposed in trench T3B-NW indicates a high water content within Unit 390 when the clay was deposited on top of it. This further validates our argument that Unit 390 was deposited subaqueously. It then seems reasonable to argue that the well-sorted sand of Unit 390 was ejected from below. (4) A liquefaction ejecta could either be a sill or a sand blow. However, in this case Unit 390 is likely to be a sand blow because the clay cap below (Units 400-427a) is probably not thick enough (only 30 cm) to resist the elevated pore-water pressure. The increased pressure in the underlying water-saturated sand can easily break through to the surface where the clay cap is thin (<1-2 m) (Obermeier, 1996). All of the arguments above suggest that Unit 390 is a sand blow. However, we are still not able to locate the vent for such a large liquefaction ejecta. It might require some luck to find it as large sand blows rarely come

from multiple vents that are closely spaced, but rather only a few vents at most that are widely spread apart (Obermeier, 2009).

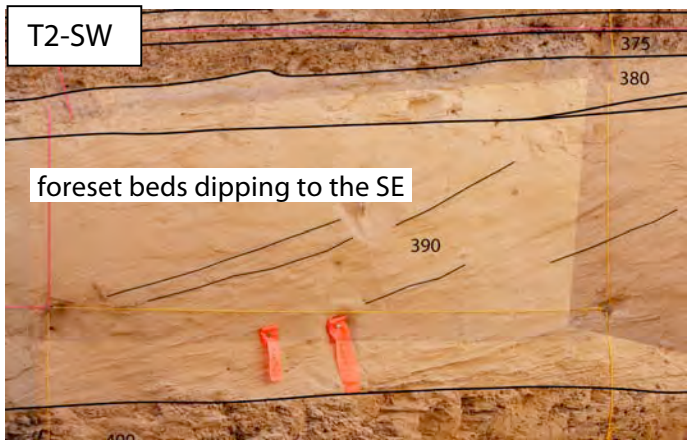

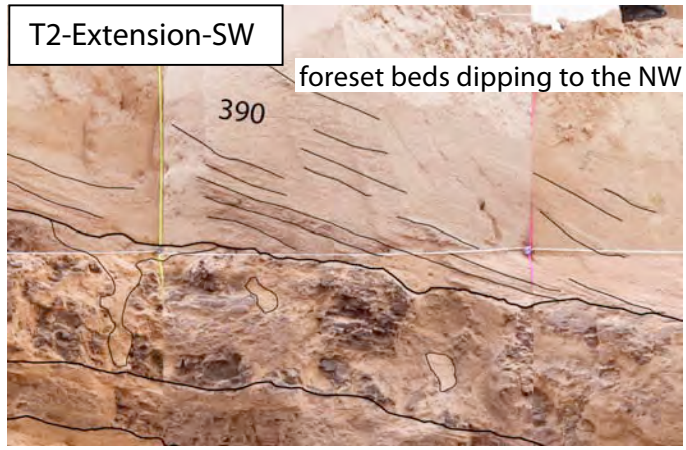

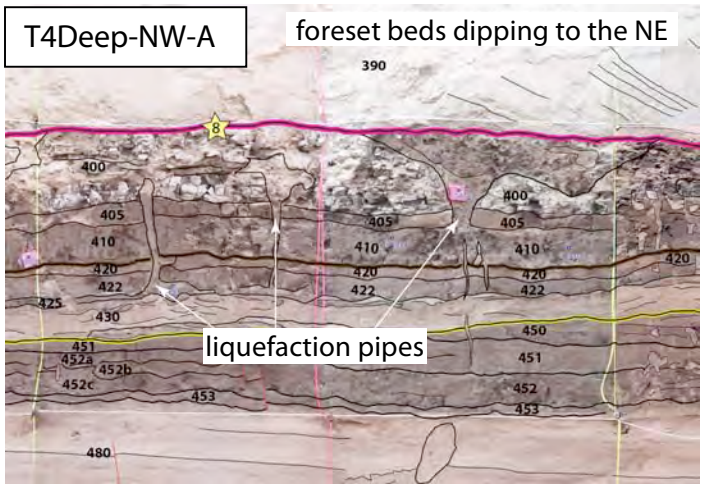

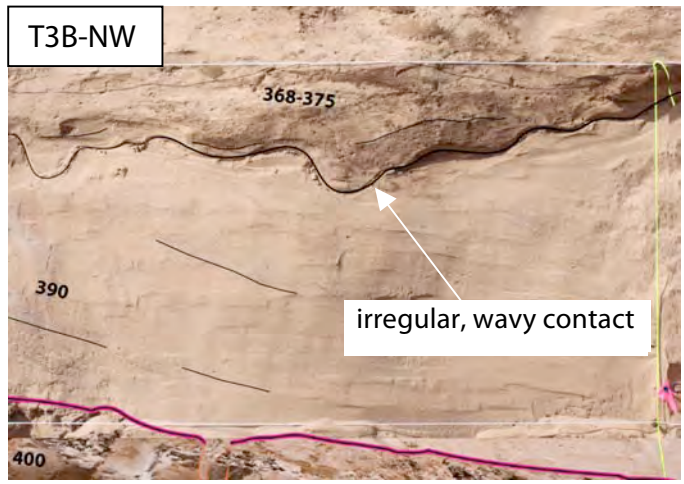

Besides the presence of the large sand blow, other paleoseismic indicators also serve as evidence for Event 8. Multiple smaller liquefaction pipes and a few splays of fault terminate at the base of the sand blow which were observed in all the exposures of the T4Deep trenches: T4Deep-NW-A, B and C, and T4Deep-SE-A and B.

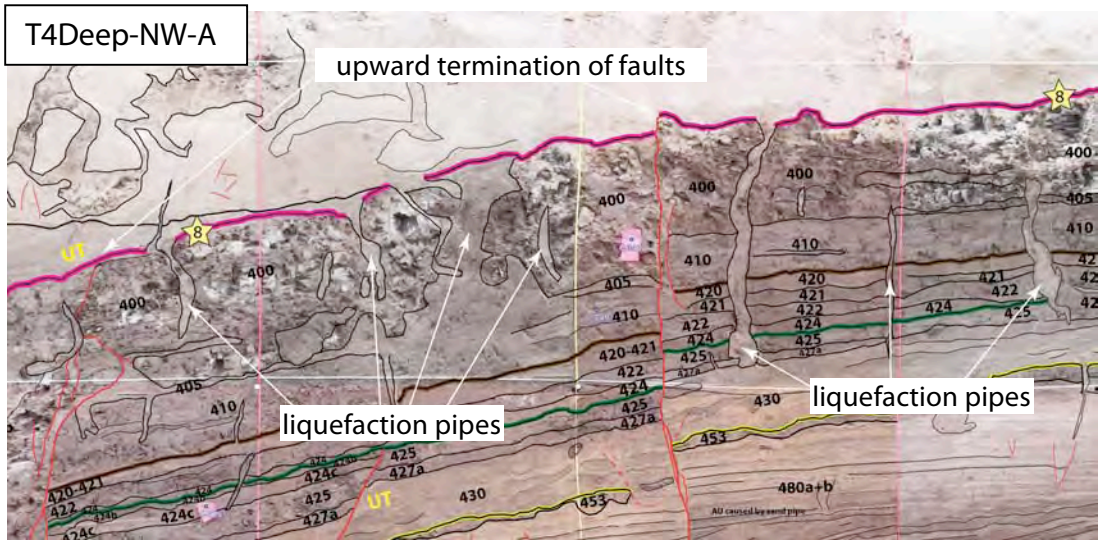

T4Deep-NW-B

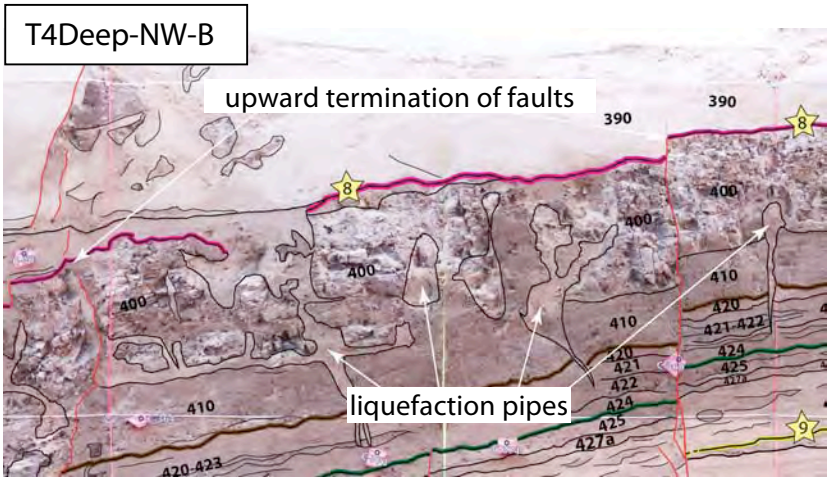

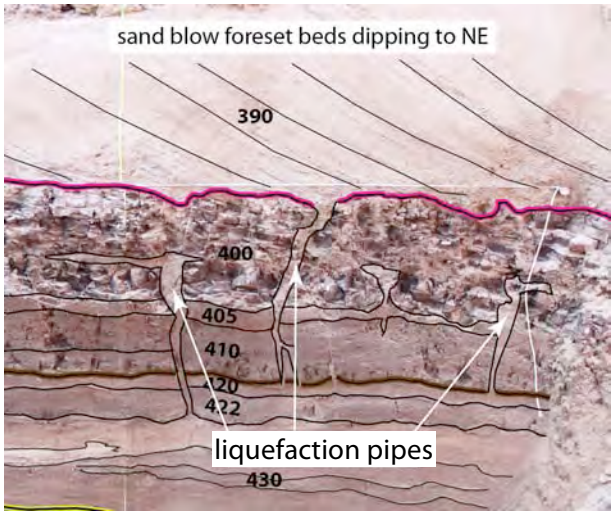

T4Deep-NW-C

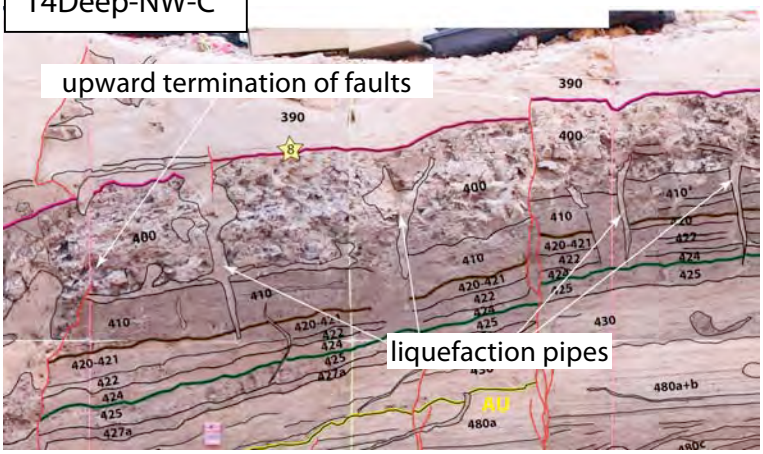

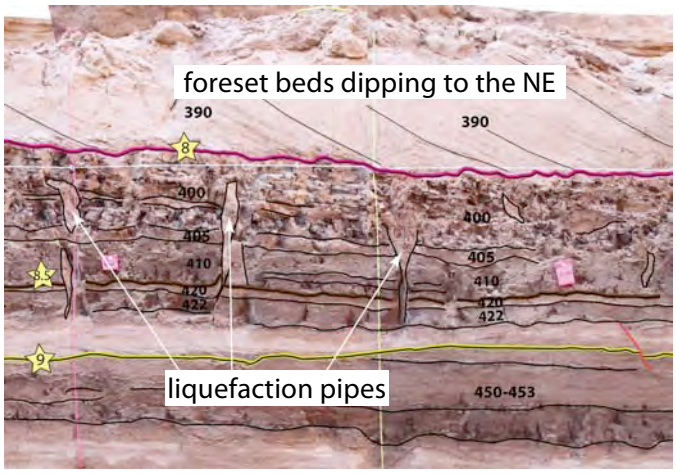

T4Deep-SE-A

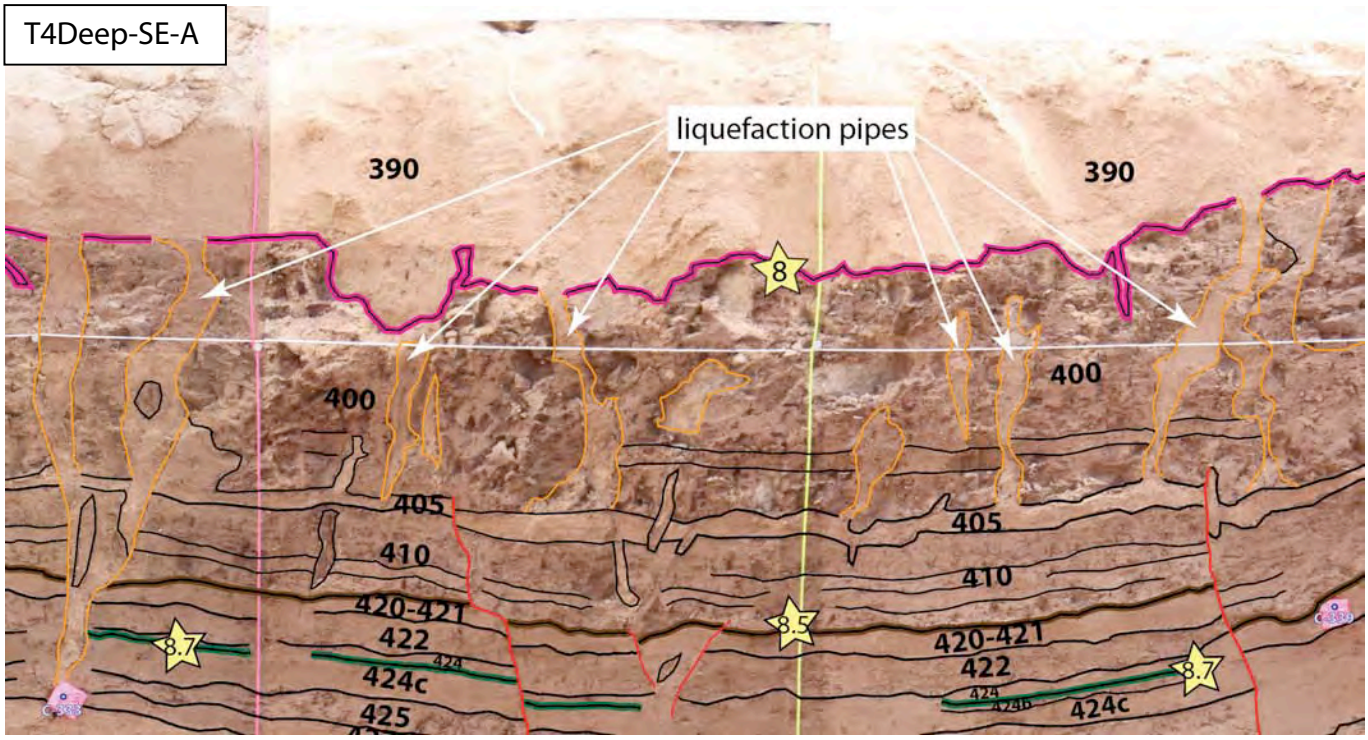

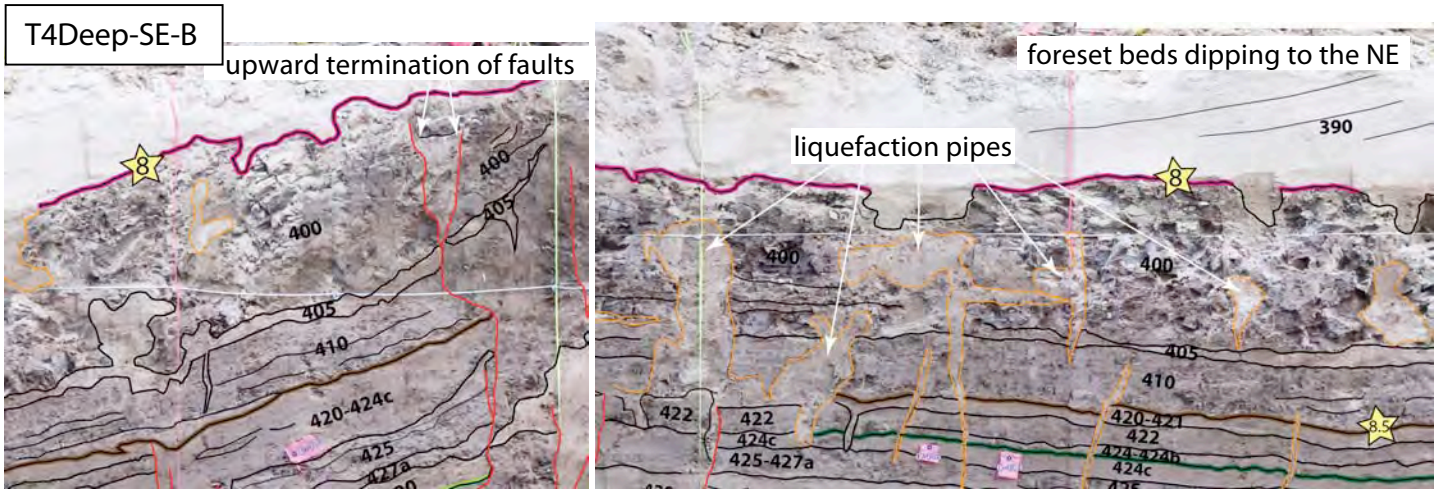

In trench T3A-SE, in addition to the fault splays, a fissure filled with well-sorted, fine sand and broken chunks of brown clay was capped by Unit 390. The sand blow was deposited horizontally on top of the tilted clay below (Unit 400), forming an angular unconformity which denotes the event horizon of Event 8.

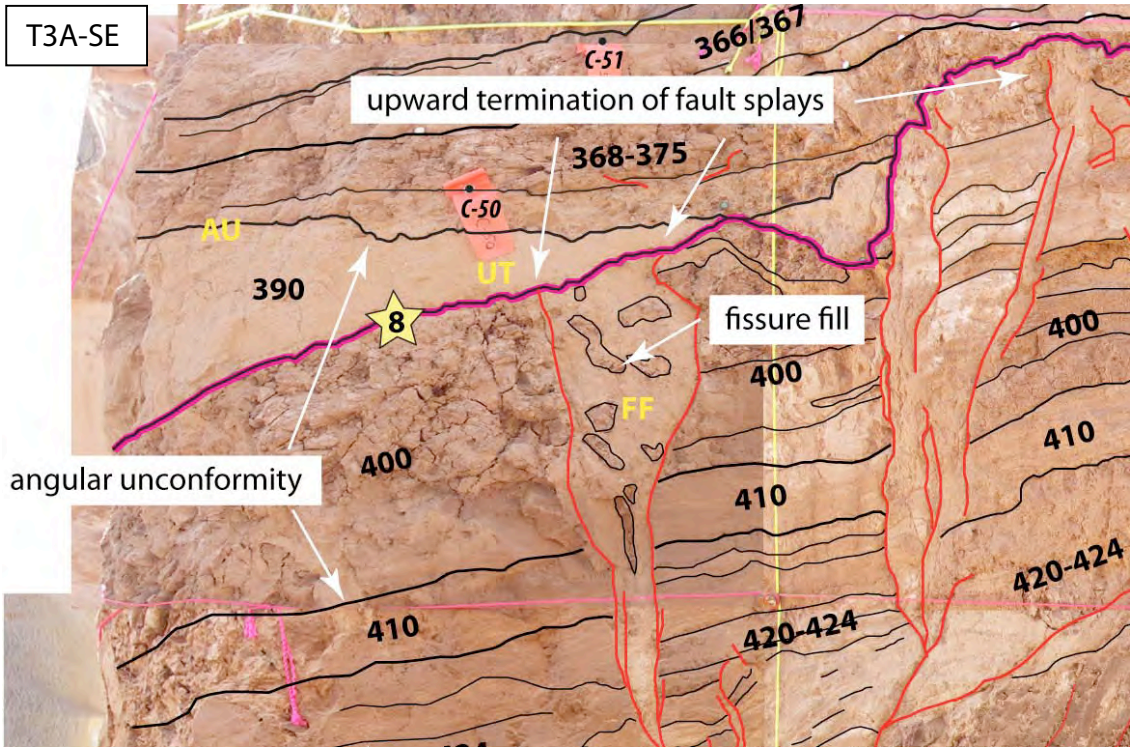

Shortly after the immediate deposition of the sand blow, a debris derived from the fault scarp was deposited on top of Unit 390, which serves as another line of evidence for Event 8 and was observed in trench T9B-SE. The scarp-derived debris interfingers with Units 368-375, therefore the debris probably was deposited when deposition of the lacustrine sediments resumed shortly after the ground shaking. Deposition of lacustrine strata continued as younger strata of Units 367 and above were deposited horizontally on top of the scarp-derived debris and Unit 390.

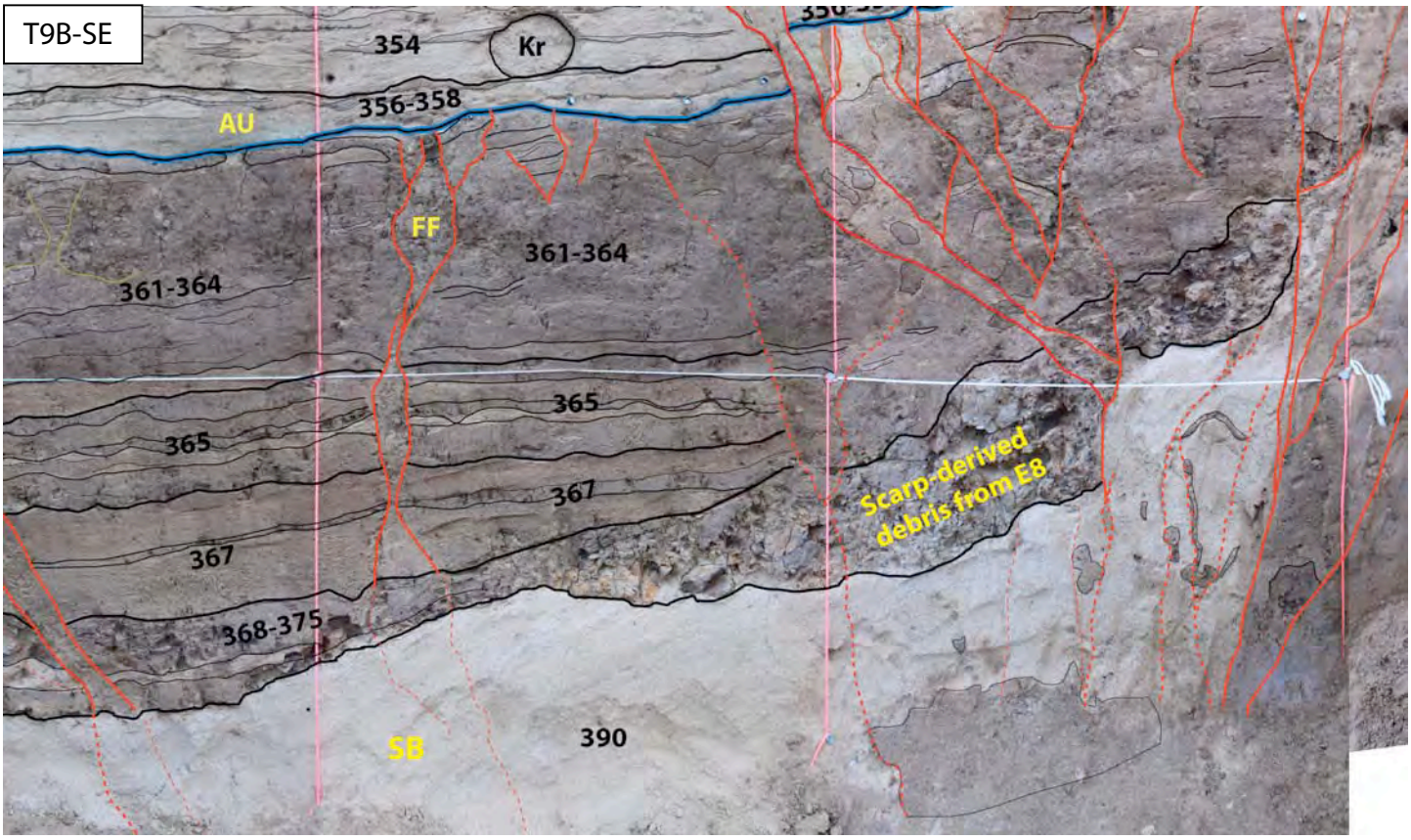

Event 8.5

The evidence for Event 8.5 is fairly weak, leading to our interpretation of Event 8.5 being an unlikely event, hence it was not assigned with a whole number. The paleoseismic indicators are only present in two cuts of the same trench: T4Deep-SE-A and B. The event horizon of Event 8.5 occurred stratigraphically at the base of Unit 410 during the early filling stage of Lake E.

Two groups of fault splays terminate upward at the base of Unit 410 as observed in two different locations on the same face of T4Deep-SE-B. However, the root of one group of fault splays could not be traced downward despite the vertical separation at the top was obvious. One possible explanation is that the displacement (if any) in the massive clay unit below is hardly discernible as the vertical separation is on the scale of mm. In addition, the lower contact of Unit 410 was obscured by a series of liquefaction pipes, therefore the exact location at where the fault splays terminate could not be assured. However, because the upper contact of Unit 410 was not vertically separated, the fault splays probably terminate somewhere as high up as the upper contact of Unit 410.

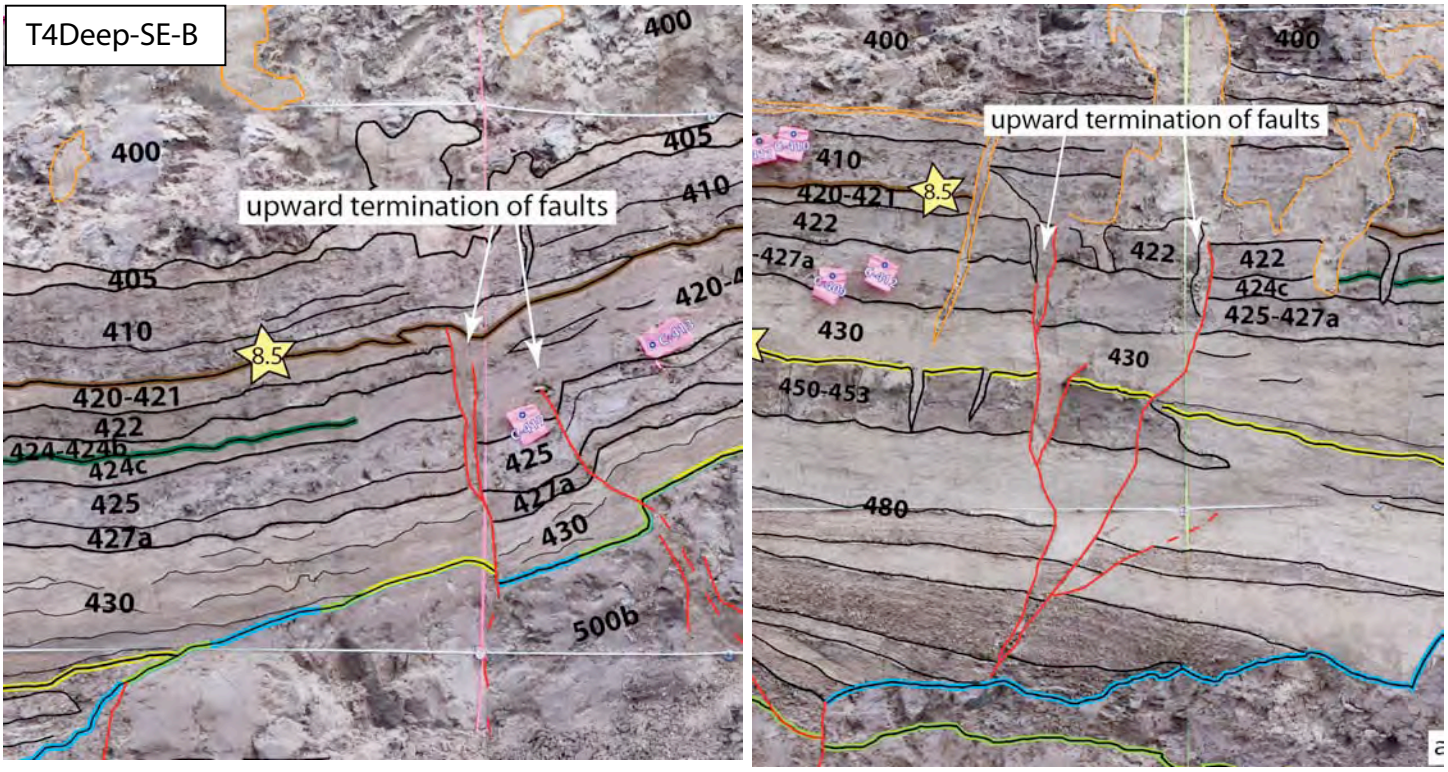

In trench T4Deep-SE-A, downward increase in vertical separation was observed on a minor fault away from the main fault zone to the southwest. The separation across the fault in the younger Units 405-410 is halved of that in the older Units 420-430, which could be explained by multiple faulting events on the same fault, making the base of Unit 410 the event horizon of Event 8.5. However, McCalpin et al. (1996) explained that this observation does not necessarily imply multiple faulting events because the same effect could be produced by faults merging and/or faults naturally dying out upward.

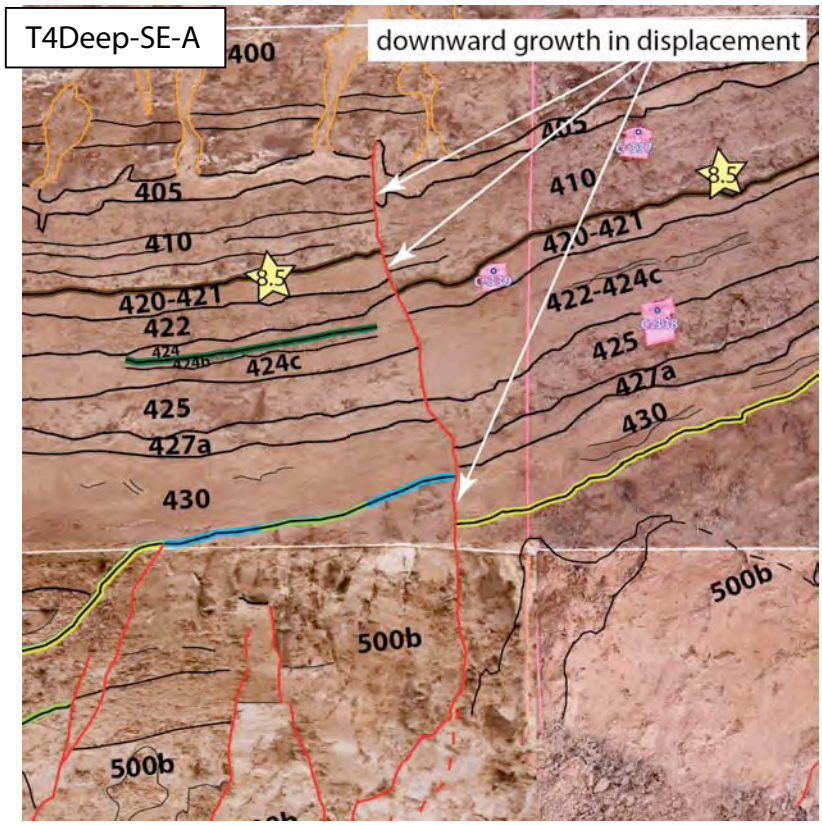

Event 8.7

T3B-NW T2-Extension-SW

Event 8.7 occurred stratigraphically at the base of Unit 424 during the early filling episode of Lake E. The T4Deep-NW-A T4Deep-NW-B event was only exposed in two cuts of the same trench, in T4Deep-NW-A and B, making the occurrence of this event uncertain. However, the upward termination of a fault in T4Deep-NW-A is clear enough to place a possible event horizon at the base of Unit 424, where vertically separated beds (Units 424b/425 and older) were capped by the undeformed, continuous younger beds (Units 424 and younger).

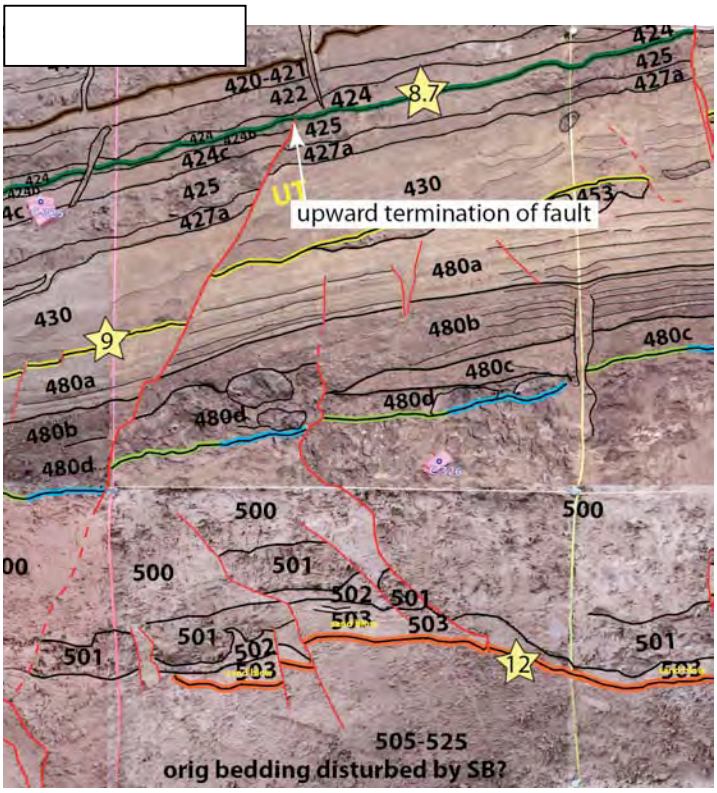

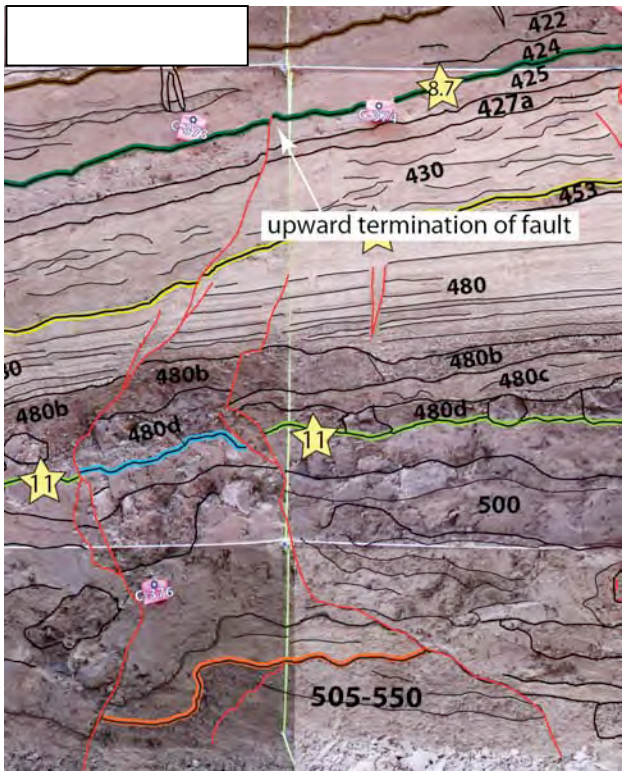

Event 9

Event 9 occurred at the base of a well-sorted, fine sandy unit (Unit 430) and at the top of a thin bed of clay that has a maximum thickness of about 15 cm (Units 450-453). We argue that Event 9 is in fact another sand blow caused by an older earthquake.

In the exposures of the fault-perpendicular trench T3B-NW and the fault-parallel T2-Extension-SW, Unit 430 consists of loose, very well-sorted fine sand with thin, continuous, planar laminations of clay near the base, which is a common texture found in sand blows.

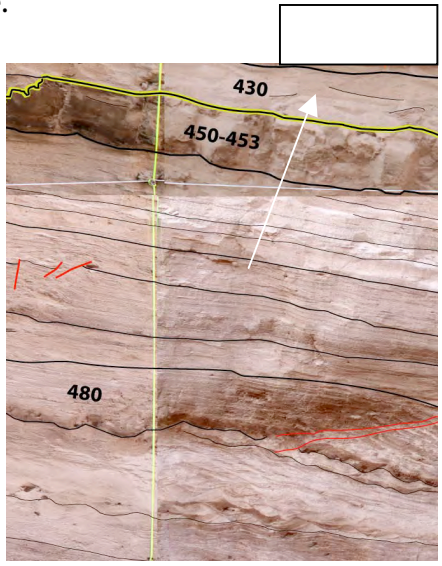

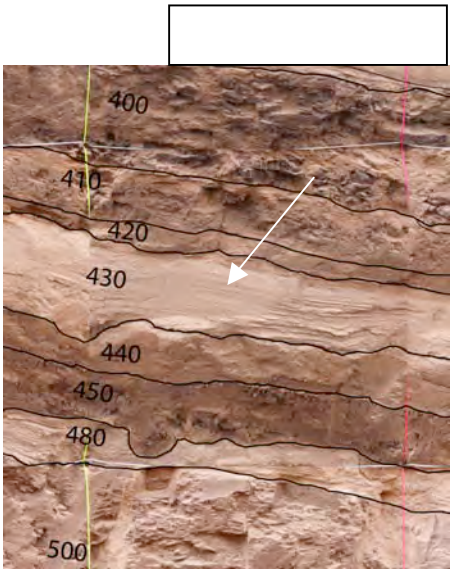

T3A-SE

In all three cuts of T4Deep-NW, Unit 430 overlies the thin bed of clay (Units 450-453) which appear to be penetrated and broken up into blocks by a series of liquefaction pipes, most of which do not extend upsection. These liquefaction pipes might have served as conduits for the deposition of Unit 430 as a sand blow. Moreover, the pervasive discontinuous wavy laminations of clay and fine sand in Unit 430 might indicate liquefaction of the sand blow itself by a later seismic event, which also could help explain the uncommon higher clay content in the sand blow as a result of material being reworked. Regardless, the liquefaction of the sand blow Unit 430 could be a very localized phenomenon because it is not present in the other two exposures mentioned earlier.

T4Deep-NW-A

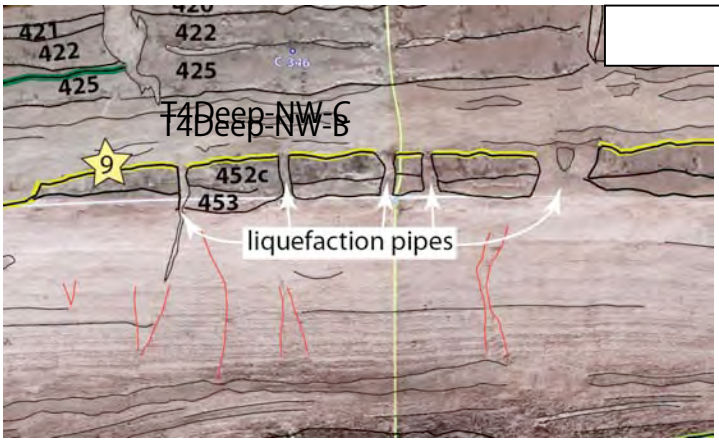

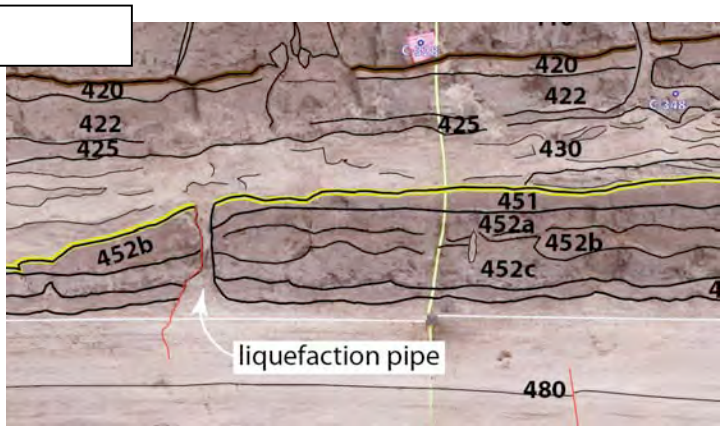

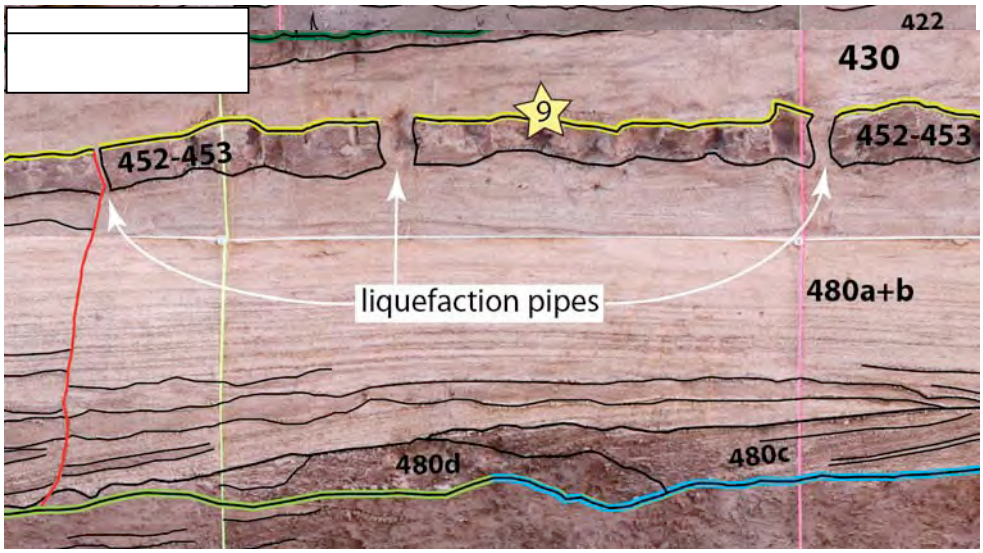

In addition, a difference in dipping angles was observed between Unit 430 and the underlying Unit 480 in trenches T3A-SE, T4Deep-NW-B and C and T4Deep-SE-A. This difference might not be a result of deformation as the beds above are more tilted than those below, but rather the result of a progradational dip formed by the deposition of a sand blow from a vent nearby.

T4Deep-NW-B

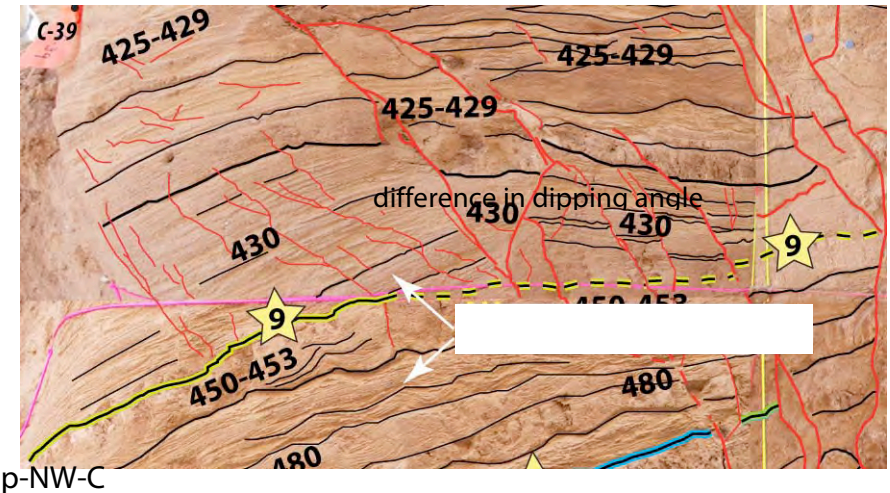

T4Deep-NW-C

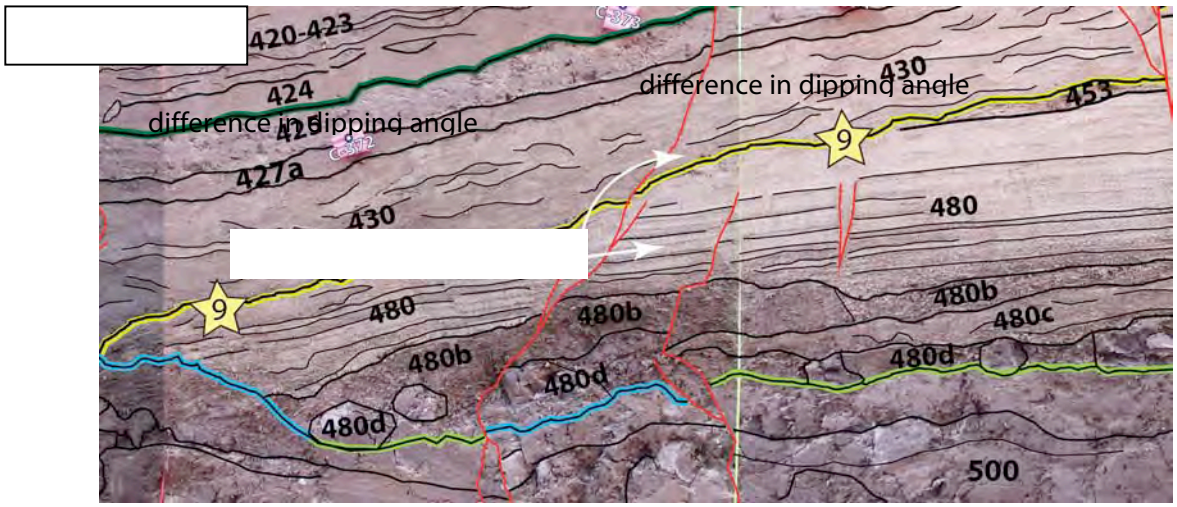

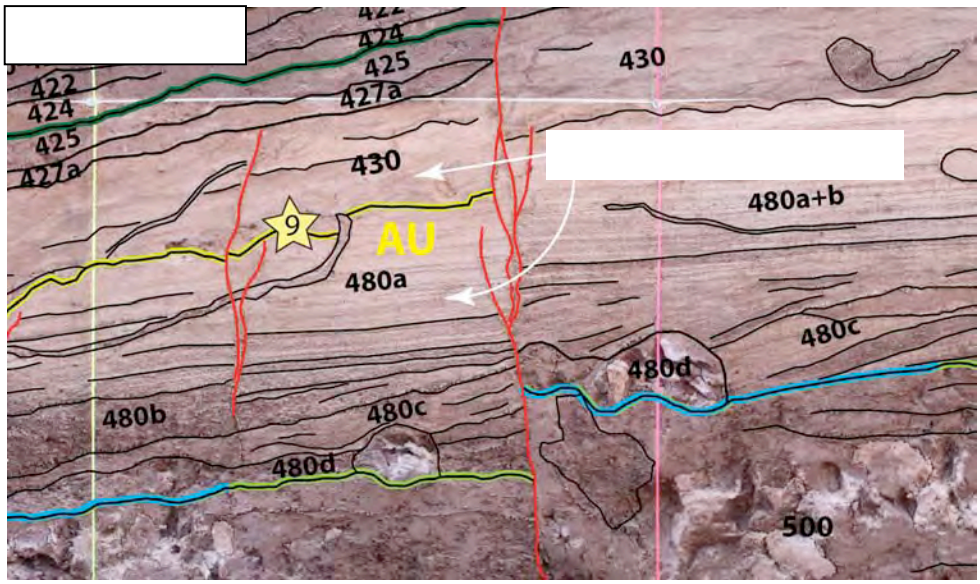

T4Deep-SE-A

T4Deep-SE-B

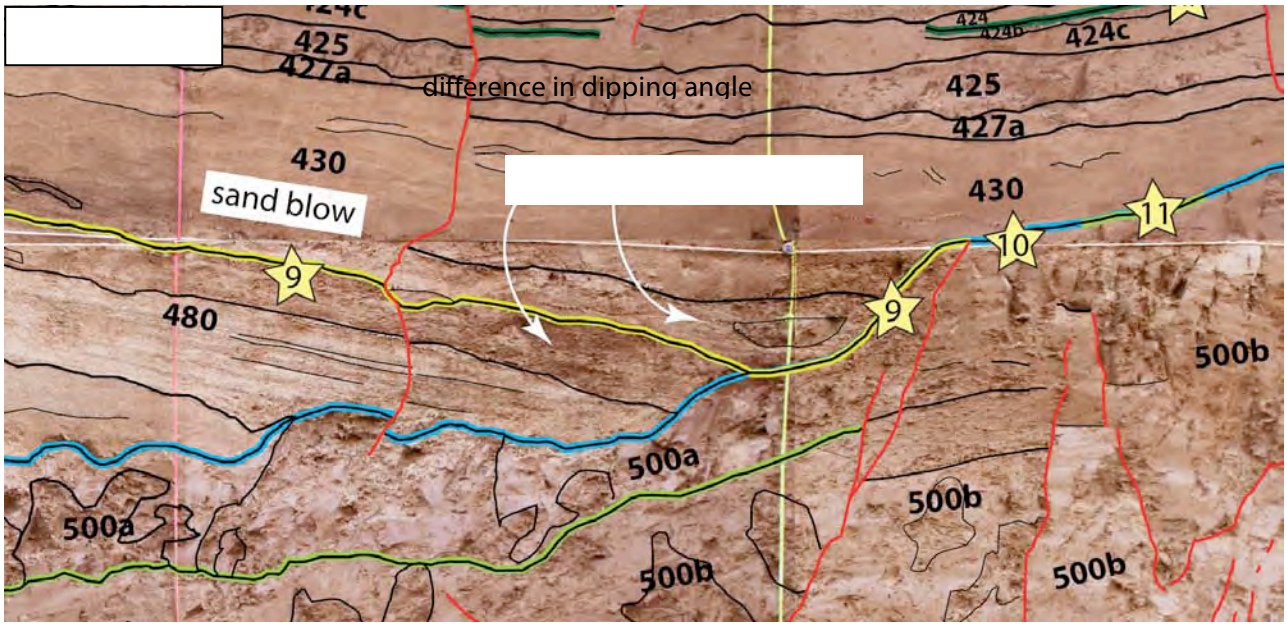

In T4Deep-SE-B, a small fault terminates upward at the base of Unit 430. However, this feature was not observed in any other exposures.

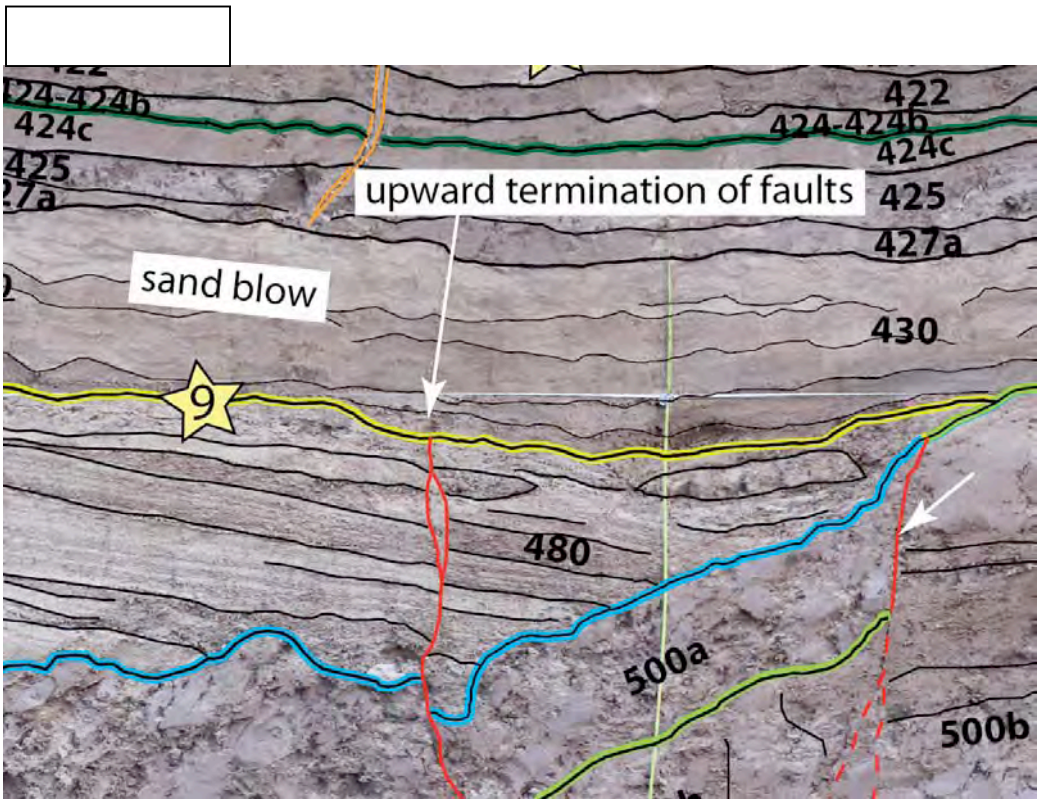

T2-Extension-SW

Events 10 / 11

T3B-NW

In some exposures, Events 10 and 11 occurred essentially at the same stratigraphic horizon. In the first part, the evidence for each event will be explained separately based on the observation in several trench exposures. In the second part, we discuss the composite horizon of Events 10 and 11 together and present additional evidence to support the occurrence of these two events.

Event 10

Event 10 occurred at the base of Unit 480, a very well-sorted fine sand with thin, continuous, planar laminations of clay closer at the base, as observed in trenches T2-Extension-SW and T3B-NW.

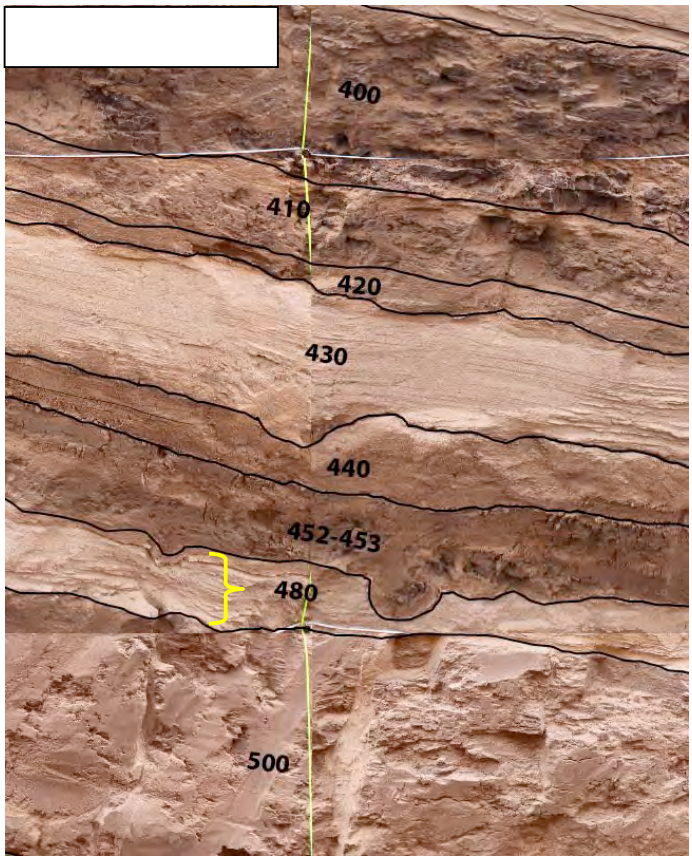

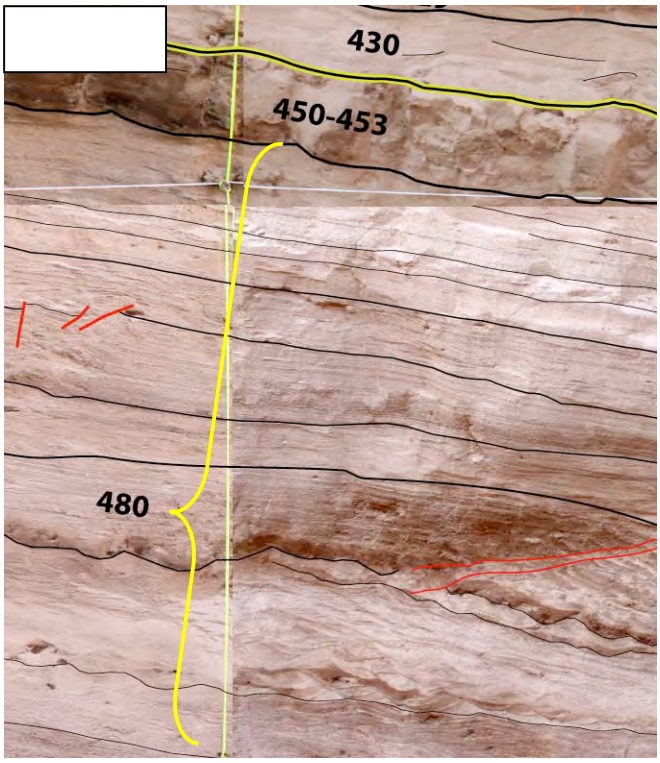

The major rationale for Event 10 is that Unit 480 is a sand blow. It is important to note that the sand blows of Unit 430 and Unit 480 were caused by two separate seismic events as they were separated by a thin package of clayey beds (Units 450-453), although in some parts of a few exposures the clay package is not present. Besides the unusually well-sorted texture of Unit 480, a difference in dipping angles exist between Unit 480 and Unit 500 as observed in T4Deep-SE-A and B. The difference could be resulted from the natural dip of sand blow progradational deposition or from the interaction of multiple sand craters.

T4Deep-SE-A T4Deep-SE-B

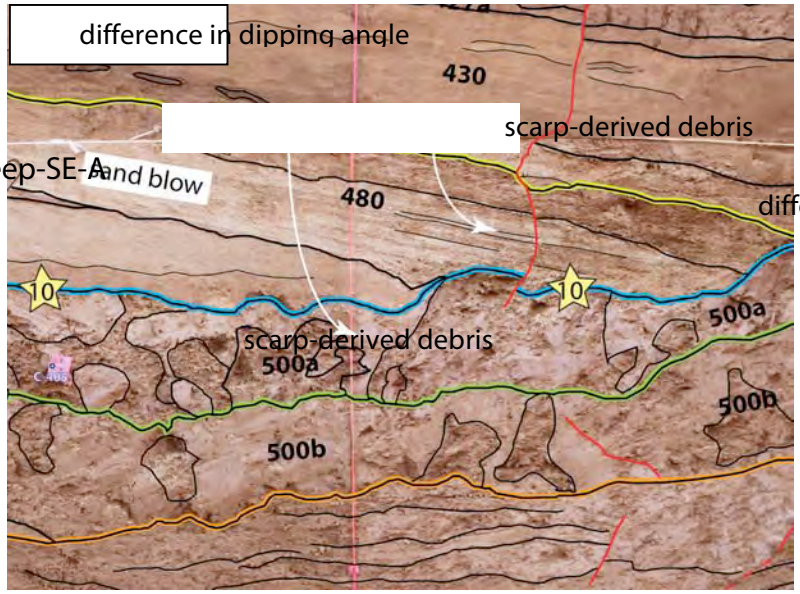

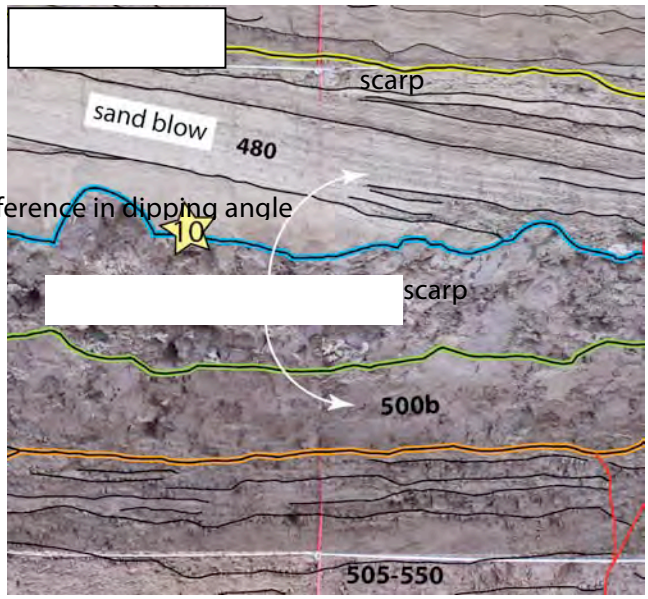

Event 11

Event 11 occurred stratigraphically at the base of Unit 500a, a unit which was interpreted to be a scarp-derived mud debris, therefore, the base of Unit 500a would denote the event horizon for Event 11 (green). Unit 500a consists of unstratified mixture of blocky clay with some fine sand and silt; the irregular upper contact of Unit 500a drapes over the scarp as seen in T4Deep-SE-A and B. Both the texture and the geometry of Unit 500a suggest a scarp-derived origin of the unit.

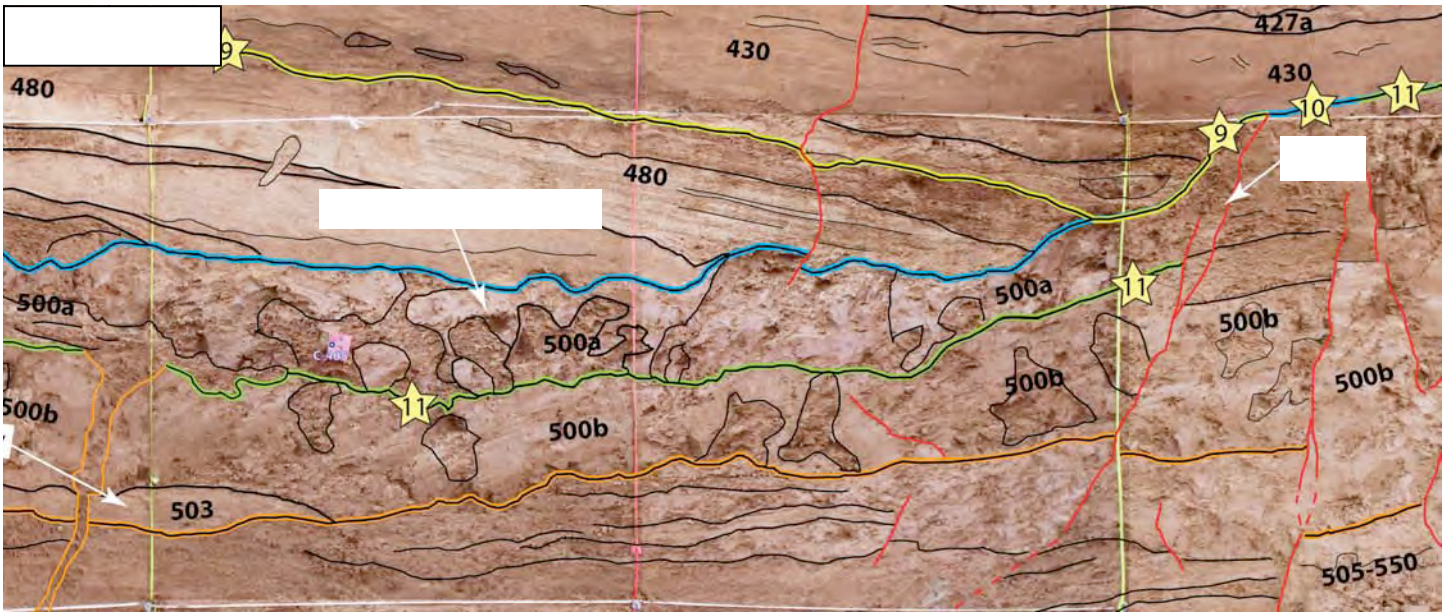

˙4Deep-NW-A

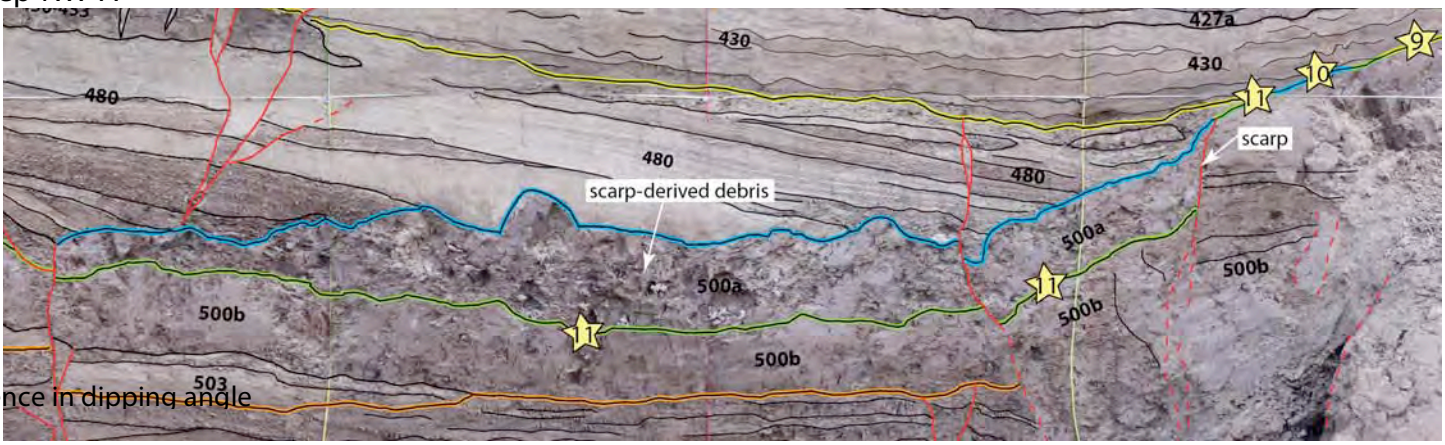

ifference in dipping angle

Events 10/11

In trenches T1-NW, T4Deep-NW and T3-NW, due to the absence of the scarp-derived debris Unit 500a, the event horizons for the two events could not be distinguished. Therefore, the evidence for both events is discussed together in the following. It is important to note that Unit 500 is presented as one whole unit in these trench logs where the scarp-derived debris is absent.

The event horizon is present at the base of 480 and the top of 500, a unit that is believed to be deposited during the filling episode of Lake F. In trenches T4Deep-NW-A and C, the depositional dip in Unit 480 further validates the sand blow nature of Unit 480. In addition, isolated clasts of clay that have a similar texture to Unit 500 were found at the bottom of Unit 480, which could be originated from liquefaction ejecta ripping off parts of Unit 500 under elevated pore-water pressure as material was being ejected to the surface. The clay clasts were not likely derived from materials shed from a fault scarp as most of them were not found close to a fault. The possibility of a subaerial erosional origin is also not likely because there is no observable signs of oxidation, e.g. red iron stains.

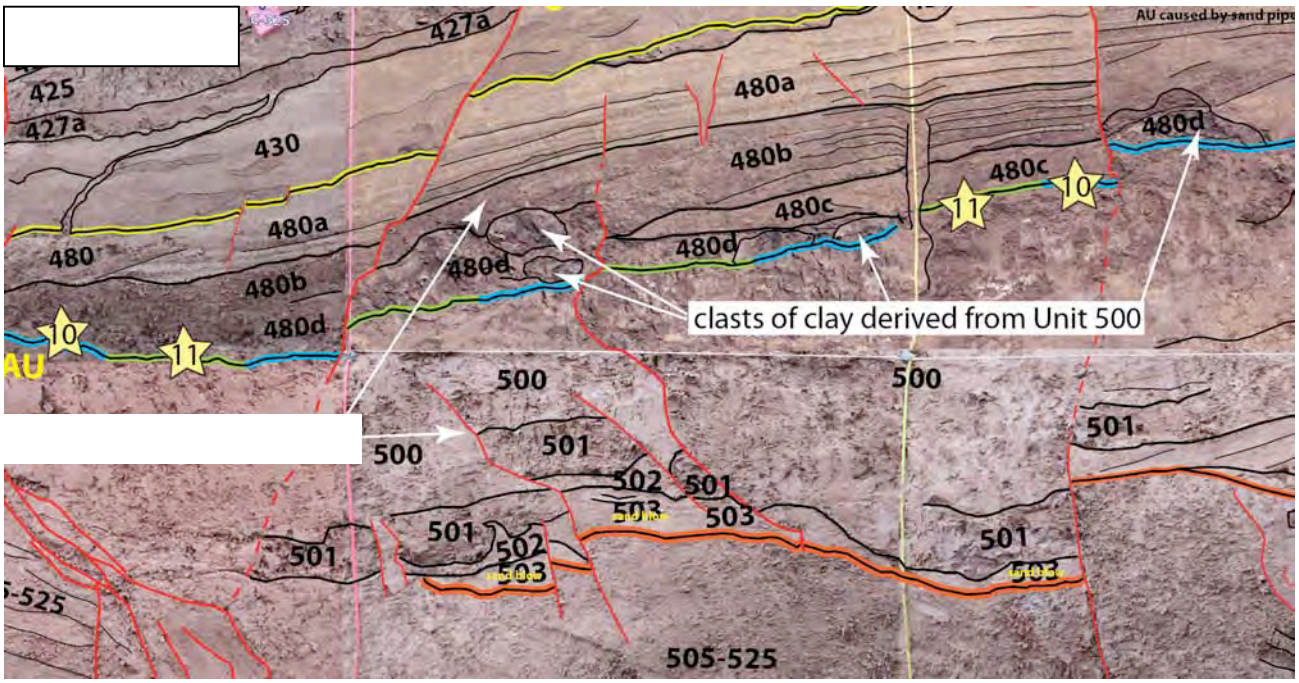

T4Deep-NW-C

difference in dipping angle

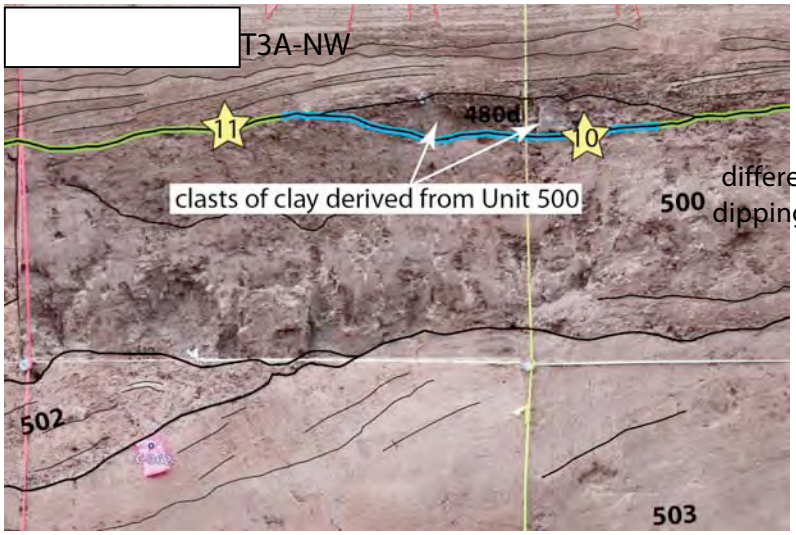

difference in dipping angle

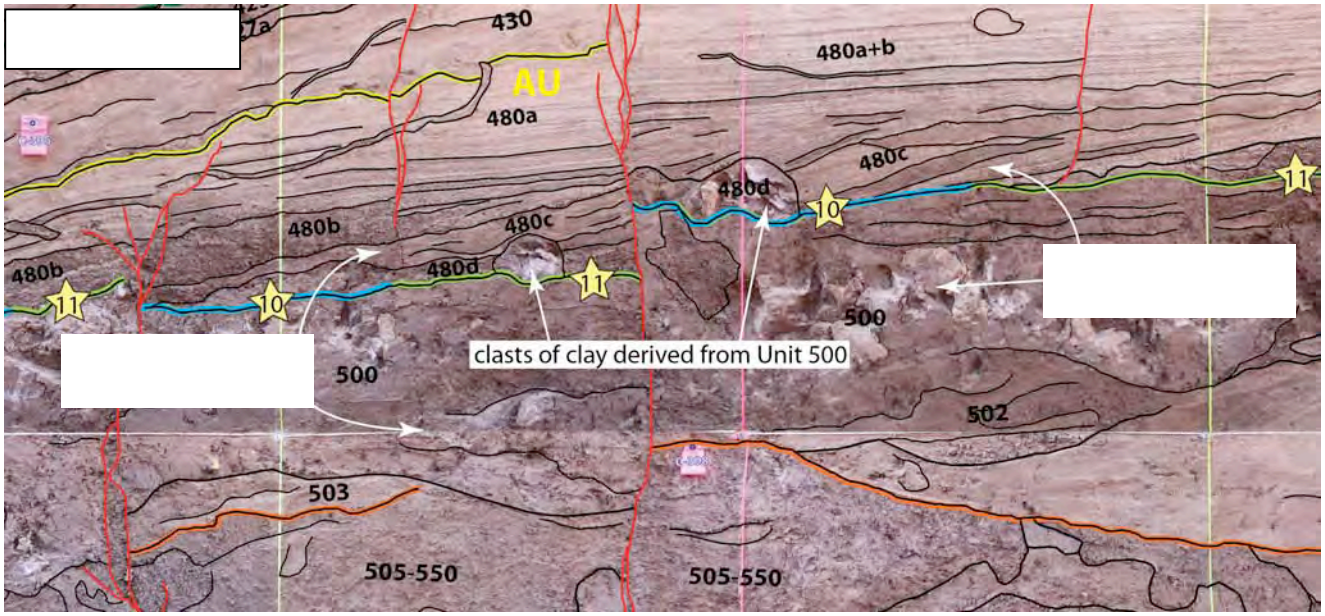

Another piece of evidence for Events 10/11 is the upward termination of fault splays at the base of Unit 480, as observed inn trenches T3A-NW and T1-NW, although the root of the faults could not be identified in T1.

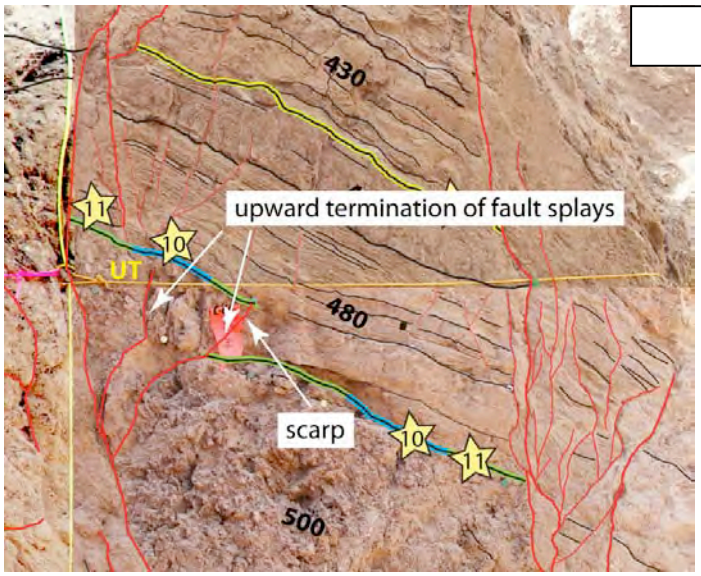

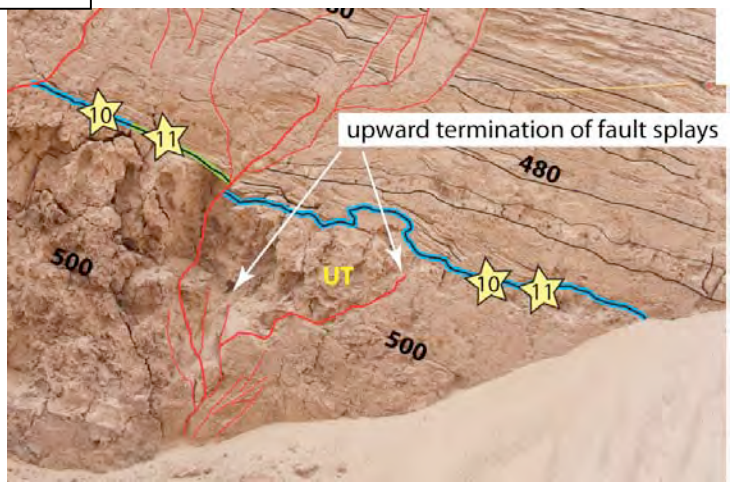

T4Deep-NW-A

T4Deep-NW-B

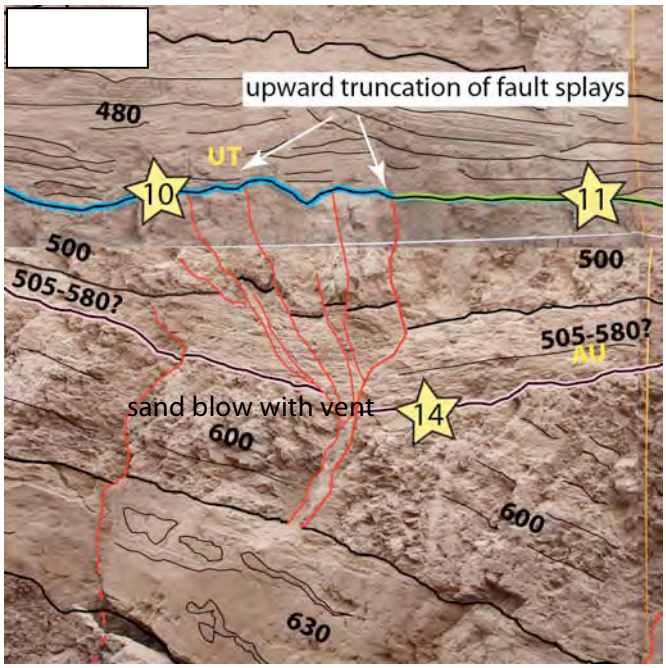

Event 12

Event 12 occurred stratigraphically at the base of Unit 503 and/or at the top of Unit 505 during the filling episode of Lake F. Paleoseismic indicators for this event are spread across different exposures including trenches T3B-NW and T4Deep.

Unit 503 was interpreted as a sand blow and was exposed in all T4Deep exposures. The unit consists of well-sorted fine sand mixed with some clay that makes it more consolidated than a typical sand blow with clean sand. Regardless of the texture, it is almost certain that Unit 503 is a sand blow because both the dome shape at the top and the vent which is about 60 cm wide are visible in all three cuts of T4Deep-NW. Hence, the base of Unit 503 marks the event horizon of Event 12. Only portions of Unit 503 were observed in the T4Deep-SE exposures.

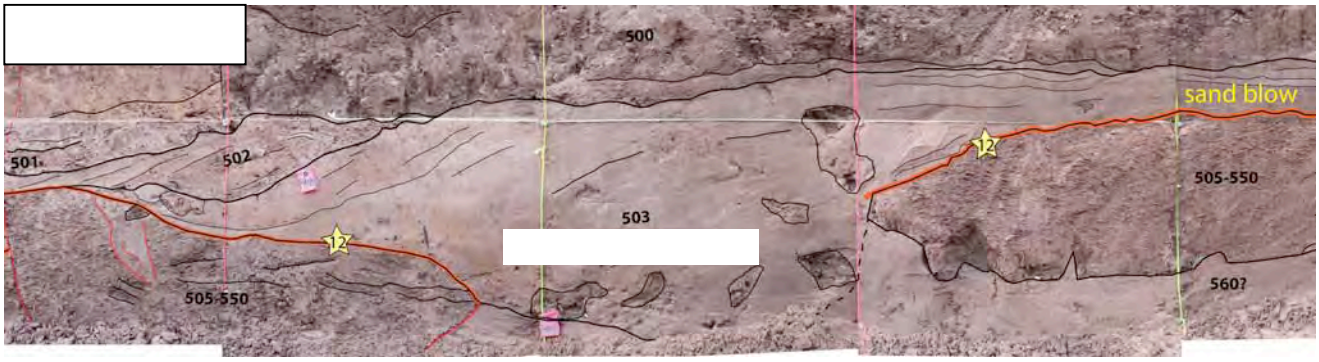

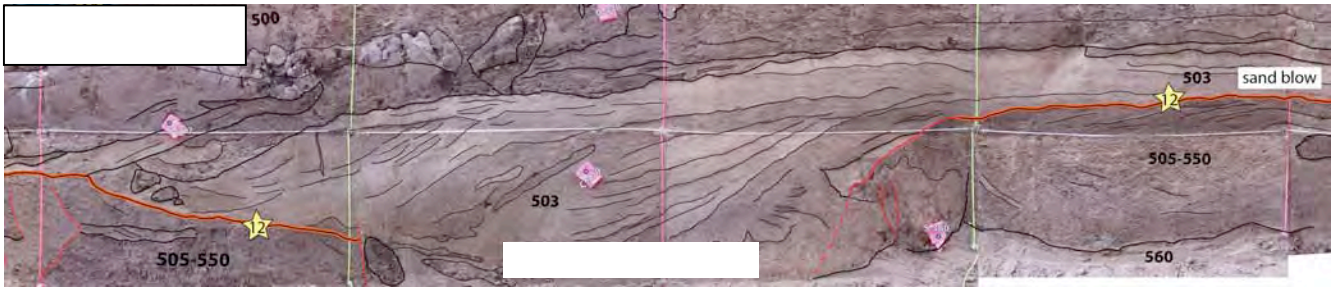

T4Deep-SE-A

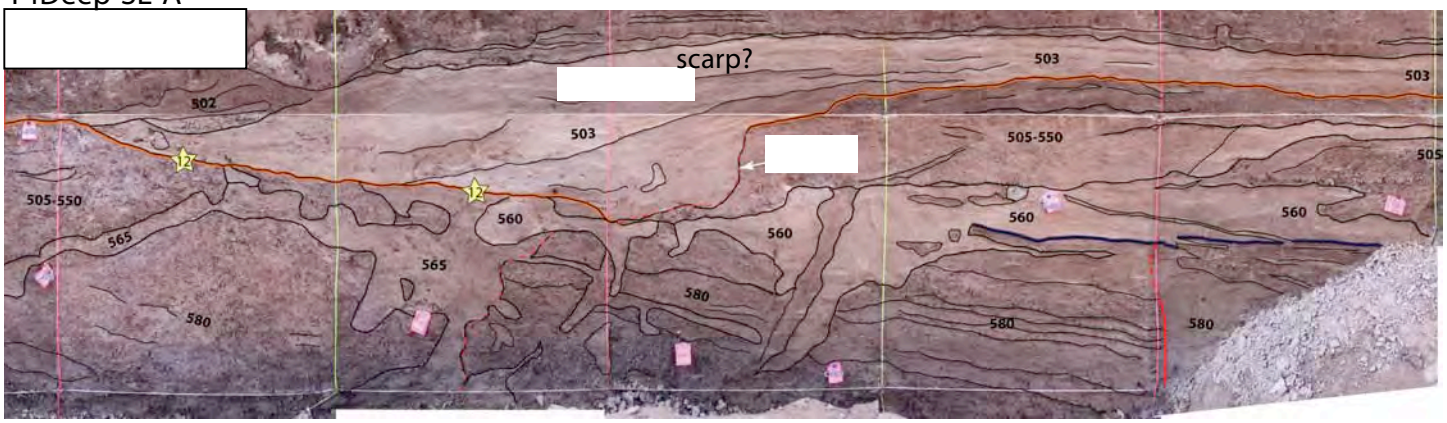

T4Deep-SE-B

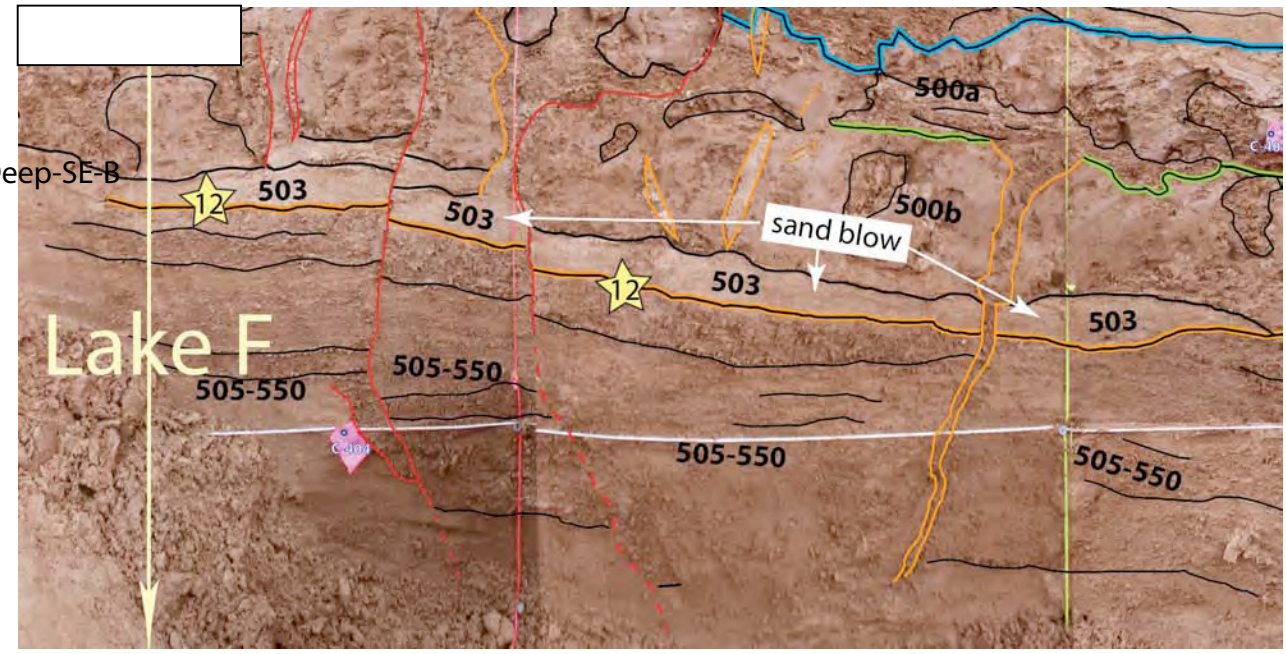

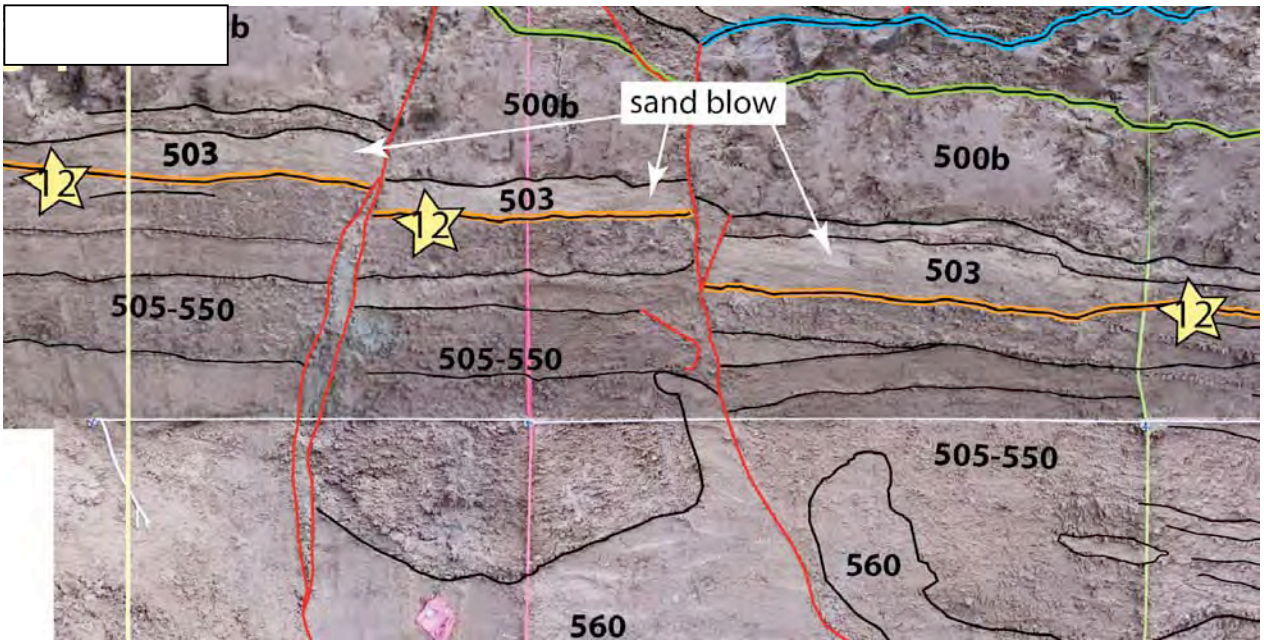

In trench T4Deep-NW-C (first figure in the previous page), a scarp might be present on the wall of the sand blow vent which could have caused the downdropping of Units 503 and 505-550 to the southwest (left in the figure). Moreover, this could further explain why the section closer to the main fault zone to the SW was downwarped toward the fault zone, in addition to the explanation of the presence of a large sand blow vent close to the fault zone. Despite the hypotheses, the presence of this fault and the corresponding fault scarp could not be assured as the fault could not be traced downsection due to multiple liquefaction units nearby obscuring the original stratigraphy and possibly the fault as well.

Additional evidence for Event 12 was observed in other exposures. Splays of fault terminate upward at the top of Unit 505 in trenches T4Deep-SE-B and T3B-NW. Also observed in trench T3B-NW was the fissure fill that was capped by Unit 500 and the angular unconformity between Unit 500 and Unit 505.

T4Deep-SE-B

T3B-NW

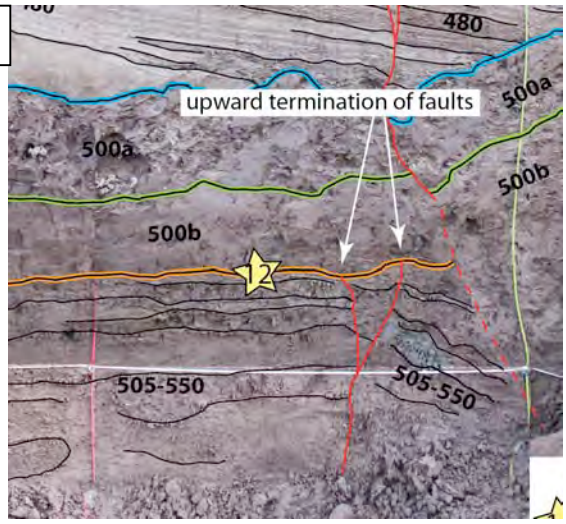

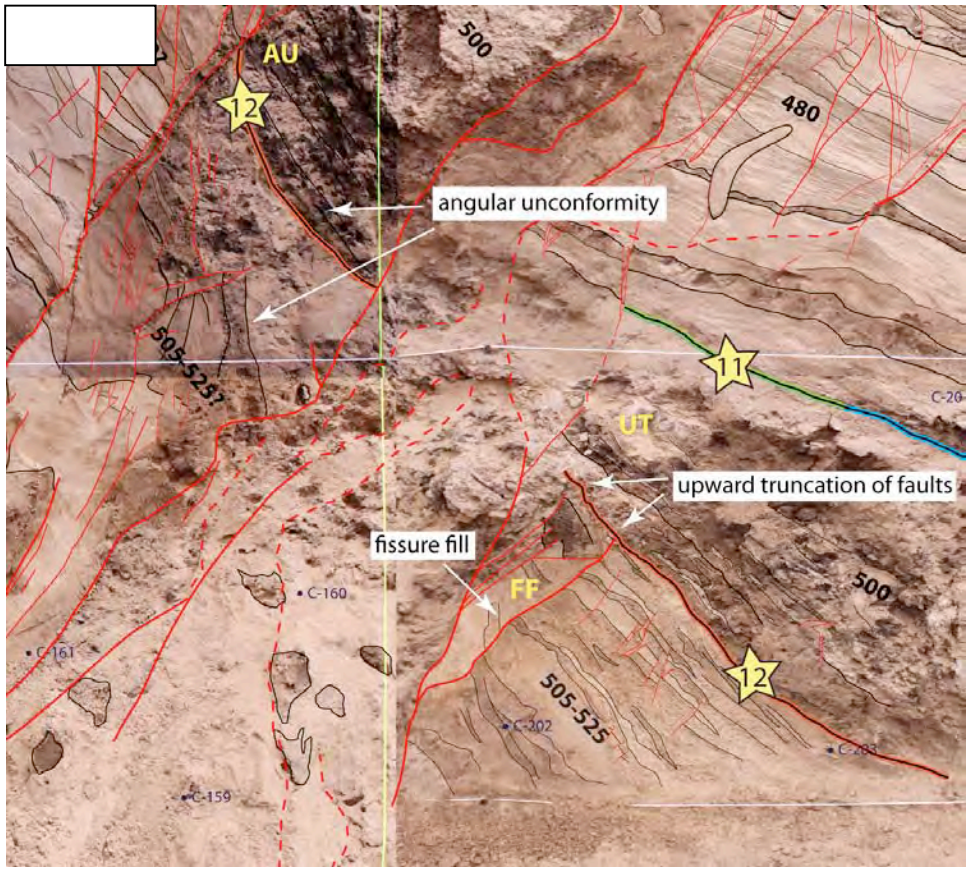

Event 13

Event 13 occurred at the base of Unit 560 and the top of Unit 580. Evidence for this event was only exposed in one trench as most of our trench exposures did not reach this depth. In trench T4Deep-NW-C, the event horizon was marked at the base of Unit 560, a unit that was interpreted to be a sand blow. The sand blow consists of well-sorted fine sand with some clay and shares a similar texture with the sand blow Unit 503 mentioned earlier. Clasts of clay were ripped off from the sidewall of Unit 580 that was in contact with the vent. It is possible that Unit 560 is a sill instead of a sand blow. However, the occurrence of Event 13 is still assured by other lines of evidence including upward termination of a fault and a clear angular unconformity between the younger horizontal strata(Units 505-550) and the older, tilted strata below (Unit 580).

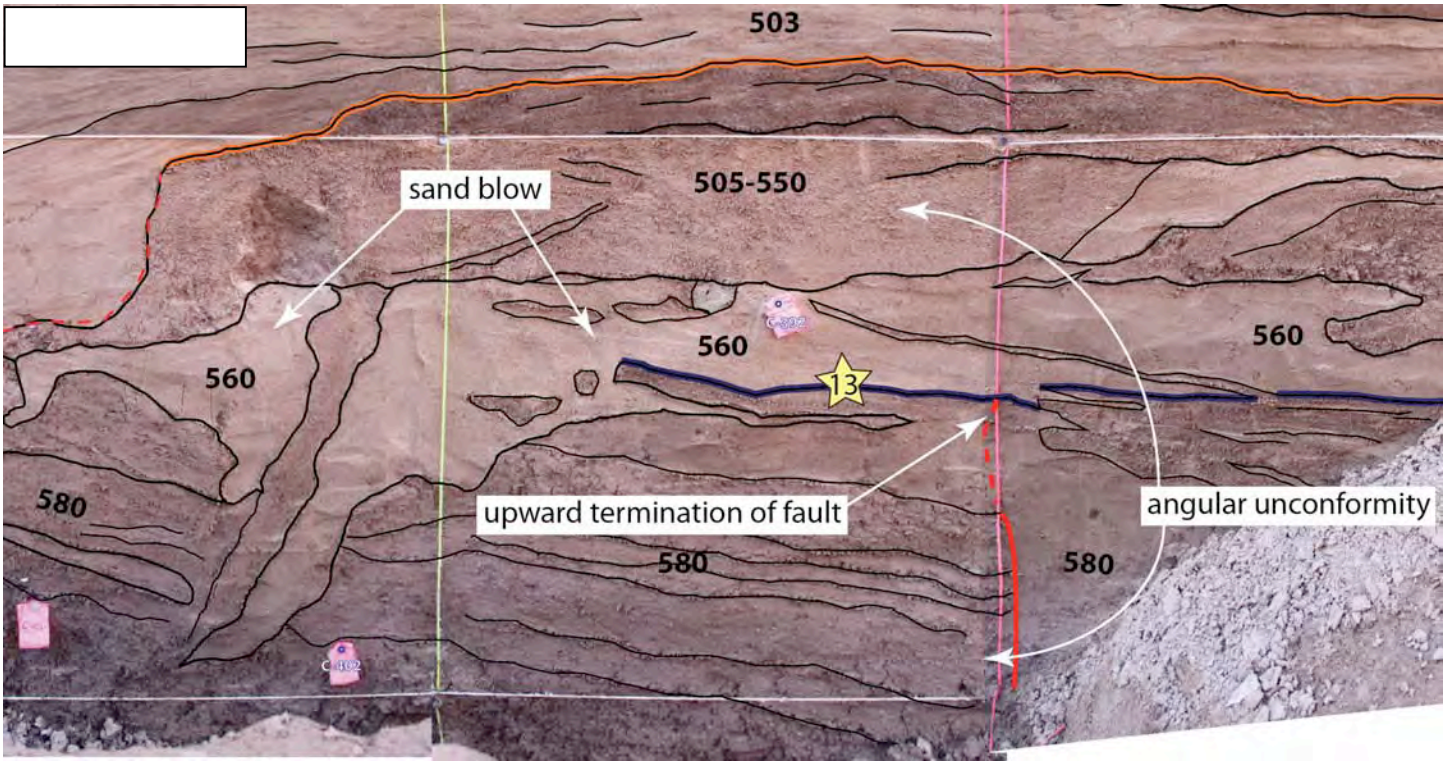

The occurrence of Events 14 and 15 are not strongly supported by multiple lines evidence, as there is only one exposure (T1-NW) in the entire trench site that contains a stratigraphic record older than Unit 600. However, each line of evidence is clear and unambiguous.

Event 14

Event 14 occurred at the top of Unit 600, probably during the dry period between Lake F and Lake G. The event horizon was marked by a sharp angular unconformity between the relatively horizontal strata above (Units 500-580) and the steeply-dipping strata below (Units 600 and 630). In addition, the dome-shaped, lenticular unit (labeled 630) was interpreted as a sand blow being ejected from the source directly below (Unit 630) via the liquefaction pipe. These features and units seem to be connected as a system because the silty texture is the same throughout, which starkly contrasts against the adjacent clayey strata (Unit 600).

T1-NW
T1-NW

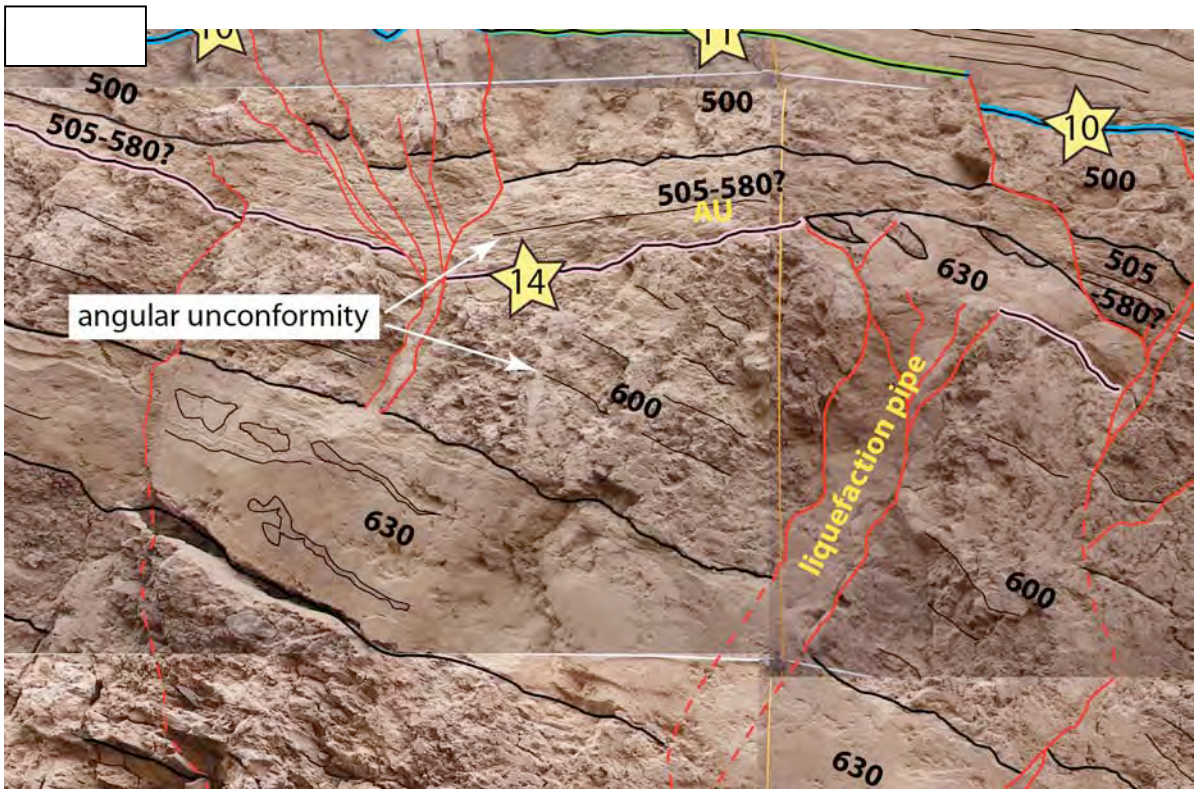

Event 15
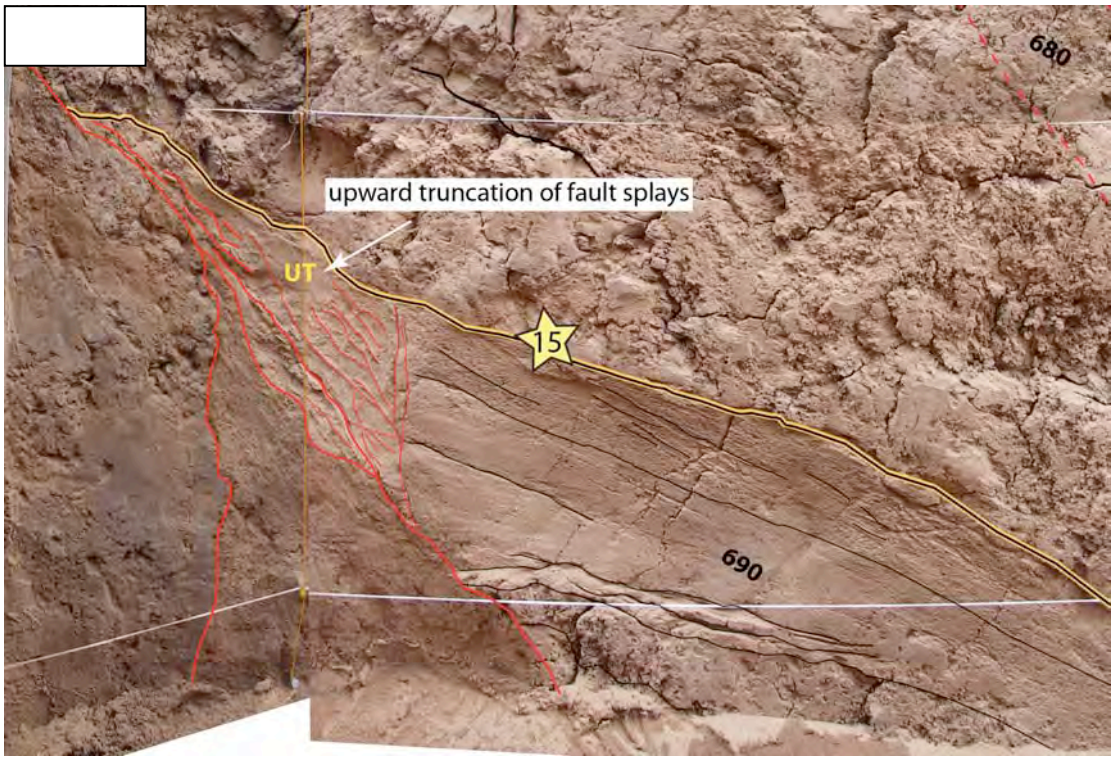
Event 15 occurred stratigraphically at the base of Unit 680 and the top of Unit 690, probably during the filling episode of Lake G. The only evidence for Event 15 is the upward termination of a series of fault splays at the base of Unit 680. Unit 680 is so far the oldest unit exposed in our trench site on the hanging wall.